Université de Montréal

Preparation, Characterization, and Rheological Properties of Star-Shaped Poly(ethylene glycol) with a Cholane Core and Study of Its Effect on Red Blood Cell Aggregation

par

Florence Janvier

Département de chimie

Faculté des Arts et des Sciences

Mémoire présenté à la Faculté des études supérieures

en vue de l'obtention du grade de Maître ès Science (M.Sc.)

en chimie

option génie biomédicale

Avril 2009

Université de Montréal
Faculté des études supérieures

Ce mémoire intitulé :

Preparation, Characterization, and Rheological Properties of Star-Shaped Poly(ethylene glycol) with a Cholane Core and Study of Its Effect on Red Blood Cell Aggregation

Présenté par :
Florence Janvier

A été évalué par un jury composé des personnes suivantes :

Suzanne Giasson, président-rapporteur
Julian Zhu, directeur de recherche
Guy Cloutier, co-directeur
Jean-François Masson, membre du jury

RÉSUMÉ

L'hyper-agrégation des globules rouges (érythrocytes) est reliée à plusieurs pathologies telles que la thrombose, l'anémie falciforme, le diabète et l'athérosclérose. Les polymères poly (éthylène glycol) PEG et le copolymère Pluronic sont utilisés pour la modification de l'agrégation érythrocytaire. Pluronic est un polymère bloc amphiphile composé d'un bloc hydrophobe de poly(propyléthylène glycol) (PPG). Récemment, des inquiétudes concernant des réactions allergiques du au PPG contenu dans le Pluronic ont été soulevées. Par conséquent, nous avons proposé l'utilisation d'un polymère PEG amphiphile en forme d'étoile composé de l'acide cholique. L'acide cholique est un acide biliaire naturel qui est synthétisé dans le corps humain. Ces caractéristiques rendent le polymère en forme d'étoile de PEG composé de l'acide cholique ($CA(PEG)_4$) très promoteur comme agent potentiel pour la réduction de l'agrégation érythrocytaire. Les polymères $CA(PEG)_4$ ont été synthétisés par la polymérisation anionique. La structure chimique et les propriétés physiques de ces polymères ont été caractérisées par la chromatographie d'exclusion stérique et la diffusion de la lumière par angles multiples. Les rayons hydrodynamiques des polymères ont été déterminés par la viscosité intrinsèque en utilisant la relation d'Einstein. Les effets des polymères $CA(PEG)_4$ sur la viscosité sanguine humaine et sur l'agrégation érythrocytaire ont été évalués et comparés aux PEGs linéaires par des mesures viscométriques et par agrégométrie. Les résultats de l'aggrégomètre ont démontré que le $CA(PEG)_4$ inhibite l'agrégation érythrocytaire mais cependant, la réduction de la viscosité sanguine n'était pas significative. L'inhibition de l'agrégation érythrocytaire du polymère $CA(PEG)_4$ en forme d'étoile était similaire à celle des PEGs linéaires.

Mots-clés : polymère étoilé de PEG, agrégation des globules rouges, agrégation érythrocytaire, polymère PEG dérivé de l'acide cholique.

ABSTRACT

Elevated red blood cell (i.e., erythrocyte) aggregation is a phenomenon closely related to several pathophysiological diseases such as thrombosis, diabetes, sickle cell disease, and athrerosclerosis. Non-ionic linear polymers such as poly(ethylene glycol) (PEG) and Pluronics have shown inhibitory effect against erythrocyte aggregation. Pluronics are amphiphilic polymers composed of a central hydrophobic moiety core, poly(propylethylene glycol) (PPG) flanked by two PEGs. Recently, a number of concerns have been raised on the allergenicity of PPG in the Pluronics. Therefore, we suggested the use of an amphiphilic star-shaped PEG polymer based on cholic acid core. Cholic acid is a natural bile acid produced in the human liver; therefore, it should confer more biocompatibility. These features made the cholic acid based PEG ($CA(PEG)_4$) an attractive polymer to be used in the reduction of erythrocyte aggregation. The $CA(PEG)_4$ polymers were synthesized by anionic polymerization. The narrow molar mass distribution of the star-shaped polymers was characterized by size exclusion chromatography alone and coupled to a multi angle laser light scattering. The addition of the laser to size exclusion chromatography provided additional information about the branching character. The hydrodynamic radius of the star-shaped $CA(PEG)_4$ was calculated from their intrinsic viscosities using the Einstein viscosity relation. The effects of the star-shaped $CA(PEG)_4$ on human erythrocyte aggregation and blood viscosity were investigated and compared to linear PEGs by means of viscometry measurements and laser aggregometry. The aggregometer data showed inhibition of erythrocyte aggregation for the star-shaped $CA(PEG)_4$ polymer, however, the reduction in blood viscosity was not significant. Compared to linear PEGs of the same molar mass, the star-shaped $CA(PEG)_4$ polymer inhibited red blood cell aggregation in a similar manner.

Keywords : Star-shaped PEGs, red blood cell (RBC) aggregation, erythrocyte aggregation , cholic acid based polymers.

TABLE OF CONTENTS

LIST OF TABLES

LIST OF FIGURES

LIST OF SYMBOLS AND ABBREVIATIONS

AROP	anionic ring-opening polymerization
ATRP	Atom transfer radical polymerization
AOROP	anionic ring-opening polymerization
CA	Cholic acid
CAME	Cholic acid methyl ester
$CA(PEG)_4$	Cholic acid PEG star-shaped polymers
dn/dc	Differential refractive index increment
DMSO	Dimethyl sulfoxide
DP	Degree of polymerization
EG	Ethylene glycol
EO	Ethylene oxide
g_M	Branching ratio
Hb	Hemoglobin
Ht	Hematocrit
IgE	Immunoglobulin E
MW	Molecular weight
PBS	Phosphate buffer saline
PDI	polydispersity index
PEG	Poly(ethylyene glycol)
PEO	Poly(ethylene oxide)
PVP	Polyvinylpyrrolidone
PPG	Polypropylene glycol
R_{ex}	Rate of exchange
R_g	Radius of gyration

R_h	Hydrodynamic radius
R_p	Rate of propagation
RBC	Red blood cell
SD	Standard deviation
SCD	Sickle cell disease
THF	Tetrahydrofuran
η	Viscosity
$[\eta]$	Intrinsic viscosity
γ	Shear rate
τ	Shear stress

ACKNOWLEDGEMENTS

I would like to thank my research director Julian Zhu for allowing me to join his group and providing the opportunity to pursue a Master's degree. Also, I appreciated his patience and his persistence. I also would like to thank my co-director Guy Cloutier. I am grateful to him for his guidance and the financial support he provided through out my research. Jonathan Armstrong also deserves credit, as he helped out with most of the blood experiments. Without him, this thesis would not have been possible. I would like to thank all the people from the laboratory of Dr. Zhu and that of Dr Cloutier (too many to name). It was a pleasure getting to know all of you. I have learned a lot from you and gained knowledge by working side by side and participating in group meetings. All of you contributed to my development as a chemist.

My family has always offered support to all my decisions, and as such, deserve thanks as well. I thank my mother for never allowing me to quit anything I started and for her motivational speeches and encouragements. I give thanks also to my sister for supporting me and the reminders "always stay positive."

Finally, and most importantly, I would like to thank God to whom all of this would not be possible without Him. "If I have the gift of prophecy, and know all mysteries and all knowledge; and if I have all faith, so as to remove mountains, but do not have love, I am nothing." 1 Cor 13:2

"The more you study, the more you find out you don't know, but the more you study, the closer you come." By Cozy Cole

CHAPTER 1: INTRODUCTION

Organ and tissue perfusion strongly depends on adequate blood flow. Subtle disturbances can lead to clinical disorders. The hyper viscosity syndrome (*i.e.*, high blood viscosity) is a condition associated with hyper red blood cell (RBC) aggregation, which can slow down the blood flow or even stop it. This form of disorder can cause ischemia and thrombosis. Moreover, increased RBC aggregation has been observed and is implicated in the pathophysiology of numerous diseases with circulatory disorders, such as cardiovascular diseases, chronic and acute inflammatory diseases, diabetes, cancers, sickle cell disease, thalassemia and trauma.[1,2,3] In fact, several studies have pointed to RBC aggregability as being a strong cardiovascular risk factor.[4,5] **Appendix 1** describes the relation between RBC aggregation and some of these pathologies.

Blood viscosity can be reduced or increased when macromolecules are added to the suspending medium. This can cause either inhibition or promotion of RBC aggregation. Non-ionic macromolecules with small hydrodynamic radius, R_h (< 4 nm) and low molar mass (< 20 kDa) are known to reduce blood viscosity when added to RBC suspension in plasma in vitro.[6] Linear Poly(ethylene glycol) (PEG) has shown to be beneficial in reducing RBC aggregation and blood viscosity.[7] Also, an amphiphilic block copolymer of PEG composed of a central hydrophobic moiety core of poly(propylethylene glycol) (PPG) to form the compound with the general formula PEG-PPG-PEG has been used successfully to reduce red blood cell aggregation and blood viscosity.[8] Though it has shown promising results for the treatment of several hyper blood viscosity disorders (sickle cell disease and myocardial infarction), severe allergic reactions occurred in 30% of patients receiving intravenous infusion of Pluronics.[9-11] This allergic reaction is thought to come from the PPG.

Similar inhibition of red blood cell aggregation and reduction of blood viscosity may be achieved in an amphiphilic star-shaped PEG. The star conformation provides an even smaller hydrodynamic radius and lower viscosity when compared to linear PEGs which should make it even more efficient in reducing RBC aggregation. Indeed, as it will

be discussed later, a more compacted structure of polymer (smaller hydrodynamic radius) tends to inhibit RBC aggregation. The high density along with the dense core of PEG stars prevent non-specific interactions with biological systems which could lead to immune responses.[12] Also, cholic acid, a natural occurring compound produced in the human liver, has surfactant properties. The cholic acid may be used as an initiating core to polymerize star shaped PEG and to confer more biocompatibility to the polymer. Preparation of such amphiphilic star-shaped PEG polymers has the potential to be used as an intravenous injection for the treatment of hyper RBC aggregation. Thus, before we describe the rational behind this work, a general background on blood, RBC aggregation, and bile acids will be provided.

1.1 Blood Components

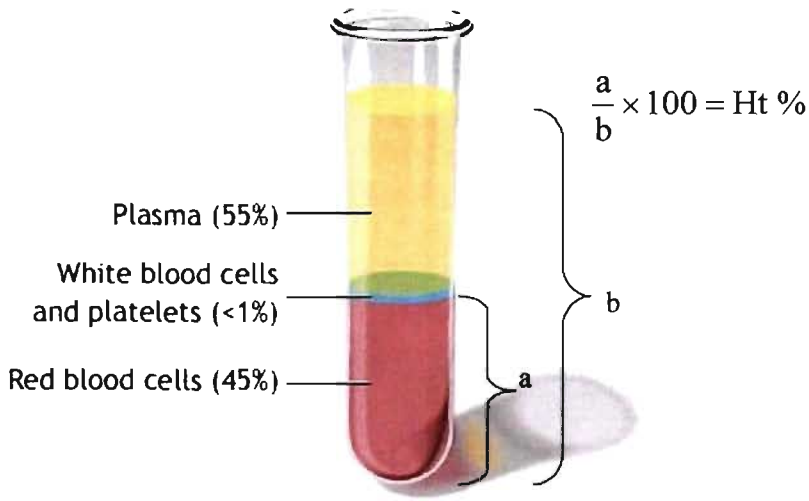

Figure 1.1. Span hematocrit tube and components of blood. The RBC volume measured as the percentage of the total blood which is referred to as the hematocrit (Ht) and is normally around 45%.[13] (Adapted from ref. [14])

Blood is a complex heterogeneous system composed of different types of cells and molecules that appears as a homogenous fluid. When blood is centrifuged and left standing in an anticoagulant tube there are three major parts that can be observed (**Figure 1.1**). The upper layer is filled with a clear liquid that is called plasma. This fluid part of blood contains no cells but does contain many proteins including fibrinogen, a key protein involved in the clotting process and various substances (ions, sugars, lipids, hormones, vitamins, and dissolved gases). Below the plasma lays the buffy coat, which contains leukocytes (white blood cells), and platelets, a subcellular protein that participates in clotting. At the bottom of the tube are the red blood cells (RBCs) or erythrocytes. RBCs are responsible of the transportation of oxygen and carbon dioxide between the lungs and other tissues. The RBC volume measured as a percentage of the total blood volume is called the blood hematocrit (Ht). Normally it is around 45%. [13]

The RBC is a highly specialized cell whose principal role is to transport oxygen from the lungs to the tissues and also carbon dioxide (CO_2) back to the lungs. This function is facilitated by its biconcave shape with a typical diameter of 7-8 μm, a thickness of 2 μm in periphery that is less than 1 μm in the center.[4] This disk shape optimizes the oxygen exchange surface with the surrounding cells. Its membrane and cytoskeleton are able to undergo marked deformation to pass through the capillaries that have 2-3 μm diameters. This deformation is mainly possible due to the membrane protein (band 3 and glycophorin) and proteins in the cytoplasma.[15] The mature human RBC looses its nucleus during the marturation process to provide more space for the transportation of hemoglobin and to facilitate the surface gas exchange. Hemoglobin (Hb) is an important constituent in RBC and is the molecule that complexes and transports oxygen in the human body. Hb is a heterodimeric tetramer composed of two α-like-globin chains and two non-α-globin chains (β, γ, or δ), conjugated to four heme groups (**Figure 1.2**). A typical erythrocyte can carry 270 millions hemoglobin molecules with each carrying four heme groups whose iron atoms temporary link to oxygen atoms.[16]

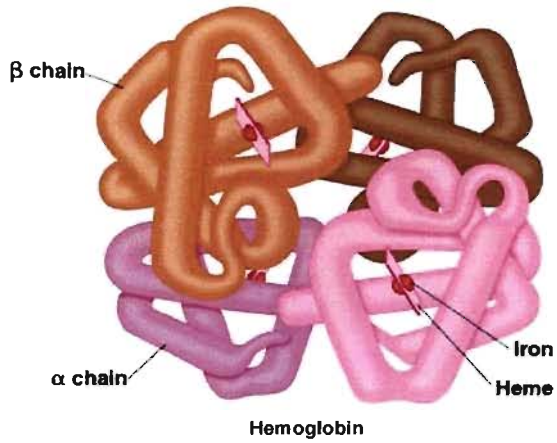

Figure 1.2. Tertiary structure of hemoglobin with the two β and α globin chains bound to four heme moieties. Reproduced from ref. [17].

1.2 Hemorheology

The terms blood rheology and hemorheology can be used interchangeably and they are concerned with the study of flow and deformation behaviour of blood and its constituents *(i.e.*, RBCs, white blood cells, platelets).[15] Henceforth, crucial for the understanding of the rheology of blood is a basic understanding of some general principles of rheology.

1.2.1 General principles of rheology

Rheology is defined as the study of flow and deformation of a material normally exerted by an external force.[18] Solids deformed when a force is applied. If the deformation is proportional to the applied force and not too large, and if the original shape is returned; the solid is said to be elastic. On the other hand, if the deformation remains permanent after the force is removed, the solid is said to be plastic. Fluids continuously deform or flow because of the applied forces. Most materials, including blood, exhibit the combined behaviour of both liquid and elasticity of a solid, also known as viscoelasticity.[18]

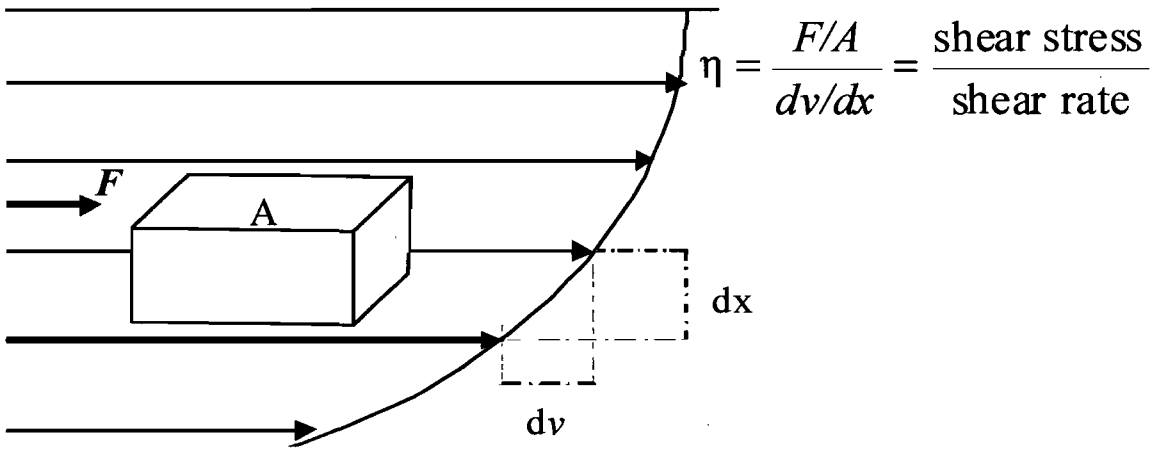

Figure 1.3. Parabolic velocity profile in laminar flow. The shear rate (*dv/dx*) is the ratio of the velocity difference (*dv*) of adjacent fluid lamina to the distance between the fluid lamina *(dx)*. The shear stress (*F/A*) is the force (*F*) applied per unit area (*A).* The viscosity (η) is the shear stress divided by the shear rate.

The degree of deformation (or flow) of a material is related to the force applied per unit area. This deforming force is termed stress and comprises two main components: (1) normal stress, the force per unit area acting perpendicular to the surface, and (2) shear stress, the force per unit area acting parallel to the surface.[18] **Figure 1.3** shows the visualization of the shear stress as the movement of hypothetical layers sliding over each other. The gradient of the velocity in the direction at right angles to the flow is called the shear rate (also called the velocity gradient or strain rate).

Under laminar flow conditions, (**see Appendix 1**), the shear rate-shear stress relationship is used to describe the internal resistance between laminas or fluid layers which is termed, the viscosity.[18] The viscosity can thus be obtained by the ratio of the shear stress to the shear rate (**Figure 1.3**). For rheological purposes, fluids can be divided in two main categories: Newtonian fluids and non-Newtonian fluids. In non-Newtonian fluids, the viscosity does not remain constant as a function of the shear rate; therefore, the

term apparent viscosity is preferably *used* to describe the viscosity at given conditions. In **Figure 1.4,** curve **1** illustrates a Newtonian fluid where the viscosity does not changes as a function of the shear rate; curve **2** shows a non-Newtonian fluid with a decrease in viscosity, which is known as shear thinning; and curve **3** shows a non-Newtonian fluid with an increase in viscosity, which is called shear thickening.

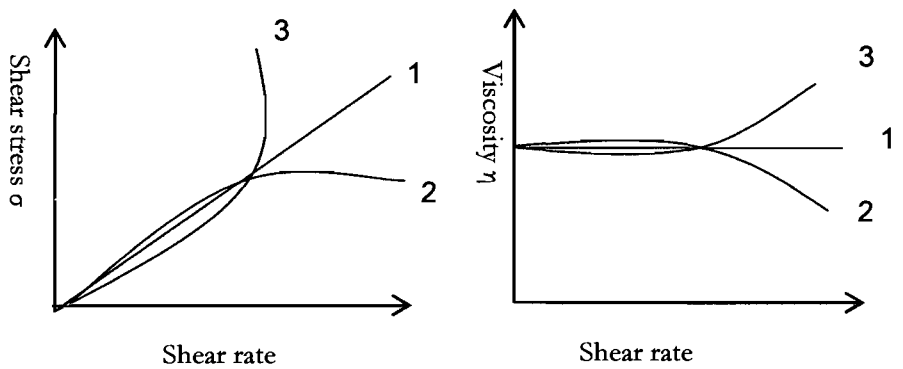

Figure 1.4. *Shear stress-shear rate* and *viscosity-shear rate* relations for **1** Newtonian fluids and non-Newtonian fluids, where 2 represents shear thinning and **3** represents shear thickening rheological behaviours.

The viscosity can be affected by several parameters such as pressure, temperature, time, shear rate, and the molecular nature of the compound.[19] The viscosity normally decreases with increasing temperature. The viscosity of all simple liquids decreases with increase in temperature because of the increasing Brownian motion of their constituent molecules, and generally the higher the viscosity, the greater is the rate of decrease.[18] The measured viscosity can either increase or decrease with time elapsed. A gradual decrease of the viscosity while subjected to constant shearing followed by gradual recovery of the structure when the stress is removed is termed *thixotropy*. The opposite type of behaviour, gradual increase in viscosity while subjected to constant shearing, without recovery of the structure is called *rheopexy*.

The rheological properties of dilute polymer solutions are mainly a function of the concentration, temperature, molar mass, and structure of the long chain molecule.[18]

Generally, for dilute polymer solutions its viscosity is much higher than that of the pure solvent. This arises because of the large differences in the size between the polymer and solvent molecules, and the magnitude of the viscosity increase is related to the dimension of the polymer molecules in solution. Therefore, viscosity measurements of dilute polymer solutions can be used to provide information concerning the effects upon chain dimensions of polymer structure, molecular shape, molar mass, and polymer-solvent interactions .[19]

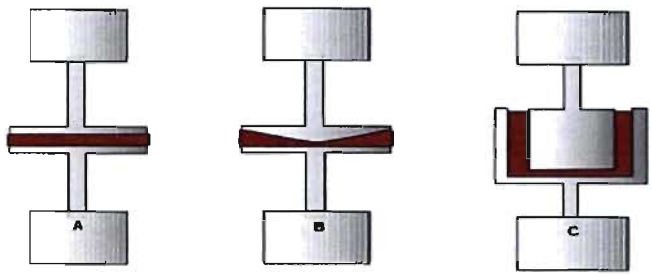

Figure 1.5. Different geometric designs that a rotational rheometer can possess: **A)** parallel plates, **B)** cone and plate, and **C)** concentric cylinders (couette).

Several methods exist to characterize the viscosity of a solution. It can be measured by a viscometer, which studies the stress-strain relations. Capillary viscometers are mostly used to study Newtonian fluids whereas viscometers and rheometers are used for non-Newtonian fluids. While viscometers are limited to the measurements of viscous flow, rheometers are concerned with the viscoelasticity properties of semi-solids. Additionally, rheometers are instruments that produce deformation under controlled conditions representative of those found in real conditions (temperature and deformation rate) and measure the consequences. The consequences are usually conveyed in terms of stress and viscosity from which a host of rheological parameters can be further computed. Rotational rheometers utilized different geometric design to produce a simple continuous shearing motion between two surfaces, one or both of which are rotating while measuring the properties of fluids (**Figure 1.5**).

1.2.2 Blood viscosity

Whole blood viscosity (RBCs, plasma, white cells, and platelets) is considered as a non-Newtonian suspension since its viscosity varies with the shear rate.[15] Blood can be viewed as a two-phase liquid, or it can also be considered as a solid-liquid suspension with the cellular components being the solid part. However, under shear, RBCs behave liquid-like and blood is considered as a liquid-liquid emulsion.[15] The amount of platelets and white cells is so small compared to red cells that they play a minor role in the whole blood viscosity. However, white cells may sometimes have some influence as they specifically adhere to the vascular endothelium in certain inflammatory diseases such as hyperleukocytic leukaemias.[20] The viscosity of blood depends on plasma viscosity, hematocrit value, and RBC rheological properties (deformability and aggregation). These parameters vary considerably in several human pathological disorders. Altered blood rheology may have severe clinical consequences.[4]

Plasma viscosity

Since plasma is the suspending medium of the cellular constituents of blood, any change of its viscosity directly affects the whole blood viscosity regardless of the hematocrit or cellular concentration.[15] The presence of protein fractions, notably fibrinogen, is the major cause of blood viscosity increase, which happens in disease states or after tissue injury. Plasma is considered to exibit Newtonian behaviour and its viscosity (1.10-1.35 cP) is constant at the body temperature. However, some have reported non-Newtonian behavior especially in diseased states.[21]

Hematocrit value

Under laminar flow, the presence of cellular constituents disturbing the flow streamlines is the main reason why whole blood viscosity (RBCs, plasma, white cells, and platelets) is higher than plasma viscosity alone. The degree of disturbance of flow streamlines, and consequently the viscosity of blood, strongly depends on the concentration of the cellular constituents or the hematocrit.[15] In general, blood viscosity

increase as the hematocrit increases and usually follows an exponential relationship, where at higher values of hematocrit; blood viscosity becomes extremely sensitive to hematocrit variations.[22]

Red blood cell deformability and aggregation

In addition to the concentration of the cellular constituents which disturbs the flow streamlines, the deformability of the RBCs under shear force is an important factor to consider. Normal RBCs are deformable bodies which align themselves in the direction of the flow. RBCs deformability and their orientation with respect to the flow streamlines are primary cellular factors affecting blood viscosity at high shear rates.[15] RBC deformability depends on the membrane and its underlying cytoskeleton: (1) the biconcave discoid shape, and (2) the hemoglobin concentration, both which determine its cytoplasmic viscosity.[23] The RBC deformability affects the entrance of blood cells into the capillaries. This is especially a concern for RBCs with reduced deformability in pathological disorders such as sickle cell disease, which may sequester the capillary entrance. The stiffening of the cell membrane or the high concentration of Hb, which increases the blood viscosity may impede RBC passage through the capillaries .[24]

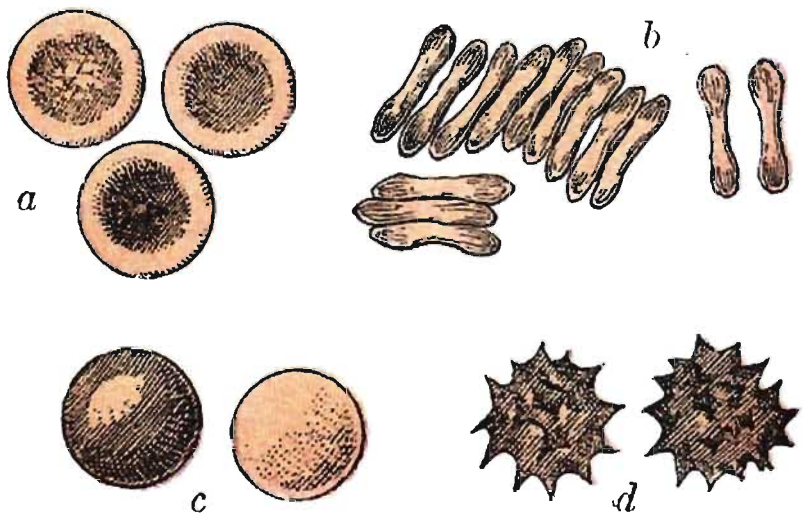

Figure 1.6. Illustration of the deformation and aggregation of human red blood cells. **a**. observed from the surface. **b**. observed in profile and forming *rouleaux*. **c** Rendered spherical by water. **d**. Rendered crenate by salt solution. Taken from ref. [25].

Another important rheological properties of RBCs is their ability to aggregate themselves in stacks and form a reversible mass known as *rouleaux,* which is a primary factor affecting blood viscosity at low shear rates. (**Figure 1.6b**).[21,26]

Typically, arteries and capillaries have high shear rate conditions, whereas blood in venules is subjected to lower shear rates. RBCs tend to aggregate and form *rouleaux* in environments of low shear rate < 10 s^{-1} (*i.e.* venules), which increase blood viscosity.[6] The decrease in shear rate causes the shear stress to increase. Thus a higher pressure gradient is required to move the blood at low flow rates. It is worthwhile to know that a certain yield stress is necessary to get the RBCs to re-flow or dissagregate.[27] The shear stress required to separate two cells in this orientation for a saline suspension of RBCs in 4% dextran was determined by Chien and coworkers to be less than 1 dyn/cm^2. [28] Upon flow rate increase, the shear force becomes strong enough to disrupt *rouleaux*. High shear rates above 100 s^{-1} typically cause disaggregation of *rouleaux* and cell deformation, which in turns improve blood flow.[29] At high shear rates, the viscosity of blood is constant (4-5 cP) and behaves like a Newtonian fluid because the level of aggregation is reduced or inexistent.[15] In clinical settings, RBC aggregation is mainly due to the increased concentration of high molecular weight plasma proteins as fibrinogen and immunoglobulins G and M (IgG and IgM).[6,30] Other plasma proteins such as haptoglobin, ceruloplasmin and C reactive protein were shown to also promote aggregation.[31]

1.2.3 Blood viscosity in rotational viscometers

Blood viscosity is usually measured in a rotational viscometer, which allows the measurement of blood viscosity over a wide range of shear rates. Rheology measurements are important in hemorheology since it predicts the behavior of blood flow in the vessels. In a static system at constant temperature, the apparent blood viscosity (η_a) is a function of the hematocrit (Ht) and applied shear rate (γ).

$$\eta_a = f(\mathrm{Ht}, \gamma) \tag{1.1}$$

Experimental apparatus have been designed to study the rheology of RBCs. They usually require blood to be sheared between two concentric cylinders (also known as Couette flow) or between a cone and plate, to create a constant shear across the blood layer (**Figure 1.5**). It is assumed that the RBCs or aggregates are uniformly distributed within the fluid layers when the viscosity measurements are obtained.

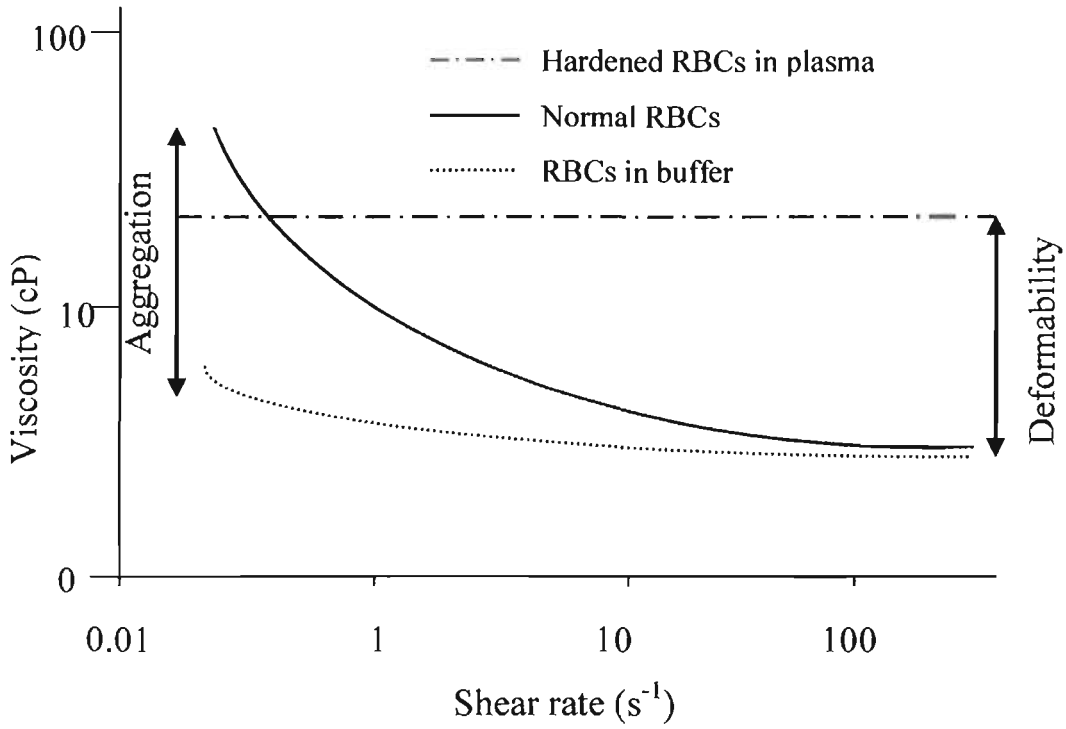

Figure 1.7. Illustration of the effect of the shear rate on the apparent viscosity of normal red blood cells (RBCs) suspended in plasma, in albumin, and in glutaraldehyde (to produce hardened cells). The increased in viscosity of RBCs at low shear rates is due mainly to RBC aggregation and the drop in viscosity at low shear rates is due mainly to RBC deformability. Adapted from ref. [32].

Chien studied the behaviour of RBCs in rotational viscometers and showed that the increase of viscosity at low shear rate was primarily due to RBC aggregation.[33] **Figure 1.7** is illustrative of that experiment. Chien incubated the RBCs in three media: saline buffer (non-aggregating medium), plasma (aggregating medium), and

glutaraldehyde (cell hardening medium). In glutaraldehyde, the RBCs hardened and the viscosity was high and constant and remained independent of the shear rate. In saline buffer, the viscosity of the RBCs remained almost independent of the shear rate and was lower than the viscosity of RBCs incubated in glutraldehyde and plasma. This showed that the drop of viscosity at high shear rates was due to the deformability of RBCs. However, at low shear rate, the viscosity of the RBCs incubated in plasma increased exponentially due to the aggregation of RBCs. The increase in the apparent viscosity of RBCs suspended in plasma was due in part to the increase in the effective particle size and greater trapping of plasma. As the shear rate decreased, the lower shear force acting on RBCs allowed the formation of aggregates, which increased the effective viscosity. At very low shear rates, the orientation of the cells relative to the flow was random but as the shear rate increased, the deformability or flexibility of red cells allowed them to orient themselves in a manner that presented minimal cross-section to the flow streamlines, and effectively reducing the apparent particle size.

1.2.4 Mechanism of red blood cell aggregation

There are two co-existing theoretical models to explain the process of RBC aggregation: bridging and depletion (**Figure 1.8**). Merrill et al. originally proposed the "Bridging Model" over thirty years ago for the plasma proteins (e.g., fibrinogen) inducing RBC aggregation.[34] Later Chien and Jan, and Brooks[27,35,36] reported that, dextran adsorption within neighboring RBCs also induces aggregation.

In the bridging model, RBC aggregation is considered as a reversible process, which depends on the equilibrium process between several parameters: the macromolecular bridging force due the adsorption of macromolecules onto the adjacent cell surfaces (F_b) and the disaggregating forces due to electrostatic repulsion (F_e), mechanical shearing (F_s) and membrane strain (F_m). The net aggregating force (F_a) can be expressed as:[34]

$$F_a = F_b - F_e - F_s - F_m \tag{1.2}$$

The bridging model postulates that RBC aggregation occurs when the bridging forces (F_b) exceeds the disaggregating forces (F_e, F_m, and F_s.). For instance, when RBCs come into close proximity, aggregates may form due to the absorption of long chains of macromolecules such as fibrinogen or dextran (a neutral polymer) with high molar mass leading to a bridging effect between cells being greater than the disaggregation forces (**Figure 1.8**). [37,38]

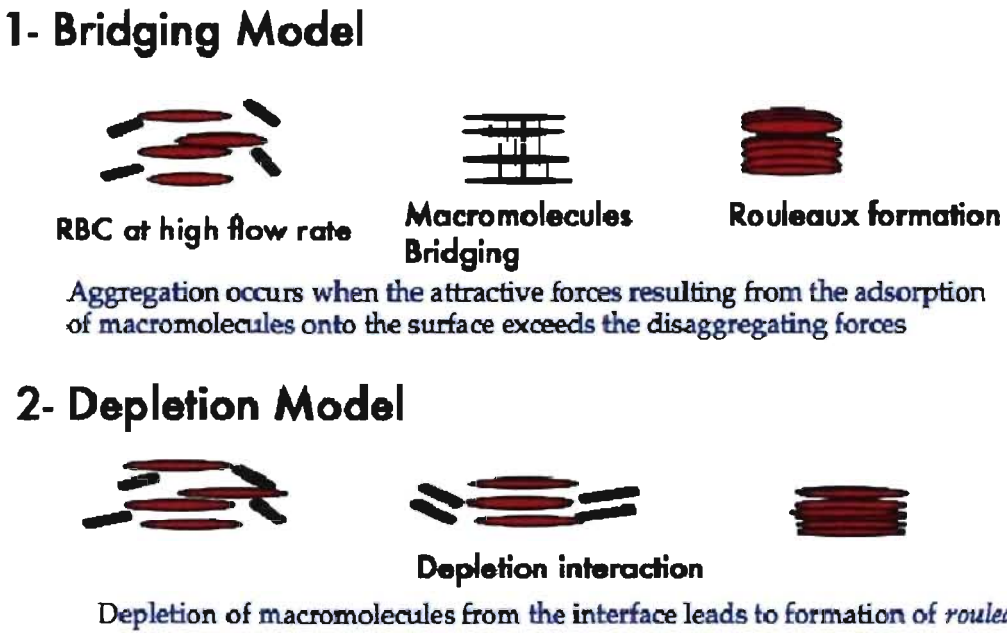

Figure 1.8. Schematic drawing of the bridging model in **1** and the depletion model in **2.** Black cylinders correspond to plasma macromolecules whereas red disks are red blood cells. Adapted from ref [39].

The "depletion model" originated from Asakura and Oosawa and was applied later to RBC aggregation.[40] This model hypothesizes that the reduced concentration or the exclusion of proteins or macromolecules (e.g. dextran > 40 kDa) is near the cell surface of RBCs compared to suspending medium or bulk solution. This exclusion of macromolecules near the cell surface leads to osmotic gradient and thus depletion layer interaction and the tendency for adjacent red blood cells to come together (**Figure 1.8**).[32,41] According to this model, RBC aggregation is induced without surface adsorption

of macromolecules but rather results from an overlap of the depletion zones, which in turn causes attraction of the cells due to the osmotic pressure.

The attraction force between the cells relies on the polymer concentration between the depletion area and the bulk solution, the thickness and density of the layer, the separation distance between RBCs, and the spatial properties of the macromolecules. For instance, when the separation distance x is much greater than the thickness of the depletion layer ξ, the force of attraction between two cells is considered negligible. The depletion layer ξ depends on the macromolecule concentration in the bulk solution and its molar mass. If the separation distance x is much more smaller than ξ, the force f of attraction between two cells can be described by:[34]

$$f \propto (R/kT\xi^3) \cdot (\pi\xi - x) \tag{1.3}$$

where R is the radius of the red cell, k is the Boltzman's constant, and T the temperature gradient.

The role of macromolecules in blood is not a factor only affecting blood viscosity but in addition they regulate many cell interactions in normal and pathological conditions. For instance, in thrombosis formation, plasma proteins participate in platelet aggregation. However, in RBC aggregation, the presence of large macromolecules or plasma proteins is necessary for RBC aggregation because RBCs suspended in saline solution alone do not aggregate (**see Figure 1.7**)

Both the bridging and the depletion models can explain RBC aggregation in their own rights and one is not necessarily better than the other. However, there is an obvious contradiction between both mechanisms. The bridging model predicts an increase in aggregation due to the increase in concentration of the macromolecules near the RBC surface, whereas the depletion model predicts the opposite.[41] Both models suggest that the total adherent force between two cells is maximal when the cells are arranged "en face" or in *rouleaux*. The mechanism of RBC aggregation and disaggregation and thus the role of macromolecules in RBC-RBC interaction are far from being understood, especially in human disease states.

1.3 Disorders Related to Abnormal RBC Aggregation

Microcirculatory disorders contribute a large fraction to the morbidity and mortality of patients and constitute a major health cost to society.[42]. The microcirculation represents the smallest vessels in the circulatory system and encompasses the capillary network with the smallest inner diameters of 4-8 μm, the arterioles with diameters up to 100 μm, and the venules somewhat larger.[42] Typically, the arterioles have a magnitude of ten times the shear rate of capillaries and venules have the lowest shear rate.[42] The blood flow in the microcirculation aims to maintain vital functions such as gas and metabolite exchanges between capillary vessels and perfused tissues. Impaired microcirculation arises as a result of diseases affecting the vascular system by inflammation, which promotes not only leukocyte adhesions but RBC hyper-aggregation degeneration.[42] Elevated RBC aggregation is observed when high protein fractions (*e.g.*, fibrinogen) are produced as a result of chronic infections, tissue damage, degenerative diseases, and cancers to name a few examples. Impaired microcirculation may have functional and structural impacts on the corresponding tissues or organs and these adverse effects may create acute and chronic symptoms such as such as ischemia and tissue infarction.[42] In addition, the migration of RBC aggregates to the center of blood vessels where the shear rate is minimum might attenuate oxygen diffusion through the cell-free layer that is observed close to the vessel wall.[32] A systematic consequence of RBC hyper-aggregation that may be observed in conditions such as hypertension is the decrease of the blood flow and reduction of the cardiac output (the amount of blood being pumped out by the heart over a particular period of time) in severe cases.

1.4 Blood Rheology Modifiers: Macromolecules

As mentioned earlier, red blood cells in the presence of high molar mass macromolecules such as plasma proteins or polymers tend to aggregate and form *rouleaux*. The rheological effect of macromolecules on blood rheology have been extensively studied and reviewed. It is general knowledge that macromolecules modify the plasma viscosity as well as the red blood cell aggregation.[6,36] Non-ionic

macromolecules with small radii or molar masses are known to reduce the in vitro blood viscosity when added to RBCs suspended in plasma.[6] Non-ionic macromolecules known to promote RBC aggregation in vivo or in vitro include dextrans with molar masses ≥ 70 kDa, poly(ethylene glycol) (PEG), and polyvinylpyrrolidone (PVP).

The effect of the hydrodynamic radius of macromolecules on RBC aggregation was investigated by Armstrong et al[6]. The three non-ionic polymers that were studied were dextran, PEG, and PVP ranging from a molar mass of 1.5 kDa to 200 kDa. The hydrodynamic radius for each polymer was calculated from their intrinsic viscosities. The study showed that the different polymers demonstrated similar effects on RBC aggregation when compared on the basis of their hydrodynamic radius. Notably, all three polymers with hydrodynamic radius < 4 nm inhibited RBC aggregation whereas those with a hydrodynamic radius > 4 nm promoted RBC aggregation. Also, the maximum optimal inhibitory effect was observed for polymers with hydrodynamic radius between 2 and 3 nm. The study also showed that this trend could be applied to common plasma proteins such as fibrinogen and albumin.

1.4.1 Dextran

Dextran has been widely used for the induction of RBC aggregation and in the study of RBC aggregation mechanism. Dextran was one of the first and principal plasma substitutes.[35,43] Dextran of MW 70 kDa with gelatin or PVP, increases the apparent blood viscosity with the exception of Dextran of MW 40 kDa which decreases blood viscosity.[44] Dextrans have been shown to absorb on the membrane surface of RBCs using several techniques such as radioactive labels.[28,35] It has also been used to support the "Bridging Model" based on the molecular weight threshold and the rate of the absorption isotherms.[39,45] Low molecular weight dextran is utilized in clinical practice to reduce the hematocrit level by hemodilution to enhance tissue perfusion and oxygenation.[46] In 1963, low molecular weight dextran was found to prevent thrombosis (clotting of the blood).[43] However, the danger of dextran has been raised concerning renal failure and the increased plasma viscosity.[47]

1.4.2 Poly(ethylene glycol) (PEG) and Pluronics

Because of their advantageous properties, PEGs have been used in a wide range of biomedical applications.[48-50] PEG is a water-soluble polymer that is non-toxic, has a good clearance from the body, and is able to escape the immune system recognition.[51] PEG may also transfer its immune properties when it is attached to another molecule.[48] Thus, a toxic molecule can become non-toxic when combined with PEG. Also, an hydrophobic moiety of a molecule can become water-soluble when coupled to PEG without loosing the biological properties of the drug.[52] PEGs bound to lymphocyte T cells (cell-cell interaction molecules) was found to reduce antigenic recognition by preventing the adhesion of molecules that are involved in immune recognition and response system.[53] In whole blood, linear PEGs with low molar mass (< 20 kDa) have shown to reduce RBC aggregation.[6] Enhance inhibiting of RBC aggregation has been reported when the terminal hydroxyl group of PEGs is modified to achieve covalent attachment with the RBC's membrane. [39,54]

Another class of polymers showing reduction of RBC aggregation is a copolymer of PEGs also known as Poloxamers or Pluronics (trademark names). Pluronics have two hydrophilic chains of PEG linked by a hydrophobic block poly(propylene glycol) (PPG) to form a PEG-PPG-PEG structure (**Figure 1.9**). In 1966, the use of the surfactant Poloxamer 188 (Pluronic F-68) of a molar mass of 8.4 kDa was originally suggested by Miyauchi et al. as a blood rheology modifier and was later found to reduce blood viscosity.[55,56] The infusion of Pluronics F-68 (80% PEG) trademarked as RheothRx® intravenously was shown to reduce blood viscosity, which in turn improved blood flow to ischemic tissues, reduced thrombosis, and hence provided a potential treatment for inherited blood diseases (e.g. ischemic vascular disease and vasoocclusive crisis in sickle cell disease).[57,58]Alernatively, Pluronics F-98 with a high molar mass of 13 kDa induces aggregation (**Figure 1.10**).[59]

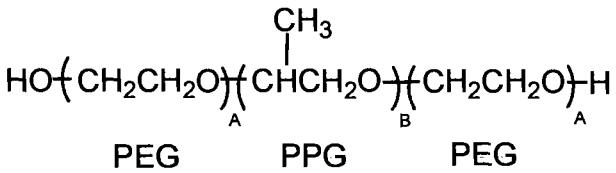

Figure 1.9. Chemical structure of Pluronics, and ABA block copolymer consisting of poly(ethylene glycol) (PEG) and poly(propylene glycol) (PPG) .

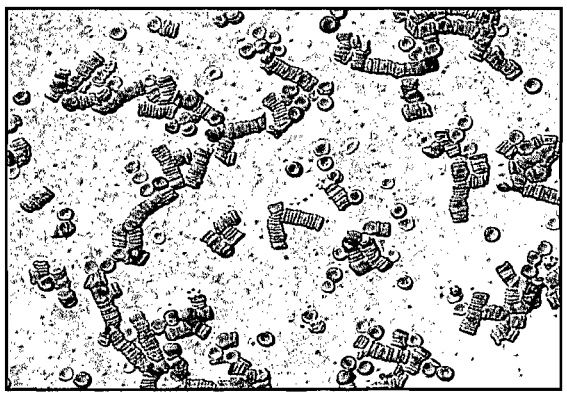

(a)

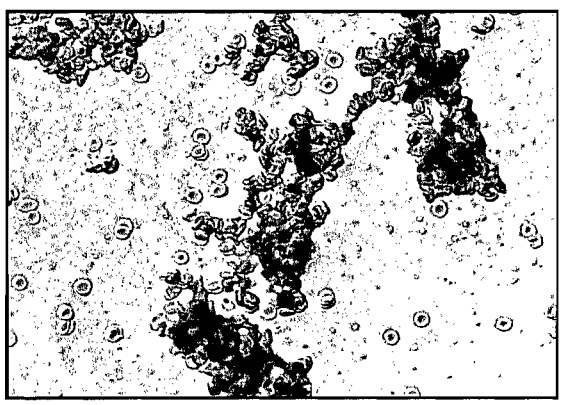

(b)

Figure 1.10. Photos by light microscopy at a magnification of 400 of **(a)** normal RBCs in plasma and **(b)** RBCs coated with Pluronics F98 (13 kDa). Acquired at the Division of Hematology and Oncology, Department of Internal Medicine of the University of Southern California.

The covalent attachment of an appropriate Pluronics to RBC surface has shown to be able to predict and control RBC aggregation due to the critical micellization temperature (CMT).[59,60] Pluronics have been widely tested in several clinical researches and have shown great benefits in intravenous infusion. The polymer has shown to be beneficial in the treatment of sickle cell disease and myocardial infarction where it accelerates thrombolysis formation, thus reducing re-occlusion and ameliorating re-perfusion injury.[61,62] It can also reduce RBC aggregation in blood and decrease whole blood viscosity in human.[63]

Adverse non-immunoglobulin E (IgE) (class of antibodies that participates in allergic response) mediated hypersensitivity reactions occurred is some individuals following intravenous injection of Pluronics F-68-based pharmaceutical, most likely by complement activation.[64] In a clinical study, Pluronic F-68 was combined with a perflurochemical (Fluosol-DA) for radiation treatment of tumors. Up to 30% of patients receiving Fluosol-DA developed hypotension and/or acute respiratory distress.[9] These events were thought to be secondary complement activation by Poloxamer micelles. Recently, these adverse reactions have been classified as "complement activation-related pseudoallergy" and occurred after the infusion of contrast media, various drug stabilizers, and drug carriers, and presumably is a reflection of an individual's immune cell sensitivity to complement derived mediators.[9,11] More recent studies by Moghimi et al provided evidence that Pluronic F-68 complement activation is an intrinsic property of the polymer and that it is independent of the polydispersity of the polymer or amount of contaminants, such as organic solvents (acetaldehyde and propionaldehyde) left during the preparations.[11] The complement activation was triggered at submicellar concentrations of the polymer and was partially due to the presence of allylic double bonds therein.

According to this review, the development of novel approaches to prevent Pluronic-mediated complement activation is obviously a necessity. New strategies may involve either biochemical modifications such as attaching an anti-body or the design of new therapeutic PEG-based polymer. Since biochemical modifications involves a thorough understanding of the specific antigen involved in Pluronic complement

activation which is not fully understood yet, we chose to explore the design of a novel PEG-based polymer. The design of the novel PEG polymer should have similar surfactant properties as Pluronic and should confer more biocompatibility or be less prone to allergenic reactions than Pluronic by being naturally derived. Also, since the size of the polymer affects the RBC aggregation, a more compact structure should be better in inhibiting RBC aggregation.[6] We chose the design of a novel amphiphilic star-shaped PEG polymer based on cholic acid, which is a natural occurring bile acid produced in the human liver.

1.5 Bile Acids and their Derivatives

Bile acids and their derivatives are currently used for biomedical and supramolecular applications.[65-67] A series of these polymers have been prepared for drug delivery systems,[68] molecular recognition,[69] dental fillings, and bone repairing materials.[70] In particular, polymeric biomaterials with the design of an amphiphilic polymers with bile acid groups in the main chain or side chain, or as pendant groups or end groups [71-73] , have attracted significant interest because of their biodegradation expected to lead to the release of endogenous compounds. In fact, the *in vitro* exposure of 3T3 fibroblasts, a cell line used to study the cytotoxicity of dental monomers to methacrylic derivatives of bile acids used as monomers in dental composites, have shown to be less cytotoxic than the commercial dentals.[74] Such results have incited efforts to improve the physical and toxicological properties of polymeric biomaterials by incorporation of bile acids into the structure of these materials.[75] The beneficial results of bile acids originate from its chemical nature, which is described in the next section.

1.5.1 Nature of bile acids

Bile acids are amphiphilic molecules existing in the bile of most living beings. They are synthesized from the oxidation of cholesterol in the liver via many enzymatic steps. About half of the cholesterol produced in the body is used to synthesize bile acids. The bile acids from humans and higher vertebrae are usually conjugated with glycine

(H_2N-CH_2-COOH) or taurine (H_2N-CH_2-CH_2-SO_3H) and are stored in the gallbladder.[76] After a meal, bile acids are released in the salt form to the small intestine to promote the resorption of fats and lipids.[66] In total about 20-30 mg of bile acids are secreted in the small intestine.[77] Then, they are either excreted or reabsorbed through the ileum naphthal in the enterohepatic circulation to be reused again. Their function is vital in the emulsification of fats, and membrane transports of vitamins.

Bile acids made in the liver from cholesterol are referred as "primary bile acids" and those produced by the action of intestinal bacteria during the enterohepatic pathway of bile acids are called "secondary bile acids". Secondary bile acids may be subject to further structural transformation by liver enzymes and thus are referred to as "tertiary bile acids". Cholic acid and chenodeoxycholic acid are primary bile acids; lithocholic acid and ursodeoxycholic acid are secondary and tertiary bile acids, respectively (**Figure 1.11**). The human bile acid pool has about 2.5–5 g of bile acids, compromising mainly ~90% of cholic acid, chenodeoxycholic acid and deoxycholic acid in a ratio of about 2:2:1 and ursodeoxycholic acid and lithocholic acid are found in the remaining 10% of the pool.[68]

Cholic acid (**CA**) is one of the most abundant bile acids in our body and is relatively easy to obtain. It is also considered useful in the synthesis of new prodrugs for liver-specific drug targeting and improved intestinal absorption.[78] The incorporation of a biocompound such as **CA** into polymers may lead to the improvement of the biological compatibility, activity, and safety of the materials in biomedical applications.[79,80]

In contrast to other bile acids, **CA** has four functional groups. The steroid possesses also an asymmetry meaning that no two positions are equivalent. For instance, the C3-OH is equatorial while the others are axial, allowing the former to possess fast chemical reactivity and to be derivatized selectively (**Figure 1.12**).[81]

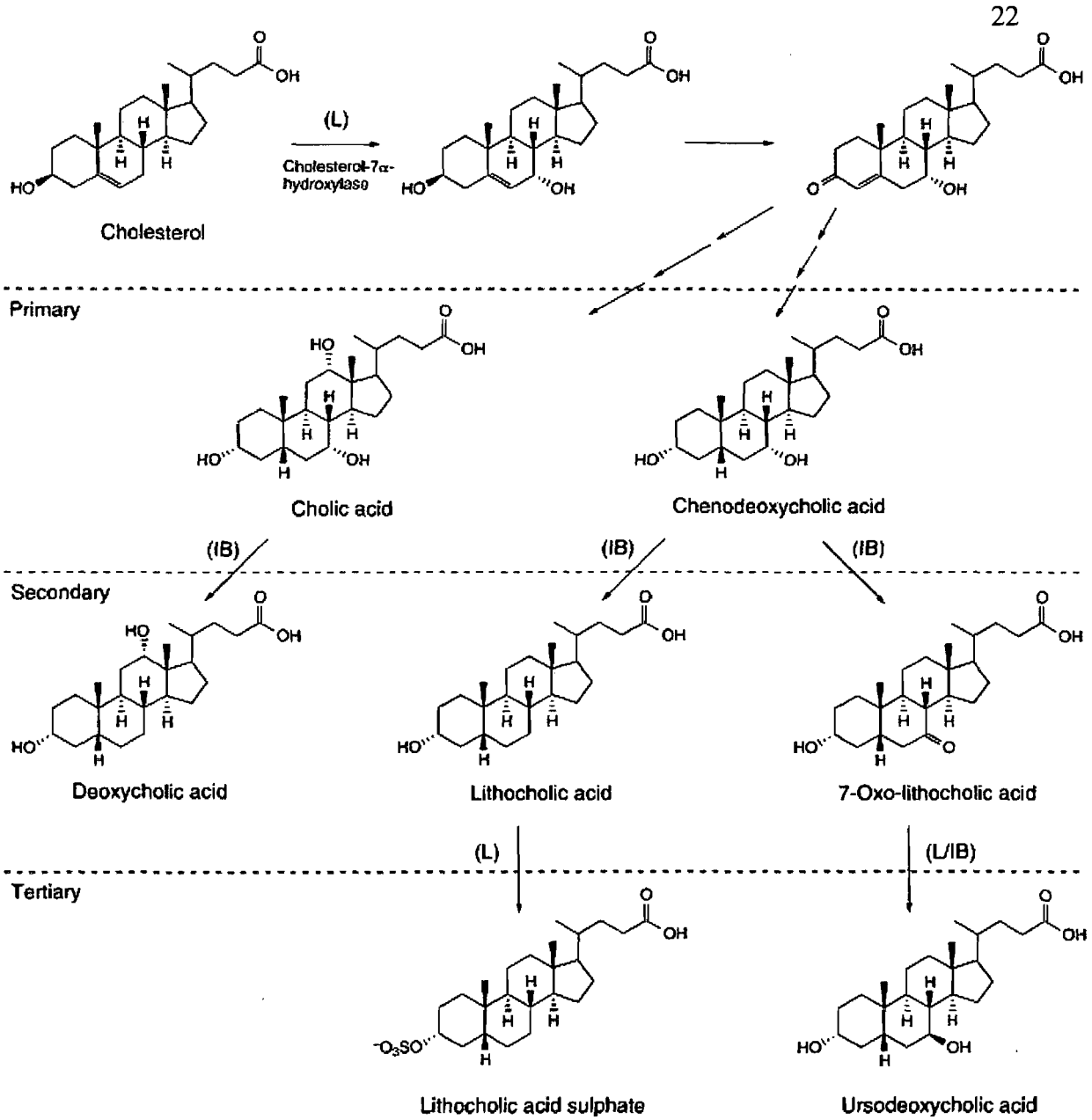

Figure 1.11. Bile acid metabolism: production of primary, secondary and tertiary bile acids occurs in the liver (L) and by intestinal bacteria (IB). Adapted from ref.[68]

1.5.2 Properties of bile acids

The chemistry of bile acids involves the usual reactions for hydroxyl and carboxylic groups. However, the rates at which each hydroxylic group reacts differ from each other and merit further elaboration. The hydroxyl groups may be oxidized or esterified with a variety of reagents. The order by which each hydroxyl group reacts is dependent on its position. The order of reactivity is $C_7 > C_{12} > C_{13}$, and $C_6 > C_3$.[76] The order of ease for acetylation, reduction, and hydrolysis is quite different. The order of reactivity is $C_3 > C_7 > C_{12}$.[76]

The reactions of the terminal carboxyl group are typical of this group and involve the esterification which is a classic reaction to protect against the oxidative and reductive reactions in the preparation of bile acids. Also, esters tend to crystallize more easily than in their natural state.[82] Other reactions with the carboxyl group include the formation of complex compounds with salt and conjugation with amino acids moiety by first coupling the carboxylic acid with azide or mixed anhydride.

Due to their unique structure with a hydrophobic β-side and a hydrophilic α-side, bile acids possess detergent and cleaning properties which differ from typical surfactants, which have a polar head and an alkyl chain. The facial amphiphilicity of the bile acids is provided by their rigid steroid backbone from having all the hydroxyl and the carboxylic groups on one side of the molecule **(Figure 1.12)**.

In a very dilute medium, these amphiphilic molecules are present as monomers and as the concentration increases these molecules form micelles at which the surface tension, electrical conductivity, viscosity, light scattering, and other properties abruptly change. Micelles are aggregates of amphiphilic molecules in water; the aggregation of these molecules is spontaneous above a well defined concentration known as critical micellization concentration (CMC).[83] The micelles are formed by the delicate balance of opposing forceswhich result in aggregates that solubilize fats. Depending on the pH, presence of ions, and temperature, bile acids easily form micelles in water at concentrations of 0.6–10 mM; this is of central importance for their physiological function.[68]

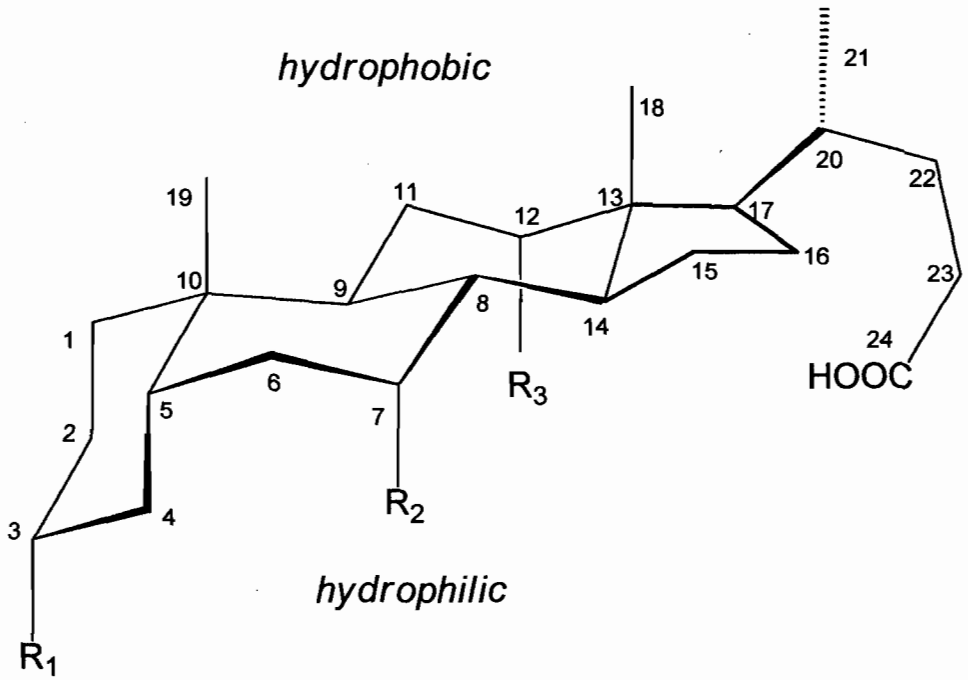

Bile Acids	R_1	R_2	R_3
cholanic acid	H	H	H
cholic acid	OH	OH	OH
chenodeoxycholic	OH	OH	H
deoxycholic	OH	H	OH
lithocholic acid	OH	H	H

Figure 1.12. The chemical structure of bile acids.

In general, micelles may be cylindrical or spherical depending on the configuration of the molecule. For instance, soaps usually adapt a spherical structure whereas bile acid micelles are almost cylindrical or even more complex structures for secondary micelles.[76] During the formation of micelles in an aqueous environment, the center of the spherical or cylindrical structure contains the hydrophobic moiety of the amphiphilic molecule and the outer layer containing the carboxylic and hydroxylic groups forms the hydrophilic moiety, which interacts with the water molecules. If the hydroxylic groups on the micelles are ionized, they attract ions on them, which in turn neutralize the charges on the micelle. In general, the micelles have a net charge and migrate in the direction of the electrostatic field. [77]

Therefore, the hydrophobicity of the cholane core as well as the amphiphilic properties and micelle formation of the bile acids may provide interesting characteristics when combined to PEG.

1.5.3 Polymers based on bile acids

The synthesis of a variety of bile acid derivatives has been described.[67,75,81] Most of the substances were developed in searching novel compounds with pharmaceutical and biomedical applications including their treatment in the bile acid deficiency and liver disease and their dissolution in cholesterol gallstones.

In our group, we have synthesized hydrogel polymers with bile acid derivates to improve their properties. For instance, hydrogel polymers of methacrylate and methacrylamide derivatives of cholic acid were made by radical polymerization of the hydroxyl group on position C3 (**Figure 1.13 a**).[86,87] Depending of the design and intended application, the bond at position C3 was either a β or an α configuration. The introduction of the 3-amino group instead of the 3-hydroxy group was carried out to improve the hydrophilicity of the monomer from ester to amide (**Figure 1.13 b**). However, the hydrophobicity was still predominant in the polymer.[88,89] In effort to improve the hydrophilicity of these methacryloy polymers, a flexible spacer group, ethylene glycol (EG) was introduced, and with variable length of EG or oligomers the water content

increased (**Figure 1.13 c**).[79] The hydrophilicity of these methacrylate esters and methacrylamide of cholic acids can subsequently be increased by copolymerization with even more hydrophilic comonomers such as methacrylic acid (MAA) and hydroxyethyl methacrylate (HEMA).[81] Some of these polymers were modified and their liquid crystal properties where the bile acids represent the mesogenic unit were synthesized.[90]

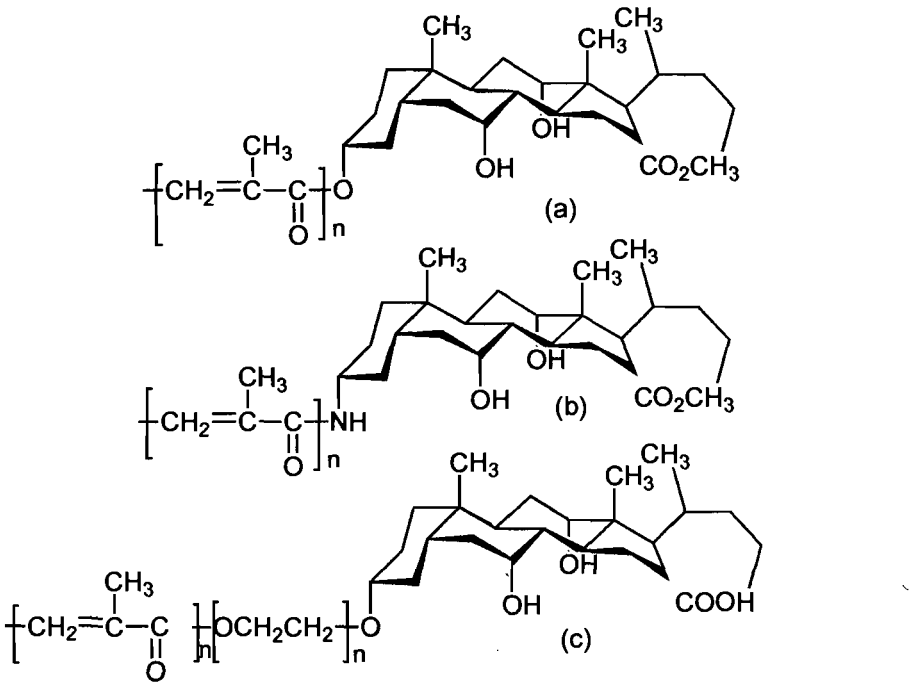

Figure 1.13. Structure of some cholic acid derivatives.

Living polymerization methods such as atom transfer radical polymerization (ATRP) have been used in the preparation of super-branched or combed-shaped polymers containing **CA** and poly(methacryloyl tri(ethylene glycol)) with much better structural control than the conventional radical polymerizations.[78] These combed-shaped polymers have shown to have semicrystalline properties and high glass transition temperature (T_g) caused by the bulky and hydroxy-containing CA residues in high density, factors that tend to raise T_g of polymers.

Star-shaped amphiphilic polymers

The design of amphiphilic star-shaped polymers is of growing interest for biomedical, pharmaceutical and biotechnology applications because these polymers can behave as unimolecular micelles or be designed to exhibit a very low critical aggregation concentration (CAC).[91,92]

Star-shaped polymer exhibit smaller hydrodynamic radius and lower solution viscosities as compared to the linear polymer of same molecular weight.[93] More importantly, star polymers with multiple end groups may confer even more advantages by being functionalized for a variety of applications. These features are very attractive for biomedical applications such as micellar drug delivery and thermoplastic hydrogels.[94,95]

The amphiphilic polymers are generally produced by modifying hydrophilic polymers such as dextran, polysaccharides, chitosan, and heparin by covalently attaching a bile acid through its carboxylic group (at position C24) or its hydroxyl groups (preferably position C3).[96] These water-soluble polymers containing bile acids as pendant groups are able to form micelles in water, which is a desirable property for drug delivery vectors. Micelles as drug delivery vectors are able to provide a set of unbeatable advantages: they can solubilize poorly soluble drugs and thus increase their bioavailability; they can stay in the blood circulation long enough providing gradual accumulation in the required area; their size permits them to accumulate in body regions with leaky vasculature; they can be targeted by attachment of a specific ligand to the outer surface; and they can be prepared in large quantities easily and reproducibly.[97] Being in a micellar form, the drug (poorly soluble drug) is well protected from possible inactivation under the effect of biological systems, it does not provoke undesirable side effects, and its bioavailability is usually increased. When bile acids are part of a water-soluble polymer, the resulting amphiphilic polymer might exhibit a better compatibility with biological systems and interact favorably with proteins, enzymes, or lipids.[98]

These polymers are mainly synthesized by copolymerization of two monomers: one water repellent such as PPG and the other water-soluble such as PEG. The other process usually involves the chemical attachment of an existing hydrophilic polymer

through attachment of hydrophobic moiety. Since bile acids show limited solubility in their acid form in water and exhibit surface-active properties in their sodium salt form, their hydrophibicity makes them attractive compounds for the preparation of amphiphilic polymers in which they are incorporated as the hydrophobic segment.[99]

Star polymers, which a number of linear arms of similar MW emanate from a central core, have drawn recent interest due to their compact structure and their interesting rheological properties.[100] Star-shaped polymers with a cholic acid core have been prepared in our laboratory by ATRP with well controlled molar masses.[101] The modified carboxylic group at position C24 along with the hydroxyl groups on positions C3, C7, and C12 were used to initiate the polymerization of *tert*-butyl acrylate (**Figure 1.14**).

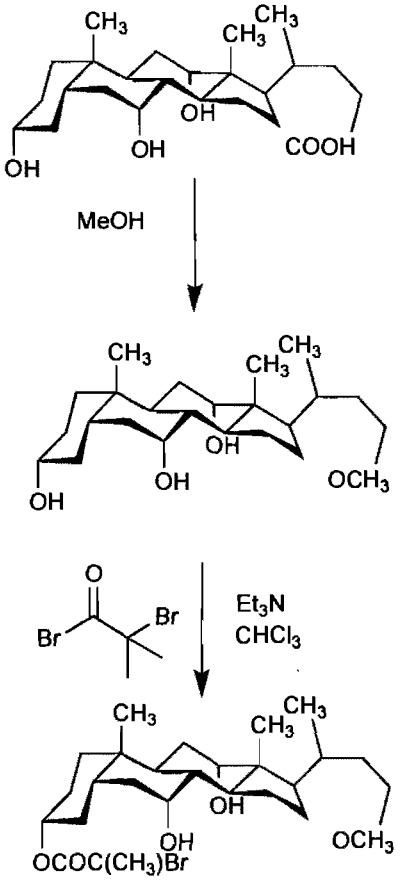

Figure 1.14. Atom transfer radical polymerization initiator from cholic acid. Hydrolysis of the *tert*-butyl groups affords a star-shaped polymer.

1.6 The main objectives

As mentioned in the introduction, elevated RBC aggregation, which increases blood viscosity, is a strong pathophysiological factor affecting many cardiovascular diseases. Block copolymers of PEG, poloxamers or Pluronics, which reduce RBC aggregation, have shown to induce adverse reactions in some patients. Hence, enhancing the biocompatibility by changing its molecular architecture and growing PEG onto a biocompatible core, such as a bile acid that is naturally found in the body, should increase its biocompatibility. When such natural biocompounds are introduced or used in the preparation of the polymer materials, they should be better tolerated biologically because of their amphiphilic properties, which allow the polymer to interact favorably with the biological environment. Even in case of a possible breakdown of the polymers, it is less likely to cause toxic effects; hence allergic reactions should be less of a concern. Also, a star shaped polymer is preferred because a small compact structure should be better at reducing blood viscosity because of its low solution viscosity compared to linear polymers of the same molecular nature. Therefore, we proposed the use of a star-shaped amphiphilic PEG polymer with cholic acid derivative as core, as a therapeutic polymer for inhibiting RBC aggregation.

In order to find an appropriate molar mass of the star-shaped polymer that might be more effective in reducing RBC aggregation and to have controlled chain lengths, several polymers of different molar masses have been prepared via living anionic polymerization. These star-shaped polymers were characterized by nuclear magnetic resonance spectroscopy, size exclusion chromatography, and thermal analysis. Rheological analysis and viscosity measurements were used to evaluate their solution viscosities.

Herein, we wish to assess the effect of the star-shaped PEG with a cholane core on RBC aggregation. To evaluate the extent of the inhibition of RBC aggregation, two experimental approaches were used: viscosity measurements and laser aggregometry. The results will be compared to linear counterparts and to reactive PEGs, which are covalently linked to the RBC membrane to study its effectiveness.

CHAPTER 2: EXPERIMENTAL PROTOCOLS

In this chapter, the preparation of the polymers and the characterization methods used for this study are addressed. Then, we present the methodologies used to evaluate the effect of the polymers on blood viscosity.

2.1 Preparation of Star-Shaped Polymers with a Cholane Core

2.1.1 Description of the experimental techniques

Anionic polymerization technique has been developed to allow the controlled synthesis of polymers with a variety of structures. This type of polymerization produces polymers with similar chain length or narrow molar mass distribution, which is termed living or chain-termination-free. Thus, living anionic polymerization is our chosen technique to synthesize well-controlled molar mass and molar mass distribution star-shaped polymers.

However, anionic polymerization must be conducted under inert conditions because of the sensitivity of the initiating system and the resulting chain ends to the traces of air and water. Therefore, very rigorous experimental conditions must be utilized in order to achieve quantitative results. For this purpose, a special setup with a high-vacuum and argon purification and special apparatus are required to exclude all impurities that may interfere with the polymerization reaction. The experimental setup is shown in **Figure 2.1**. This system is primarily composed of an oil pump capable of producing a strong vacuum and an argon line. The pressurized argon passes through a column filled with drying agents (silica) and then, the gas passes through the manifold. Afterwards, the gas passes through a pressure release system that is controlled via a stopcock, which is connected to the mineral oil bubbler. The pressure release device is simply a needle syringe in an Erlenmeyer flask sealed with a septum and copper wires. However, there is always the danger of pressure building up to the point of fracturing the apparatus when gases are used in a vacuum system. Consequently, a slight pressure difference is required

to facilitate the diffusion of gas or the transfer of intermediates into another flask. Thus, the purpose of the pressure release system serves to relieve such pressure in the apparatus while maintain an air-tight system.

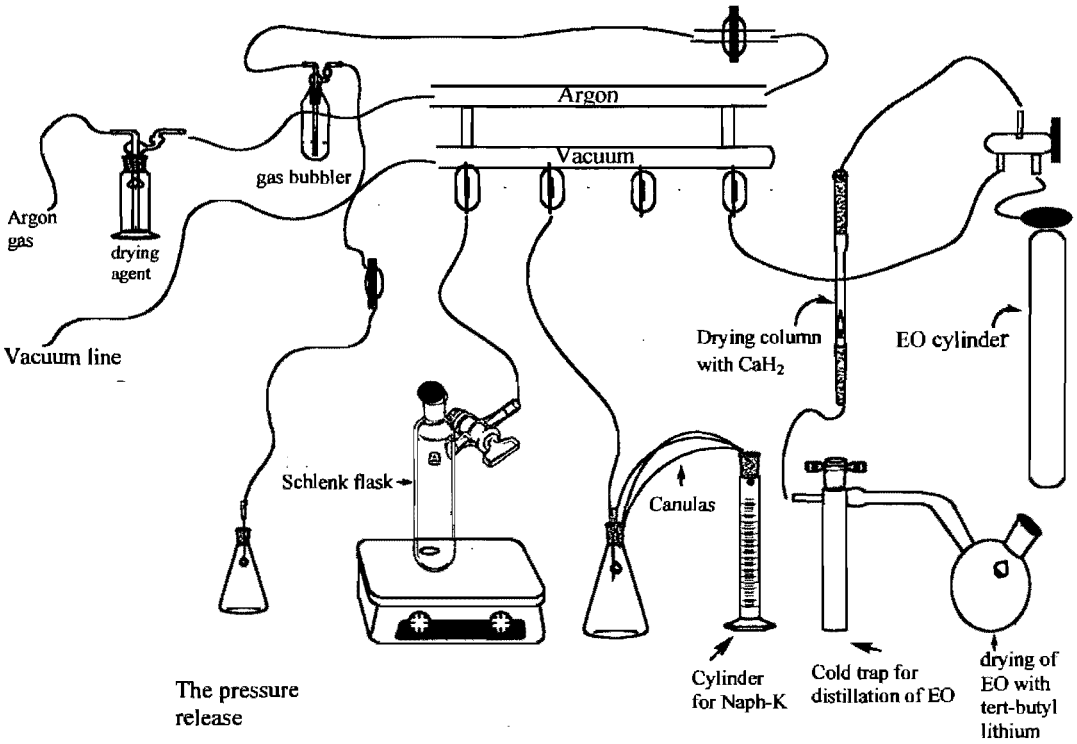

Figure 2.1. Setup for the anionic polymerization with the argon, manifold and the vacuum pump system.

Treatment of glassware

Flasks, reactors, and other glassware were washed with chromic acid cleaning solution (caution, very corrosive), and then rinsed with distilled water followed by an acetone-wash, to be finally dried in an oven at over 100°C. After removal from the oven, the cleaned glassware was connected to the manifold and evacuated with the vacuum line. The glassware was heated with a hand torch adjusted to give a white to blue flame until the yellow flame was given off from the glass surface. During the heating process, the glassware was continually being evacuated, then, allowed to cool down followed by a stream of argon gas. This cycle was repeated at least three times.

2.1.2 Materials

Solvent Purification

Tetrahydrofuran (THF) (> 99%, Aldrich) was purified by distillation with a heating mantle over sodium metal (Aldrich) and benzophenone (Aldrich) through a distillation column, which was connected to an argon line. The appearance of the characteristic blue color indicated that the THF was dried. The THF was collected in a flask into which small lumps of potassium (98% in mineral oil, Aldrich) and naphthalene (Aldrich) were added to obtain a concentration varying from 0.24 ~ 0.50 M depending on the preparation. The flask containing the initiator solution was sealed and stored at 4°C. The concentration was determined by titration with a standard solution of 0.05 N HCl.

Ethylene oxide (EO) was purchased from Aldrich and was dried by passing through a calcium hydride column and the EO vapors were condensed by using a cold trap where a dry ice-acetone bath was used. EO was subsequently distilled in 1.6 M n-butyl lithium solution in hexanes (Aldrich). Dimethylsulfoxide (DMSO from Aldrich) was dried overnight with calcium hydride and subsequently distilled just before the polymerization and transferred to the reaction flask under argon gas prior to use. Cholic acid (98%, CA) and aminoethanol (98%) was purchased from Aldrich and used as received.

2.1.3 Preparation of cholic acid methyl ester (CAME)

The esterification of cholic acid (**CA**) was achieved according to a previously published method and is briefly discussed here.[102] CA was weighed (7.31 g, 18 mmol) and added directly to a 250 mL round bottom flask. Methanol was added (70 mL) to the reaction flask with a few (3-5) drops of concentrated HCl. The reaction vessel was equipped with a distillation column and a magnetic stirring bar. The mixture was refluxed and stirred for 6 hours at 65°C in an oil bath. The flask was cooled down at room temperature and placed in a refrigerator at 4°C overnight to precipitate the crystals. The crystals were filtered and washed 3 times with chilled methanol. The crystals were dried

overnight under reduced pressure to remove any residual methanol. The yield of the product was 95%. ^{1}H NMR (400 MHz, $CDCl_3$, ppm): δ = 0.68 (3H, s, C18-CH_3), 0.89 (3H, s, C19-CH_3), 0.98 (3H, d, J = 6.2 Hz, C21-CH_3), 3.42 (1H, m, C3-COH), 3.66 (3H, s, C24-OCH_3), 3.85 (1H, s, C7-CH), 3.98 (1H, s, C12-CH), 1.0-2.5 (various CH and CH_2).

2.1.4 Preparation of (2'-hydroxylethylene)-3α,7α,12α -trihydroxy-5β-cholanoamide (CA-$NHCH_2CH_2OH$)

In a 250 mL reaction flask equipped with a distillation column, 5 g of **CAME** (12 mmol) was added with 30 mL of 2-aminoethanol. The mixture was stirred at 90°C. The reaction was monitored with thin layer chromatography (TLC). After 4 hours, the reaction was cooled to room temperature. A 50:50 mixture of ice and water was poured into the reaction flask to yield a milky white precipitate. The precipitate was filtered and was recrystalized by adding hot methanol until it dissolved and then, ethyl acetate was added in excess. The final product was dried in the oven under vacuum. The yield of the product was 90%. ^{1}H NMR (400 MHz, DMSO-d_6, ppm): δ = 0.58 (3H, s, C18-CH_3), 0.81 (3H, s, C19-CH_3), 0.92 (3H, d, J = 6.4 Hz, C21-CH_3), 1.0-2.2 (m, protons on the steroidal skeleton backbone), 3.08 (2H, q, J = 6.04 Hz, C25-NCH_2), 3.18 (1H, m, C3-CH), 3.35 (2H, m, C26-CH_2O), 3.60 (1H, s, C7-CH), 3.77 (1H, s, C12-CH), 4.01 (1H, d, J = 3.3 Hz, C12-COH), 4.10 (1H, d, J = 3.5 Hz, C7-COH), 4.32 (1H, d, J = 4.3 Hz, C3-COH), 4.62 (1H, t, J = 5.5 Hz, 26-COH), 7.75 (1H, t, J = 5.5 Hz, 24-CONH).

2.1.5 Anionic polymerization of ethylene oxide

Several samples of different molar mass of star-shaped PEG polymers with a cholic acid core (**CA(PEG)$_4$**) polymer were obtained according to the synthetic route shown in **Figure 2.2.** The cholane derivative, **CA-$NHCH_2CH_2OH$** was weighed and then added to the reactor vessel under argon gas. Then, a low vacuum was introduced for a few minutes to remove any moisture residual before being placed under argon gas once again. Then, 90 mL of freshly dried DMSO was subsequently added to the reactor vessel via a

canula and the solution was stirred with a magnetic stirring bar. The solution was clear and colorless

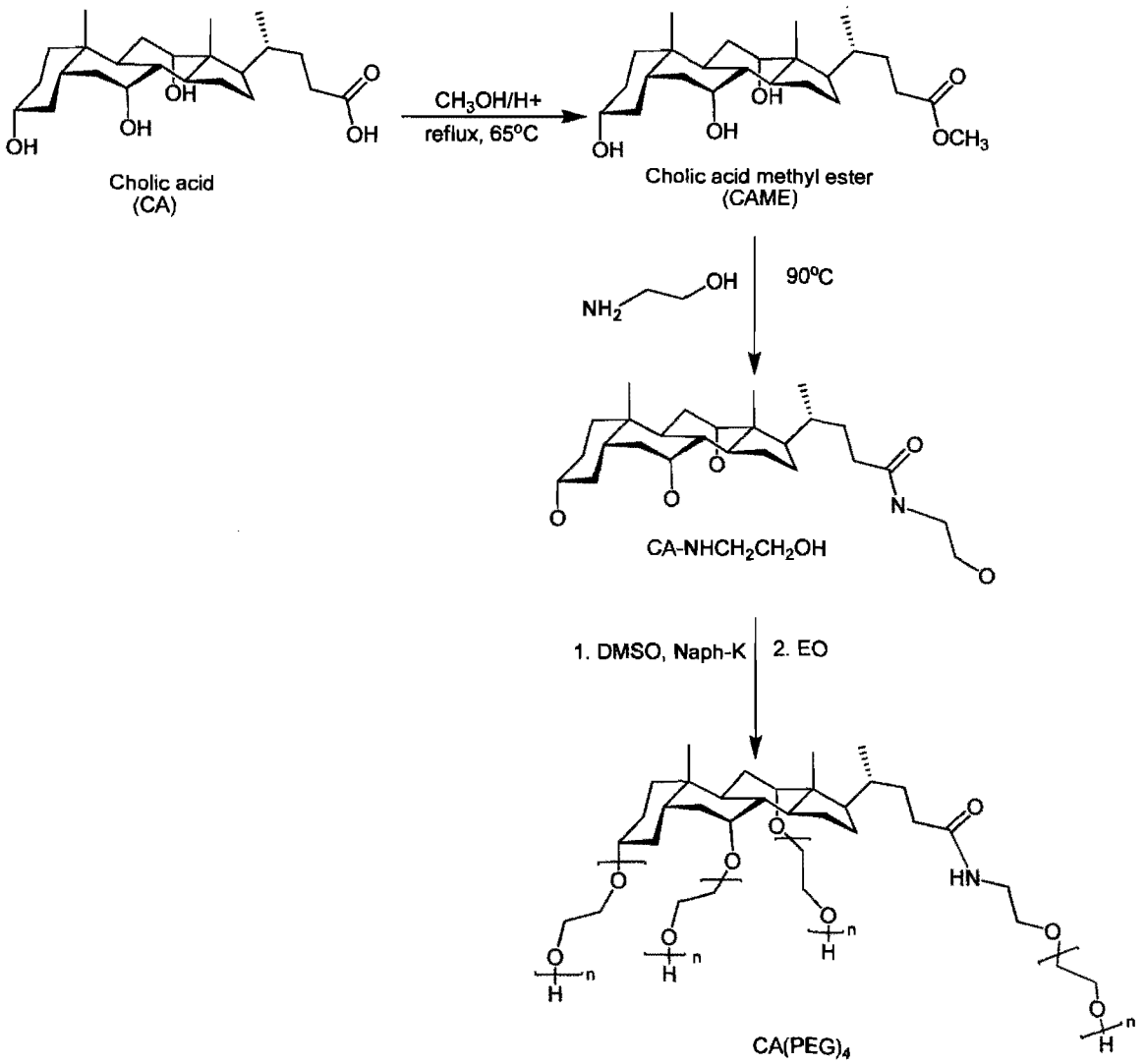

Figure 2.2. Synthesis route for $CA(PEG)_4$ star polymers.

A calculated amount of initiator to reach a 25% deprotonation (potassium naphthalene solution in THF) was collected in a graduated cylinder (see **Figure 2.1**) by pressure difference with argon gas by using a canula. This step is crucial because any leak in the system can deactivate the initiator and caution must be taken to avoid introducing

excess amount of initiator into the reactor vessel, which may lead to the activation of small PEG chains. In order to transfer the initiator from the graduated cylinder into the reactor vessel, the pressure was reduced in the reactor vessel by connecting it to a canula via the pressure release system (see **Figure 2.1**). Then, the initiator was added dropwise into the reactor vessel via a canula using high pressure of argon. After the transfer of the initiator, the reactor vessel was placed back under a stream of argon. The mixture quickly became dark green, which persisted for a few minutes until it became clear and colorless again. At this stage, if the dark green color disappeared too quickly, it usually meant that some contaminants were present in the reactor vessel and that the desired molar mass would not be attained. In the special apparatus composed of a graduated cylinder connected to a round bottom flask (see **Figure 2.1**), a vacuum was introduced just for a few seconds and then closed before ~ 5 mL of *tert*-butyl lithium was introduced into the round bottom flask part via a canula. Then, the *tert*-butyl lithium was cooled down with a dry ice-acetone bath. The graduated cylinder of the special apparatus was also placed in the dry ice-acetone bath. With a low vacuum on, a predetermined amount of ethylene oxide (EO) was collected directly in the special apparatus with the graduated cylinder and then, the vacuum line was closed. For instance, to synthesize a 15 kDa star-shaped polymer, the amount of mL of EO was calculated using the following formula:

$$\text{mL of EO} = \frac{0.75\ \text{mmol}\ A \times 4 \times 83\ \text{equiv of PEO} \times 44.05\ \text{g/mol}}{0.882\ \text{g/ml}} \qquad (2.1)$$

where A is the molar concentration of **CA-NHCH$_2$CH$_2$OH** (MW of 451.65 g/mol)

4 is the number of arms of the star-shaped polymer

83 is the equivalence of EO units per arm

44.05 g/mol is the MW of EO

0.882 g/mL is the density of EO gas.

The graduated cylinder of the special apparatus was placed in dry ice-acetone bath to distill EO in the flask. Distillation was aided by wetting a paper towel with dry ice-acetone bath and brushing the side walls of the apparatus so that EO could distill in the flask faster. This step was very useful especially when large amounts (> 10 mL) of EO had to be distilled. Normally, it could take up to thirty minutes or even an hour for the vapors of EO to condense in the graduated cylinder. In the meantime, the *tert*-butyl lithum line was closed. When the desired amount of EO was collected, the *tert*-butyl line was opened. It is noted here that an excess of 1 or 2 mL of EO was added to the calculated amount of EO so that it could compensate for the EO loss during transfer. The EO was distilled into the tert-butyl lithium flask by warming it from the contact with a hand or with the aid of warm water in a beaker and cooling the receiving end of the flask with dry ice-acetone bath. After drying EO with tert-butyl lithium, it was transferred back into the modified graduated cylinder by cooling the receiving end and warming the round bottom flask. Gloves were worn at all times during the transfer process. In the meantime, the reactor vessel containing the DSMO solution was also cooled down with a dry ice-acetone bath so that when the EO would be transferred, it would not be evaporated. The EO was transferred to the DMSO solution in the same manner as the initiator. The DMSO solution was mixed well and let warmed back to room temperature before heating. The polymerization proceeded at 40°C for 48 hours and the argon feeding line was closed. The reaction mixture was quenched with a few drops of concentrated HCl until the pH paper indicated a neutral pH value. Then, the DMSO solution was extracted 3 times with hexane to remove the naphthalene residuals and after it was evaporated under vacuum, THF was added to dissolve the polymer until the salt appeared, which was then filtered out of the solution. The THF was also removed under vacuum. The viscous polymer solution was purified by several solvent extractions with THF and diethylether to yield a white to yellow powder. The polymers synthesized are listed in **Table 2.1** and will be referred to by their sample number through out this manuscript.

Table 2.1. List of the four armed star-shaped PEG polymer with a cholic acid core synthesized by anionic polymerization

Sample	EO units (X 4 arms)	Molar Mass
1	106	19.1 kDa
2	84	15.3 kDa
3	69	12.6 kDa
4	55	10.1 kDa
5	51	9.5 kDa
6	40	7.5 kDa
7	39	7.3 kDa
8	32	6.0 kDa
9	26	5.0 kDa
10	25	4.8 kDa
11	20	4.0 kDa
12	17	3.5 kDa
13	16	3.4 kDa
14	15	3.2 kDa
15	11	2.4 kDa
16	8	1.8 kDa
17	7	1.6 kDa
18	5	1.3 kDa

2.2 Characterization Methods

Nuclear magnetic resonance (NMR) spectroscopy

^{1}H NMR spectra of the CA(PEG)$_4$ polymers and cholic acid derivatives were recorded on a Bruker AMX400 spectrometer operating at 400 MHz for ^{1}H. The cholic methyl ester (CAME) was dissolved in deuterated chloroform ($CDCl_3$ with a peak that appears at 7.24 ppm) and the other compounds were dissolved in deuterated dimethyl sulfoxide (DMSO-d_6 with a solvent peak at 2.5 ppm).

Differential scanning calorimetry (DSC)

The thermal transitions of the polymers were analyzed on a TA DSC Q1000 differential scanning calorimeter (DSC). A precise amount of polymer between 3-10 mg was placed in an aluminum capsule under a nitrogen atmosphere with a flow of 50 mL/min. The heating rate was 10°C/min and the data were treated using a Thermal Analysis 2000 system. See **Appendix 2** for more details.

Matrix-assisted laser desorption/ionization time-of-flight (MALDI-TOF) mass spectrometry

MALDI-TOF mass spectrometry was carried out on a Bruker Daltonics Autoflex MALDI-TOF mass spectrometer. The instrument is equipped with a standard nitrogen laser (λ=337 nm) to desorb and ionize the samples. The instrument was operated in the positive ion linear mode with an accelerating potential of +20 kV. All spectra were collected with an average of 200 shots. All samples were analyzed with dithranol (1,8-dihydroxy-9[10H]-anthralenone, Sigma) as the matrix and LiCl was used as the saturated salt solution. About 10 mg of dithranol was dissolved in 0.5 mL of methanol to prepare a saturated solution and 10 mg of LiCl was dissolved in 1.5 mL methanol. The polymer solutions were prepared by dissolving 2.5 mg of the polymer in 0.5 mL methanol. The final mixture solutions were prepared with the following mixing formula:

20 μL of matrix + 2 μL of a polymer solution + 2 μL of LiCl solution

Then, 0.5 to 1 μL of sample solution was deposited on the sample plate and air-dried. A peptide (1 to 4 kDa) and a protein (3 to 25 kDa) calibration standard were used to calibrate the molar masses of the star polymers.

Size exclusion chromatography (SEC)

Size exclusion chromatography (SEC) was performed on a Breeze system from Waters equipped with a 717 auto sampler and a 1525 Binary HPLC pump. The chromatogram was recorded at a flow rate of 1 mL/min in THF at 25°C, and a Waters 2414 system with a refractive index detector installed with three Styragel columns HR3, HR4 and HR6 (all three 7.8 × 300 mm) in series (from Waters) were used for the resolution of the different samples. About 2 mg of polymer were dissolved in 1 mL of THF. The calibration curve was made with linear PEGs standards (Polymer Laboratories LTD) with molar mass of 1900, 6450, 11 840, and 22 450 kDa. About 5 mg of each PEG standards were dissolved in 5 mL of THF. However, if star-shaped PEGs standards were available they would be preferable than linear PEGs since they would have a similar hydrodynamic radius. The linear calibration curve was extrapolated to estimate the number-average molar mass (M_n) and the weight-average molar mass (M_w) of the polymers (**See Appendix 2**).

Light scattering (LS) experiments for the determination of M_w of the $CA(PEG)_4$ polymers and PEG standards (Polymer Laboratories LTD) were performed on a chromatographic system consisting of a Waters 510 HPLC pump, pre-guard + two columns (PLAquagel-OH-30 8 μm, 10^3 Å and 10^5 Å), a Dawn EOS multi-angle light scattering detector (λ = 690 nm), coupled to a Optilab Rex refractive index detector, and a Wyatt QELS quasi elastic light scattering, all from Wyatt Technology Corporation. Data were collected and analyzed by the ASTRA software (Wyatt Technology Corporation). The *dn/dc* (differential refractive index increment) was determined online assuming a total mass recovery or offline by determining the refractive index at several concentrations. Water and phosphate buffer solution (PBS) at a flow rate of 1 mL/min were used at the mobile phase and 0.05% of sodium azide was added to prevent bacteria formation. The normalization and the alignment of the instrument were carried out by PEG standards, Pullulan-5 and Pullulan-100 using rms radii of 2 nm and 10 nm, respectively.[103] About 10 mg of polymer was dissolved in 1 mL of water or PBS to get a good signal from the light scattering detector.

Viscosity measurements

Viscosity measurements were made with the Viscosity Monitoring Electronic instrument (Cambridge Applied Systems) at 25°C to determine the hydrodynamic radius (R_h) of the synthesized polymers. Solutions of $CA(PEG)_4$ polymers in doubly distilled water were prepared and left standing at room temperature in a sealed vial for 24 hours to get clear solutions. The viscosity measurements for each solution were measured five times.

Rheology measurements were made on an AR2000 rheometer (TA Instruments) using a couette measuring cell. Solutions of star-shaped $CA(PEG)_4$ polymers in water and in PBS (10 mL) for different MW were prepared to study the effect of shear rate on the viscosity at 25 and 37°C. The rheological measurements of continuous and steady states were recorded.

2.3 Blood-Related Experiments

The effect of the $CA(PEG)_4$ polymers and linear PEGs on RBC aggregation was studied with Contraves LS-30 couette viscometer, Myrenne aggregometer and direct microscopic techniques. Because of the non-conclusive results of preliminary experiments, expertise was sought and measurements were performed at the Department of Physiology and Biophysics of Kerck School of Medicine at the University of South California by Dr. Armstrong.

2.3.1 Materials

The $CA(PEG)_4$ and the linear PEGs polymers used for the *in vitro* studies of their effect on RBC aggregation and their molar mass are listed in **Table 2.2**. Their molar masses were measured by size exclusion chromatography in THF and the molar mass of the linear PEGs comes from the specification of the manufacturing companies.

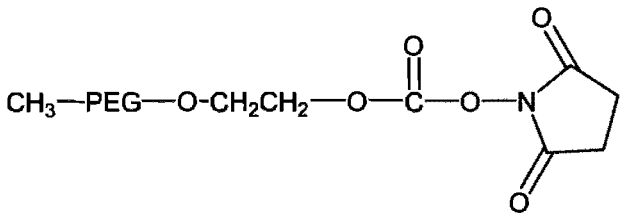

mPEG-succunimidyl proponiate (mPEG-SPA)

Figure 2.3. Structure of monomethoxy PEG succinimidyl propionate (mPEG-SPA)

Also, a monofunctional succinimidyl propionate derivative of monomethoxy PEG (mPEG-SPA) from *Netkar Therapeutics* of molar mass of 20 kDa was used as an appropriate positive control for polymer binding to the RBC's membrane (**Figure 2.3**).

Table 2.2. Linear and star-shaped PEG polymers with a cholic acid core ($CA(PEG)_4$) that were used to evaluate their effect on red blood cell aggregation.

Samples	EO units (X 4 arms)	M_n	M_w	PDI
1	106	19 110	19 340	1.01
2	84	15 320	16 050	1.05
3	69	12 660	13 120	1.04
4	55	10 080	10 600	1.05
5	51	9 500	9 970	1.05
11	20	4 040	4 230	1.04
PEG-2k (Fluka)	-	1 900	1 960	1.03
PEG-5k (Sigma)	-	5 120	5 240	1.03
PEG-7k (Sigma)	-	6 850	7 000	1.03
PEG-12k (Fluka)	-	10 800	11 250	1.04
PEG-22.8k (Polymer Labs Standard)	-	21 500	22 800	1.06
mPEG-SPA (*Netkar Therapeutics)*	-	20 000	-	-

For samples 1 to 5 , and 11, the molar mass were determined by SEC in THF

2.3.2 Sample blood preparation

Addition of CA(PEG)$_4$ and linear PEGs to RBC samples

To eliminate the effect of hydrophobic interactions with plasma proteins (e.g., albumin), the CA(PEG)$_4$ polymers were added to washed RBCs in buffer, incubated, then washed again and resuspended in autologous plasma. In this protocol, plasma dilution was equivalent for all samples. An equivalent volume of buffer was added to aliquots (blood samples).

Freshly drawn blood from three healthy human donors was anticoagulated with EDTA (1.5 mg/mL) and centrifuged at 1750 *g* for 10 minutes. The plasma was removed and saved, and the white buffy coat, which contains the white blood cells and platelets, was discarded. The RBCs were washed three times with isotonic 10 mM Dulbecco's PBS (pH 7.4, 285 mOsm/kg) and spun at 1400 *g* for six minutes. The RBCs were resuspended in plasma and adjusted to a 42% hematocrit (Ht). 2 mL aliquots of blood were pipetted into 3 mL polypropylene containers (16 samples per donor). Stock solutions of the CA(PEG)$_4$ polymers and PEG standards listed in **Table 2.2** were prepared in PBS (10 mM) to get a concentration of 100 mg/mL. The stock polymer was added to each blood sample to get final dilutions of 1.3, 4.0, and 6.7 mg/mL with an hematocrit value of 40.3%.

Addition of linear reactive PEG (mPEG-SPA) to RBC samples

Freshly drawn human blood was anticoagulated with EDTA and centrifuged at 1750 *g* x 10 minutes. The plasma was removed and saved, and the buffy coat aspirated. The RBCs were washed a further 3 times with PBS (2 x spins at 1400 *g* x 6 minutes, and a final spin at 1750 *g* x 10 minutes). Washed RBCs were resuspended to 10% Ht in 15 mM triethanolamine buffer. An amount of 100 mg mPEG-SPA was weighed into a 50 mL polypropylene tube. One mL of cold 10 mM HCl/saline was added to each polymer to dissolve it (~20 seconds). Then, 10 mL of RBCs in triethanolamine buffer were immediately added top each polymer sample (giving a total polymer concentration of ~9

mg per mL of suspension, or 100 mg per mL of packed RBCs). The samples were incubated at room temperature for 90 minutes. Thirty mL of PBS were added, and samples centrifuged at 500 *g* x 10 minutes. The RBCs were washed twice with PBS (500 *g* x 10 minutes). RBCs were then transferred to a 3 mL polypropylene tube and 1.5 mL of autologous plasma added, mixed, and then centrifuged at 1400 *g* x 6 minutes.
RBCs were resuspended to a 40% Ht with autologous plasma.

Microscopy

The morphology of the $CA(PEG)_4$-RBCs and the control RBCs at a physiological pH was studied by light microscopy. For the control sample (no polymer added) and 6.67 mg/mL samples only (highest polymer concentration), 50 µL of blood sample was diluted with 250 µL of plasma and mixed. Then, 1 drop was placed on a glass slide. A cover slip was put over the sample that was allowed to stand at room temperature for 10 minutes. Microscopic images were recorded at 400 magnifications.

Viscosity Measurements

The apparent viscosity of the RBC suspensions of linear PEGs and the $CA(PEG)_4$, at 25 °C, was measured over a range of shear rates (0.1-94.5 s^{-1}) using the Contraves LS-30 Couette viscometer (Contraves LS 30, Contraves AG, Zürich, Switzerland). The Contraves LS-30 rheometer is a Couette concentric-cylinder viscometer operated at a constant shear rate and equipped with a thermostated sample bath.

Myrenne aggregometer

RBC aggregation was quantified using a photometric Rheoscope (Model MA-1 Aggregometer, Myrenne GmbH, Roentgen, Germany) interfaced with a computer.[6] Stasis and very low shear conditions were produced using a transparent cone-plate geometry. This method employs the light transmission of Schmid-Schonbein et al.[104] The blood sample is placed in a photocell which is perpendicular to the light source. The principle of

this technique is based upon the increase of light transmission through a RBC suspension, which occurs when individual cell aggregates into *rouleaux;* gaps in the suspending medium between the aggregates allow more light to pass through the RBC suspension. The Myrenne aggregation parameter M, is obtained by first shearing the sample at a high shear rate (600 s^{-1}) to assure *rouleaux* disruption and RBC orientation with the flow. After abrupt cessation of the rotation, the variation of the light transmission is recorded for 10 seconds, the average change in the light transmission over this period is taken as the M value (arbitrary units). If no aggregation takes place, then the light transmission does not change and M = 0. The *rouleaux* formation process reduces the light scattering and allows for more light to pass through the photocell, resulting in a positive M value, for which the magnitude increases with the extent of aggregation. Therefore, an increase in either M (stasis) or M1 (at 3 s^{-1}) indicates enhanced RBC aggregation. Note that M thus reflects aggregation in the absence of shear and M1 reflects aggregation when fluid movement tends to promote cell-cell interaction and both M and M1 increase with increasing RBC aggregation.[6] For this study, a normalized Myrenne aggregation data (M and M1) were determined by dividing the M values of the test samples by the M values of the RBCs with no polymers added (control sample). M index greater than unity reflect RBC aggregation. Aggregation measurements for all samples, Myrenne M and M1 values were recorded in duplicate per donor.

2.4 Statistical Methods

Data are presented as mean ± standard deviation (SD). Comparisons between data groups were carried out pair-wise using ANOVA with the *Bonferroni test* using the data software OriginPro 8 (OriginLab, MA, USA). Associations between variables were assessed by least-squares linear regression.

CHAPTER 3: CHARACTERIZATION OF THE STAR-SHAPED CA(PEG)$_4$ POLYMERS

3.1 Preparation of the Cholic Acid Derivatives and CA(PEG)$_4$

The synthetic route of the cholic acid derivatives and CA(PEG)$_4$ polymers are shown in **Figure 2.2** and listed in **Table 2.1**. The first step consists of the esterification of the carboxylic acid group at position C24 of **CA** to an ester group. This reaction has been reproduced several times and resulted in high yield (>90%) and the NMR spectrum of compound **CAME** is provided in **Figure 3.3**.

The second step involves the preparation of the compound **CA-NHCH$_2$CH$_2$OH** via the nucleophilic acyl substitution reaction of the ester group of **CAME** and aminoethanol. In this reaction, the nucleophilic amine attacks the electrophilic carbon of the ester and the nucleophilicity of the amine is dependent on its lone pair. If acid was added, the basic amine would get protonated and the lone pair would become unavailable for nucleophilic attack. The reaction would not be favored thus heating is used to drive the reaction forward. The mechanism is illustrated in **Figure 3.1**.

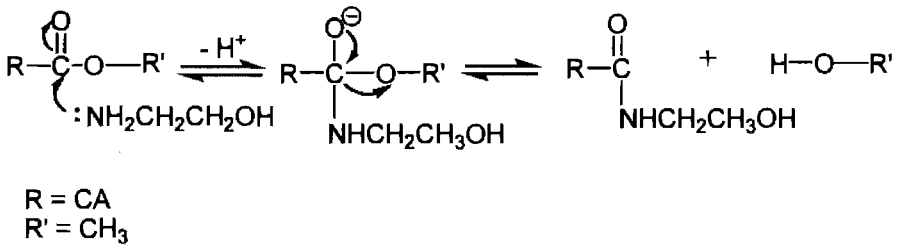

Figure 3.1. Mechanism of nucleophilic acyl substitution

In this mechanism, the stronger base (amine) is used and the weaker base (methanol) is produced. Also, before the alcohol (leaving group) portion of the ester departs, it picks up an H^+ so that it can leave as the weak base alcohol (R'OH) rather than as the strong base alkoxide ion ($R'O^-$). This is because weaker bases make better leaving groups.

The precursor **CA-NHCH$_2$CH$_2$OH** with four alcohol groups was used as a multifunctional alkoxide macroinitiator for the AROP of EO. The macroinitiator was prepared by a partial deprotonation by reacting with a solution of naphthalene potassium in THF. The macroinitiator reacted with naphthalene potassium to completion at room temperature which was evident by the stable green color that slowly disappeared when all the hydroxide groups had been reacted. However, in some cases the green color disappeared too quickly probably due to moisture content which impeded the polymerization process.

In a "core-first" approach with the multifunctional alkoxide macroinitiator, there is a high tendency of strong aggregation of the propagating alkoxides which usually leads to poor solubility, hence resulting in poor molar mass control and broad molar mass distributions.[100] Therefore, the extent of the deprotonation of the macroinitiator was restricted to 25% in most cases. Under such homogenous conditions, the exchange of protons between dormant hydroxyl groups and active alkoxides were rapid enough to generate a dynamic equilibrium as shown in **Figure 3.2**.

In this case, the extent of aggregation is limited because the rate of exchange (R_{ex}) is rapid with respect to the rate of propagation (R_p). This implies that the synthesis of PEO chains under controlled conditions from precursor **CA-NHCH$_2$CH$_2$OH** and the predictable molar masses with narrow molar mass distribution can normally be achieved. These conditions worked well for low molar mass CA(PEG)$_4$ polymers but proved to be problematical for generating higher molar masses in a predictable manner. For polymers of molar mass greater than 10 000 g/mol, the EO had to be in excess. For example to synthesize the CA(PEG)$_4$ with 15 000 g/mol, an excess of equivalent EO for a molar mass of 20 000 g/mol had to be used in order to get the desired molar mass. Prior to the addition of EO, the reactor vessel was cooled in a dry-ice acetone bath. Perhaps, during the slow heating to 40 °C, some of the EO may have evaporated.

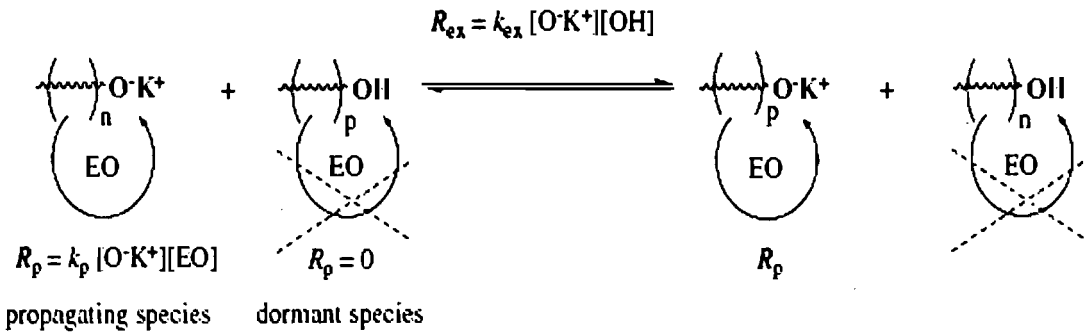

Figure 3.2. Exchange of protons between dormant hydroxyls and active alkoxide species is fast during the anionic ring opening polymerization (AROP) of ethylene oxide (EO) where the rate of exchange (R_{ex}) is much higher than the rate of propagation (R_p) or $R_{ex} >> R_p$ Reproduced from ref [105].

Anionic ring-opening polymerization (AROP) of ethylene oxide required a reactive initiator, naphthalene potassium, and a polar solvent, DMSO, which were used to allow high solvation of cations for a fast polymerization rate. Because of the low solubility of the precursor **CA-NHCH$_2$CH$_2$OH** and to prevent aggregation of the propagating alkoxides, DMSO was chosen as the solvent for the polymerization rather than THF due to its more dissociating properties and higher rate of propagation.[106] However, a potential problem associated with DMSO is the possibility of chain transfer of the propagating alkoxides to DMSO. Chain transfer of the growing alkoxides to DMSO gives rise to "dimyl" carbonions ($CH_3(SO)CH_2^-$) that may be capable of initiating a polymerization.[107] This implies that higher concentrations of the propagating alkoxides in the solution may lead to a higher probability of forming linear chains by chain transfer to DMSO. This will be shown in the SEC traces discussed later in the chapter.

The production of "ideal living polymer system", where polymers with infinitely high molecular weight are synthesized, is an extremely difficult task. The presence of impurities, which cannot be fully removed from the reaction mixture, and that are introduced with monomer or precursor as well as with solvent, leads to side reactions. In

the case of AROP, active centers are mainly deactivated by reaction with electrophiles such as traces of water, oxygen, carbon dioxide and other impurities that cause the termination of the chain. Therefore, they must be rigorously excluded from the polymerization system. This difficulty was circumvented by changing the apparatus from a round bottom flask to a Schlenck flask, which limited leakage from the pressure build-up during the polymerization. In fact, the use of the Schlenck flask led to more predictable high molar masses.

This makes anionic ring-opening polymerization a very demanding technique (ultra purity of reagents and solvents, high vacuum, etc.), somewhat limiting applicability of anionically initiated polymerizations. It may take much care to avoid and reduce the presence of some termination species and some slow side reactions, which annihilate the growing ends. If the rate of these side reactions in the system is sufficiently slow, there is the possibility to achieve the desired narrow distributed polymers, with relatively high molar masses.

3.2 Characterization of the Star-Shaped Polymers

The cholic acid derivatives were identified by NMR spectroscopy and the $CA(PEG)_4$ polymers were characterized by NMR spectroscopy, GPC, SEC-MALS, MALDI-TOF, DSC, viscometer, and rheometer.

3.2.1 NMR spectroscopy

Proton nuclear magnetic resonance (^{1}H NMR) spectroscopy is one of the most powerful techniques for elucidating the structure of chemical species. The identification of **CAME** was confirmed by the NMR spectrum shown in **Figure 3.3(a).** There is a sharp singlet at 3.66 ppm indicative of the methyl ester group OCH_3. This is a characteristic feature of the methyl protons of the bile acid methyl ester. The distinguishing features of ^{1}H NMR spectrum of cholic acid are also present with two singlet peaks at 0.69 ppm for 18-CH_3 and 0.89 ppm for 19-CH_3. The methyl proton signal of C21 is a doublet because its resonance is split in two due to the neighboring proton on proton signal C21.

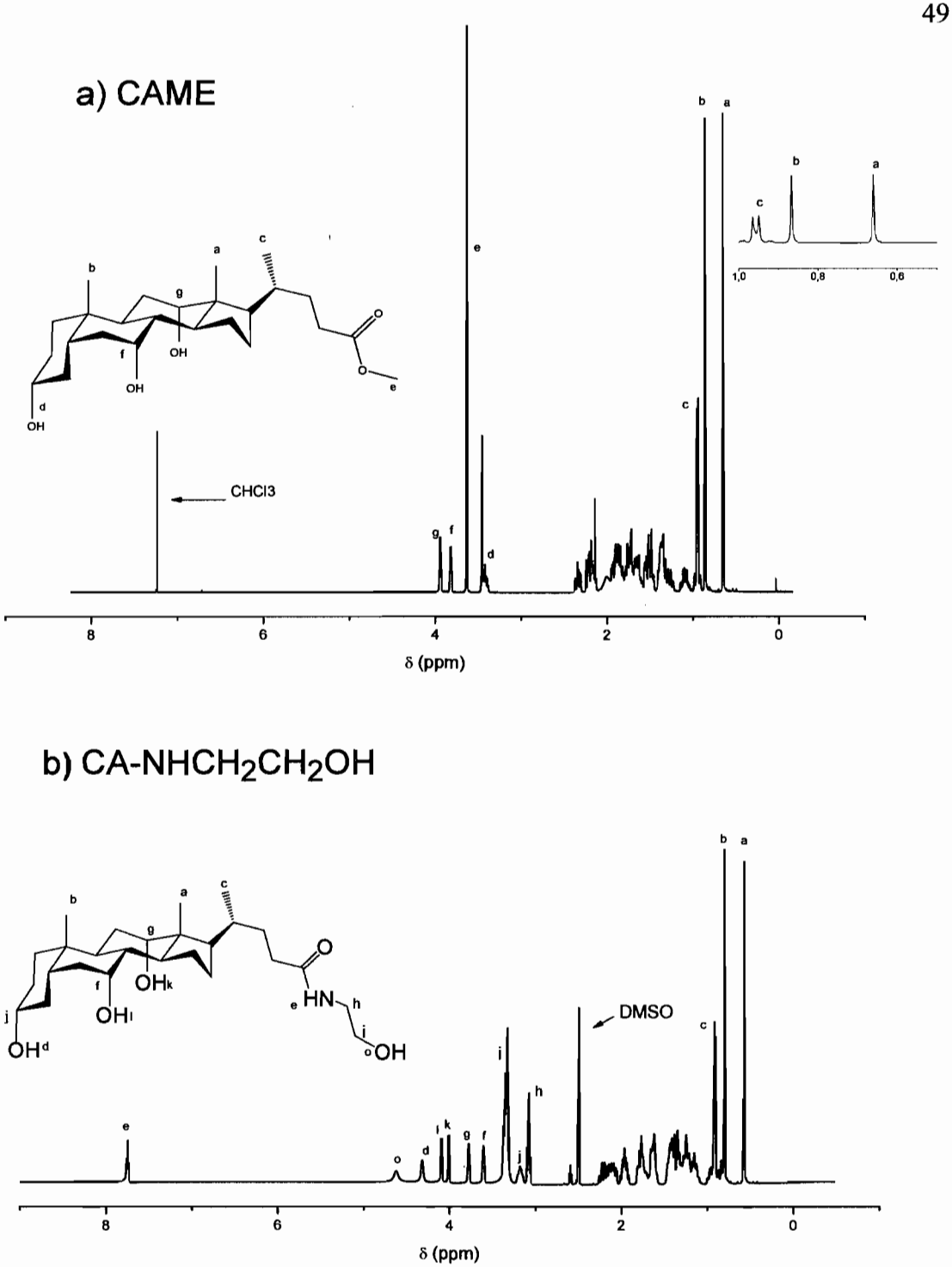

Figure 3.3. ^{1}H NMR spectra of a) CAME in $CDCl_3$ and b) CA-$NHCH_2CH_2OH$ in DMSO.

The hydroxyl group at C3 is split into a quintet due to the four protons on the neighboring carbons. For N equivalent, the spin nuclei splits the resonance by a nearby spin or group of equivalent spins into N + 1 with the intensity following the distribution of the Pascal's triangle. The multiplicity arises from the spin coupling between neighboring protons that are non-equivalent or that resonate at different frequencies. According to this simple multiplicity rule, the areas enclosed by the components of a multiplet should be the ratio of whole numbers. The overlapping resonance peaks around 1.0-2.60 ppm are attributed to the other CH_2 and CH of the steroid backbone.

The NMR spectrum in **Figure 3.3(b)** confirmed the structure of the compound **CA-HCH_2CH_2OH** by the complete disappearing of the methyl ester peak. The resonance peak of NCH_2 at 3.08 ppm on position C25 is split into a quartet due to the three protons of the neighboring nucleus. The expected quartet at 3.35 ppm of CH_2 of C26 is overlapped with the water peak of DMSO (3.3 ppm). The proton (CONH) on C24 situated closely to the nitrogen was deshielded due to the high electronegativity of the nitrogen and as a result appears further downfield (7.75 ppm). The nucleus examined can be shield or deshield by the magnetic field of neighboring nuclei. The first order effects are applied when the chemical shifts of the coupled nuclei are far enough apart and the second order effects are applied when the chemical shifts approach one another, the interactions get stronger and two things occur. Firstly, the energies of the spin states shift and secondly, the probabilities of transitions between levels also change as a result, the positions and intensities of peaks will not match those predicted.

The coupling constant, J (in Hz), is an important parameter that provides information about the number of different type of atoms that are close to each other in the molecule. It also quantifies the strength of the interaction. Coupling constants are independent of the strength of the applied field; therefore, it is an intrinsic property of the molecule. The coupling constants J were calculated by taking the peak-to-peak distance of each region in Hz. The protons at position C24 and C26 had the same coupling constant (J = 5.5 Hz) meaning that they are coupled to the same type of nucleus since protons are coupled if they have the same coupling constant. The NMR spectrum of $CA(PEG)_4$ for the repeating unit of 7 of EO is shown in **Figure 3.4**. The methylene

protons of PEG are present around 3.4-3.5 ppm. Only a few of the cholane backbone chemical shifts are visible because they are smaller compared to the PEG chains. The other NMR spectra of the polymers can be found in **Appendix 3.**

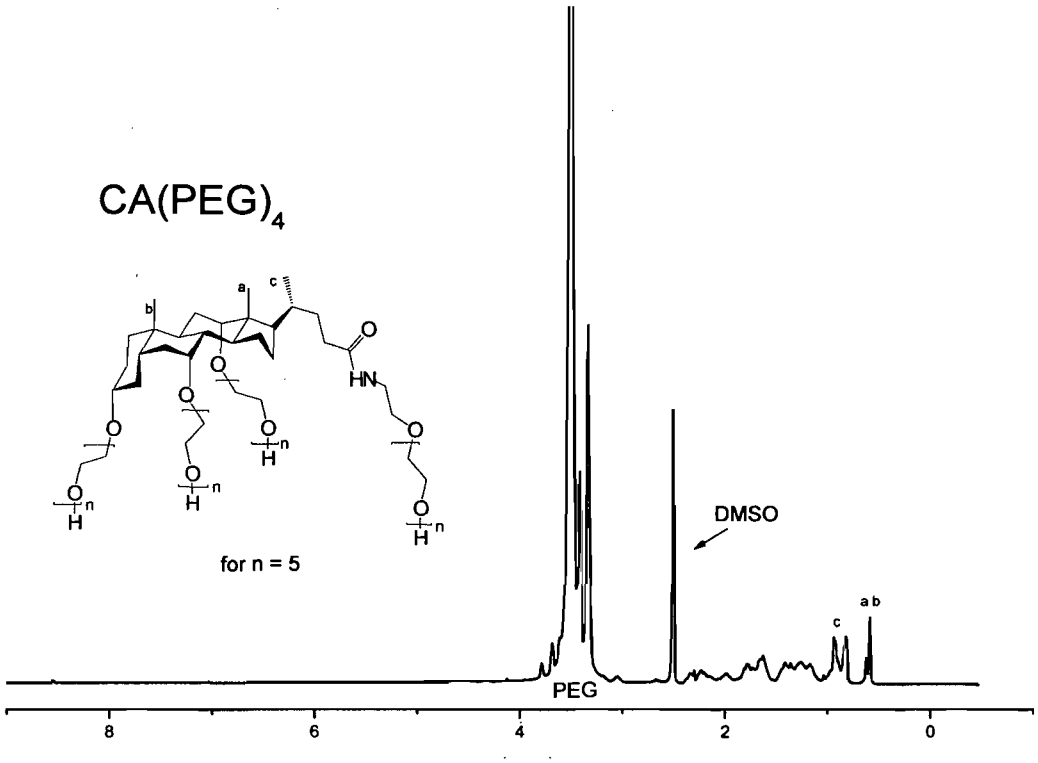

Figure 3.4. ^{1}H NMR spectrum of a CA(PEG)$_4$ polymer of **sample 18.**

3.2.2 Thermal analysis

Differential scanning calorimetry (DSC) was used to analyze the thermal properties of the CA(PEG)$_4$ polymer samples as a function of temperature (see **Appendix 2**). **Figure 3.5** shows an evident glass transition (T_g) for **sample 18**, which has only 5 units of ethylene oxide (EO) per chain, and it does not show any crystallization or melting peaks. This is probably due to the PEG chains being too short; hence, it is unable to form

any crystalline domain. However, when the PEG chains are too long, their entanglements with each other may also impede the formation of crystals.[108]

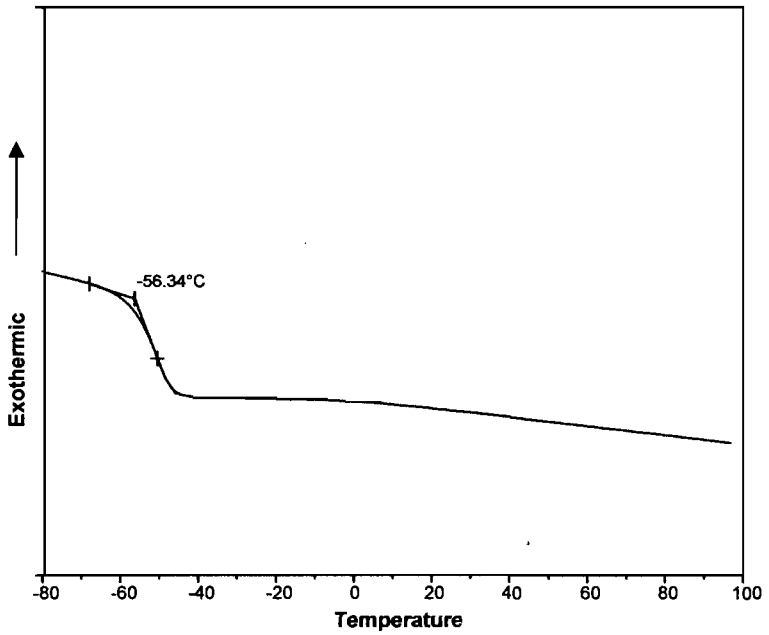

Figure 3.5. DSC trace of $CA(PEG)_4$ of **sample 18** showing the glass transition temperature, T_g.

The high molar mass of the $CA(PEG)_4$ polymers (**Sample 1 - 4**) show only melting peaks (**Figure 3.6**). These uncrystallized arms might be located in the amorphous layers, and thus can explain the no show of the crystallization peak. The existence of globular structure of star-shaped PEGs could decrease the intermolecular interaction and restrict the macromolecular conformation, which considerably refines the crystallization behavior of polymers. The thermograms in **Figure 3.6** also show that the polymers were produced under controlled living conditions because the melting peaks are narrowed except for the thermogram of **sample 2** which reflects bimodal characteristic since it has a slight shoulder near the melting peak.

In **Figure 3.7**, the melting peaks were plotted as a function of the molar mass. **Figure 3.7** shows that the melting temperature becomes slightly raised with increasing

molar mass. Thus, the melting points of the polymers seem to depend on the size of the crystalline domains, which may be larger with increasing length of the PEG.

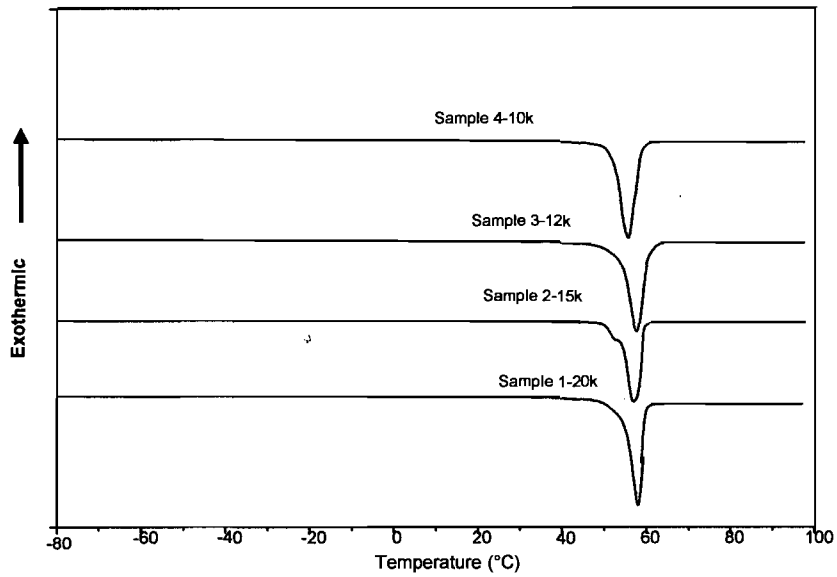

Figure 3.6. DSC traces of $CA(PEG)_4$ polymers with different molar mass showing different melting temperatures, T_m.

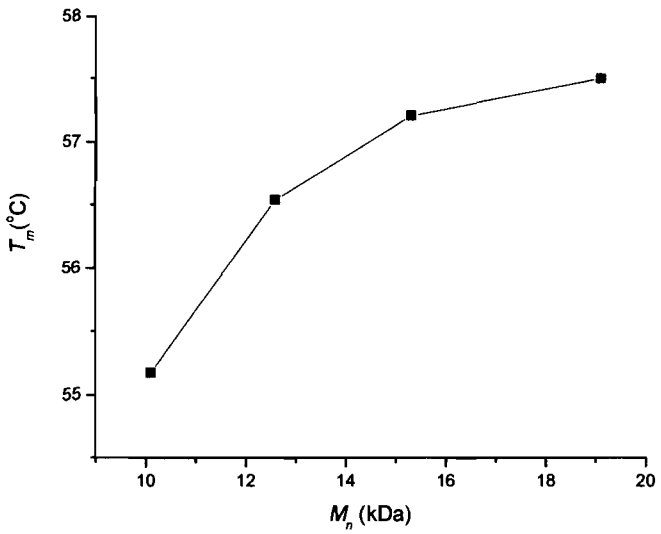

Figure 3.7. Relationship between the melting temperature (T_m) and the molar mass of the $CA(PEG)_4$ polymers.

3.3 Determination of the Molar Mass Distribution

In general, polymers do not have a single molar mass but rather have a molar mass distribution as they are made from chains of various lengths so that statistical techniques of analysis are needed to characterize them. The molar mass distribution (also known as the molecular weight distribution) is a term used to describe such a distribution (see **Appendix 2** for details). Many properties and processing methods of polymers show a strong dependence on the size of the polymer chains, so that it is essential to characterize their dimensions. Polymers with a narrow molar mass distribution can be obtained by anionic polymerization or by other living polymerization techniques. In this work, the molar mass distributions of the polymers were determined by size exclusion chromatography (SEC), SEC- MALLS, and MALDI- TOF.

3.3.1 MALDI-TOF

MALDI-TOF mass spectrometry can provide the necessary additional molecular information for a large variety of polymer classes. It is becoming routinely used for the determination of the polymer molecular weight determination, copolymerization structure, end-group analysis, and homogeneity (see **Appendix 2**).[109] **Figure 3.8** shows a typical MALDI-TOF spectrum for the $CA(PEG)_4$ polymer of **sample 18.** The use of MALDI-TOF gives irrefutable evidence of the formation of the polymers, showing signals of the EO repeating unit. The mass peak difference between each peak is 44.05 Da, which equals the mass of the repeating unit of EO. In this study, it was attempted to use MALDI-TOF to determine the MW of all the polymers but only the smallest molar mass was able to generate a good spectrum. It has been reported that mass discrimination for the lower mass components are favoured compared to the higher mass components resulting in a significantly lower average molar mass.[110] This mass discrimination effect is thought to be caused by several factors, including sample preparation, mass-dependent desorption/ionization, ion focusing/transmission, and mass-dependent ion detection.[110] Thus, the results are liable for lower molar mass. The MALDI-TOF results are influenced by the difficulty of getting higher molecular weight compounds out of the matrix support.

It is highly probable that the high molecular weight fractions of the polymers were never ionized, thus significantly lowering the molecular weight distribution. In addition, the success of a good MALDI-TOF spectrum also depends on the relative ratio of analyte to matrix. That is why we used a 2:1 and 1:1 matrix to analyte ratio but it did not make a difference in the results. The matrix roles are to separate analyte molecules from each other, absorb laser energy, and propel analyte molecules into the test chamber in the gas phase. If the matrix molecule concentration was less than was needed to separate all analyte molecules, the inter/intra molecule interaction among the analyte molecules might hinder the ionization/desorption efficiency. Furthermore, with low matrix concentration not enough laser energy is absorbed; both phenomena result in low signal counts. On the other hand, a large amount of matrix dilutes the overall analyte concentration, also causing low signal counts.

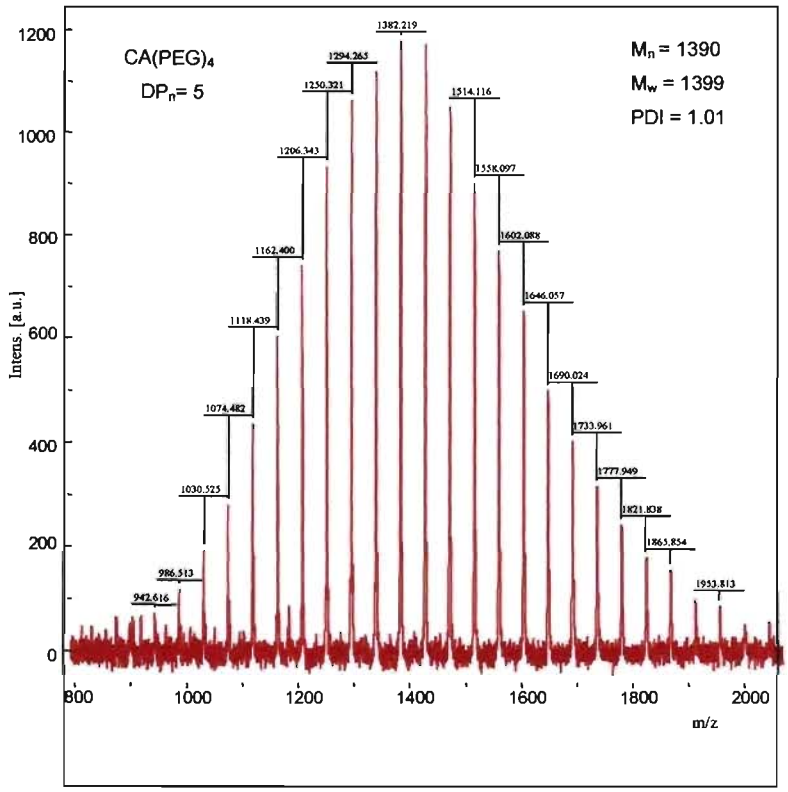

Figure 3.8. MALDI-TOF mass spectrum of $CA(PEG)_4$ polymer of **sample 18** obtained by using a N_2 laser at 337 nm wavelength with a 20 kV extraction voltage. Dithranol was used as the matrix in a saturated salt solution of LiCl.

3.3.2 SEC (size exclusion chromatography)

Size exclusion chromatography (SEC) technique is based on the observation that the lower molar mass specimens are retained longer in the column because they can diffuse more readily in the pores of the gel. Hence, the high molar mass species come out of the column before the lower molar mass molecules.

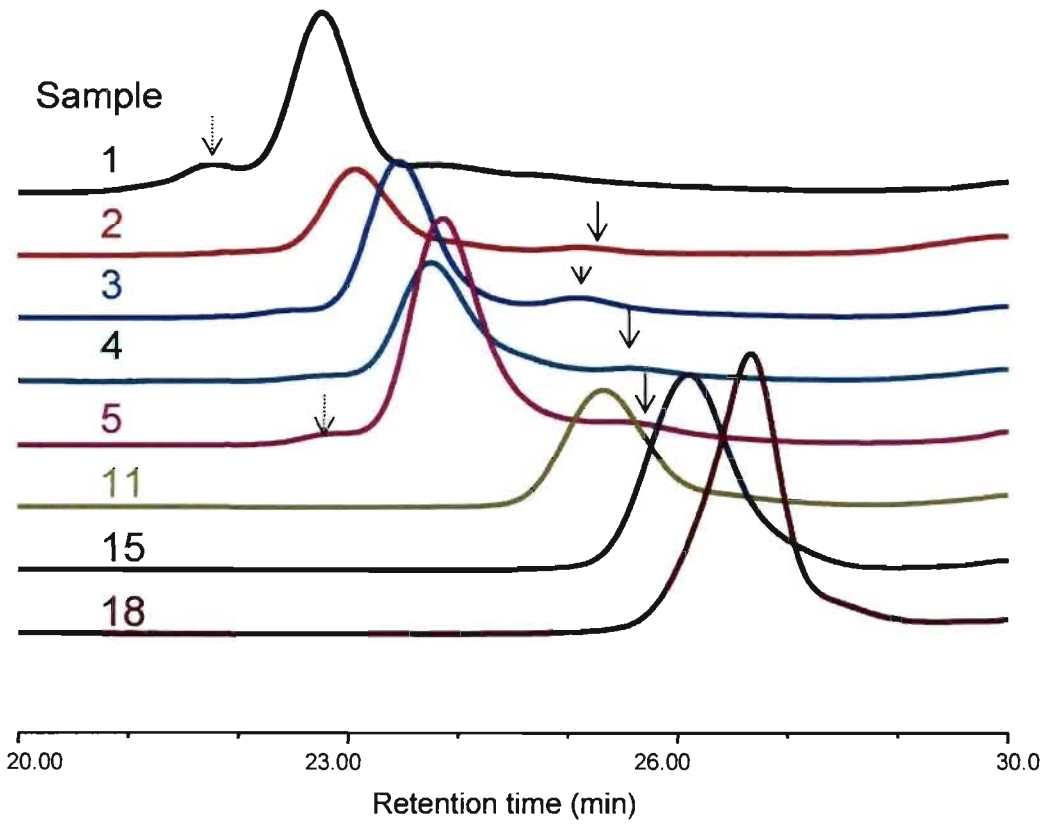

Figure 3.9. SEC traces of several molar masses of $CA(PEG)_4$ polymers in THF. Molar mass of **sample 1** = 19.1 kDa , **sample 2** = 15.3 kDa, **sample 3** = 12.6 kDa, **sample 4** = 10.1 kDa, **sample 5** = 9.5 kDa, **sample 11** = 4.0 kDa, **sample 15** = 2.4 kDa, and **sample 18** = 1.3 kDa. Sample details can be found in **Table 3.1**. Lined arrows indicate traces of low molar mass samples and dotted arrows indicate the presence of high molar mass.

Table 3.1. Molar mass of $CA(PEG)_4$ polymers obtained by size exclusion chromatography (SEC) measurements in THF.

Sample	EO units (X 4 arms)	M_n (g/mol)	M_w (g/mol)	PDI
1	106	19 110	19 340	1.01
2	84	15 320	16 050	1.05
3	69	12 660	13 120	1.04
4	55	10 080	10 600	1.05
5	51	9 500	9 970	1.05
6	40	7 450	7 680	1.03
7	39	7 320	7 616	1.05
8	32	6 020	6 840	1.14
9	26	5 080	6 420	1.20
10	25	4 850	6 490	1.33
11	20	4 404	4 230	1.04
12	17	3 470	3 570	1.05
13	16	3 420	3 580	1.04
14	15	3 160	3 350	1.11
15	11	2 380	2 540	1.07
16	8	1 850	1 930	1.05
17	7	1 640	1 760	1.07
18	5	1 330	1 360	1.02

Traces of low molar mass fractions were observed for the higher molar mass polymers **(samples 2, 3, 4 and 5)** shown in **Figure 3.9** and are indicated by a lined arrow. This could be related to a small extent of incomplete anionic ring-opening polymerization initiation resulting in fewer arms, or a small extent of chain-transfer reactions resulting in some smaller arms and some linear chains. These low molar mass fractions could not be separated by solvent extraction which led to a slight broadening of the molar mass distribution.

The amount of the initiator needed for the polymerization was small because only 25% deprotonation was required,[111] therefore, it was hard to measure the precise amount of initiator due to the imprecision of measurements of volumes smaller than 1 mL. Thus, the excess amount of initiator may have activated the polymerization of some linear PEG chains. Another possible way to explain the presence of small linear PEG chains in the SEC traces is from the distillation of the EO in *tert*-butyl lithium in hexane solution. In the final preparation, the EO is distilled out of the *tert*-butyl lithium solution in hexane by warming the round bottom flask to condense the EO vapors into the graduated cylinder, which is being cooled in a dry-ice acetone bath. If the temperature was too high, the *tert*-butyl lithium might have initiated the polymerization of some linear PEG chains.

As also seen in **Figure 3.9**, the SEC traces show the presence of high molar mass fractions especially for **samples 1** and **5,** which is indicated by a dotted arrow. This could be related to the formation of aggregates. The low molar mass **sample 18** shows a low molar mass tail in the otherwise narrowing peak at the highest M_n = 1.3 kDa (**Figure 3.9** and **Table 3.1**), which can indicate slow propagation of a fraction of the chains.[14] This can be due to non-uniform concentrations at the gas-liquid interface, resulting from ineffective mixing in the highly viscous reaction system at these molar masses.

In general, the SEC is a good method to determine the molar mass of polymers. The results greatly depend on structural resemblance of the standards, which are used to make the calibration curve, to that of the polymer being analyzed. In SEC measurements, the polymer molecules are fractionated according to the hydrodynamic volume. The size of star polymer molecules is known to be smaller than that of linear ones having the same molar mass.[112] Therefore, the SEC method underestimates the molar mass of the star polymers due to their compact volumes compared to linear polymers.

Moreover, amphiphilic macromolecules, which contain segments of with very different polar properties, have their distribution of the chemical composition change with the overall interactions with the solvent, thus, disturbing the relationship between the hydrodynamic volume and the molar mass. Therefore, the true molar mass cannot be obtained using SEC alone.

The addition of a multiangle laser light scattering detector (MALLS) to SEC enabled molar mass to be determined absolutely and independently of any calibration or reference standards from each slice of the polymer fraction (see **Appendix 2**). The precision of this method requires that the concentration of each eluting fraction be known as well as the specific differential refractive index increment, *dn/dc.* The *dn/dc* describes the change of the refractive index of a polymer solution relative to the change of the polymer concentration. The *dn/dc* value depends on the polymer composition, solvent, and wavelength. [113] The determination of *dn/dc* is done using one of the two following methods described below. The online method allows the calculation of the *dn/dc* from the peak of the injected sample of known concentration and volume. It also assumes that 100% of the injected polymer elutes from the column. On the other hand, the offline method calculates the *dn/dc* from a slope obtained by preparing several known concentrations using the differential refractive (DRI) detector with the following equation:

$$\Delta n = \frac{dn}{dc} \times c \tag{3.1}$$

where Δn is the differential refractive index and c is the concentration of the sample. Such an example is shown in **Figure 3.10** where the *dn/dc* was measured offline and gave the same values as the *dn/dc* measured online. Therefore, for several of the polymers studied, the *dn/dc* online was sufficient for the calculations of the molar mass.

The SEC-MALLS technique assumes that the molar mass of each elution slice contains molecules of a single molar mass, or at least a very narrow distribution. The molar mass for each slice is calculated according to the Zimm and Stockmayer equation:[112]

$$\frac{R_\Theta}{K^* c} = MP(\Theta) - 2A_2 cM^2 P^2(\Theta) + \ldots \tag{3.2}$$

where R_Θ is the excess Rayleigh ratio; K^* is a constant; c is the solute concentration (g/mol); M is the weight-average molar mass; $P(\Theta)$ is the form factor or "scattering

function" and approximately equal to $1\text{-}2\mu^2\langle r^2\rangle/3!+\ldots$, where $\mu=(4\pi/\lambda)\sin(\theta/2)$, and $\langle r^2\rangle$ is the mean square radius; and A_2 is the second virial coefficient (mL mol/g^2). For vertically polarized incident light with a wavelength λ_0 in vacuum, K^* is denoted by:[113]

$$K^* = \frac{4\pi^2 n_0^2}{\lambda_0^4 N_A}\left(\frac{dn}{dc}\right)^2 \tag{3.3}$$

where n_0 is the refractive index of the solvent, N_A is the Avogadro's number, and *dn/dc* is the specific refractive index increment.

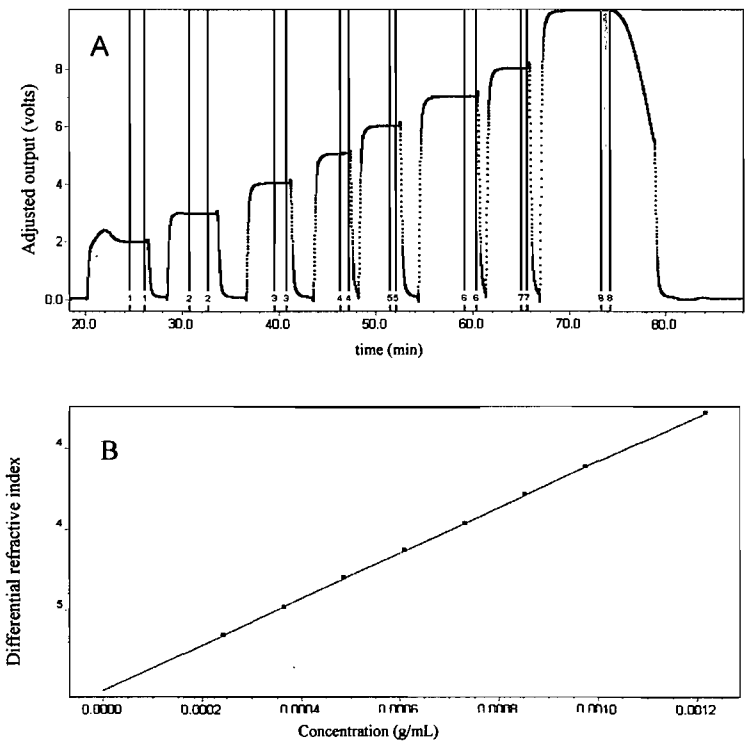

Figure 3.10. Determination of *dn/dc* offline of **sample 13** (3.4 kDa) of CA(PEG)$_4$ polymer in water. **(A)** shows the area selected of the differential refractive index data and **(B)** shows the slope of the resulting RI data. *dn/dc* offline = 0.1412 ± 0004 mL/g and *dn/dc* online gave 0.1417 mL/g.

The concentration of the polymer is measured for each elution slice using a refractive index detector. A plot of $R_\Theta/(K^*c)$ or $(K^*c)/R(\Theta)$ as a function of $\sin^2(\Theta)$ is constructed at each retention time to give M and the root mean square (RMS) radius distribution. These plots are commonly referred to as Debye and Zimm plots respectively. M can be determined from the intercept at zero angle whereas the slope yields the mean square radius.[113] The second virial coefficient, A_2, is essentially zero if the concentration is sufficiently small ($A_2 c = 0$). When $A_2 = 0$, the **Equation 3.2** can be simplified to give:

$$M = \left(\frac{K^* c}{R_0} \right)^{-1} \tag{3.4}$$

and

$$\left\langle r^2 \right\rangle^{1/2} = \frac{\sqrt{3\lambda_0}}{4\pi n_0} \sqrt{m_0 M} \tag{3.5}$$

After the concentration, molar mass, and mean square radius have been determined for each slice, the molar mass and the square radius can be calculated. The radii of the star-shaped polymers are not shown here due to the large errors in their estimations. This is because the size of the polymer molecules in the solution is small enough such that the particle scattering function $P(\Theta)$ becomes unity and the scattered light is no longer angular dependant. Therefore, no meaningful R_g values could be obtained. Also the resolution limitations of the instrument are dependant on the wavelength of the laser which is 690 nm. The minimum reliable size that can be measured with the instrument is 10 nm and the size of the $CA(PEG)_4$ polymers are smaller than 2 nm, which will be discussed later.

Molar mass obtained with SEC-MALLS for the $CA(PEG)_4$ polymers in water and in phosphate buffer saline (PBS) solution are given in **Table 3.2.** Note that **Table 3.2** shows data for the *weight average* of the molar mass (M_w). Marked differences are observed for the polydispersity index (PDI) and M_w obtained with SEC only and SEC coupled with MALLS. This is due to the occurrence of peak broadening observed with SEC, which caused each elution slice to contain a non-monodisperse mixture. As a result

of this effect, SEC with MALLS has a tendency to overestimate the *n* average molecular weight, in spite of these broadening effects; we may in practice still make the assumption that each slice is monodisperse (only one molar mass is present).[113] There is no obvious difference between the M_w obtained in water and in PBS except that the molar mass obtained in PBS appeared slightly larger. Although SEC-MALLS is an absolute method, the changes in the composition of the amphiphilic polymer also alter the *dn/dc*, which may cause errors in the measured molar mass.[114] Therefore, great caution has to be exercised when interpreting the molar mass data for the amphiphilic star polymers.

Table 3.2. Molecular weights for $CA(PEG)_4$ polymers in water and PBS obtained by conventional SEC and SEC-MALLS measurements.

Sample	SEC		SEC/MALLS			
	THF		Water		PBS	
	M_w (g/mol)	PDI	M_w (g/mol)	PDI	M_w (g/mol)	PDI
1	19 340	1.01	22 540	1.12	28 130	1.47
2	16 050	1.05	21 500	1.22	20 370	1.32
3	13 120	1.04	13 890	1.11	15 840	1.30
4	10 600	1.05	13 800	1.04	13 430	1.25
5	9 970	1.05	9 980	1.05	10 460	1.07
6	7 680	1.03	8 100	1.18	8 730	1.15
7	7 616	1.05	10 300	1.91	10 360	1.07
8	6 840	1.14	6 130	1.24	7 410	1.21
11	4 230	1.04	4 840	1.05	5 780	1.04
12	3 570	1.05	4 240	1.03	5 930	1.06
13	3 580	1.04	4 630	1.09	5 500	1.08

SEC in THF data are taken from Table 3.1

Examples of molar mass distributions for the $CA(PEG)_4$ star-shaped polymers are given in **Figure 3.11**. A small peak is observed in the high molecular weight distribution

especially when water was used as the solvent. This is probably due to some aggregation of the PEG polymers in water. As mentioned in **Section 2.2,** a concentration of about 10 mg/mL was used to dissolve the polymers. Such a high concentration was necessary in order to achieve a decent detector signal. The aggregates were greatly reduced when a salt solution of PBS was used (**Figure 3.11.b**) A bimodality distribution was observed for the high molar mass polymer **sample 1,** which is indicative of non-controlled anionic polymerization as discussed in the preparation method.

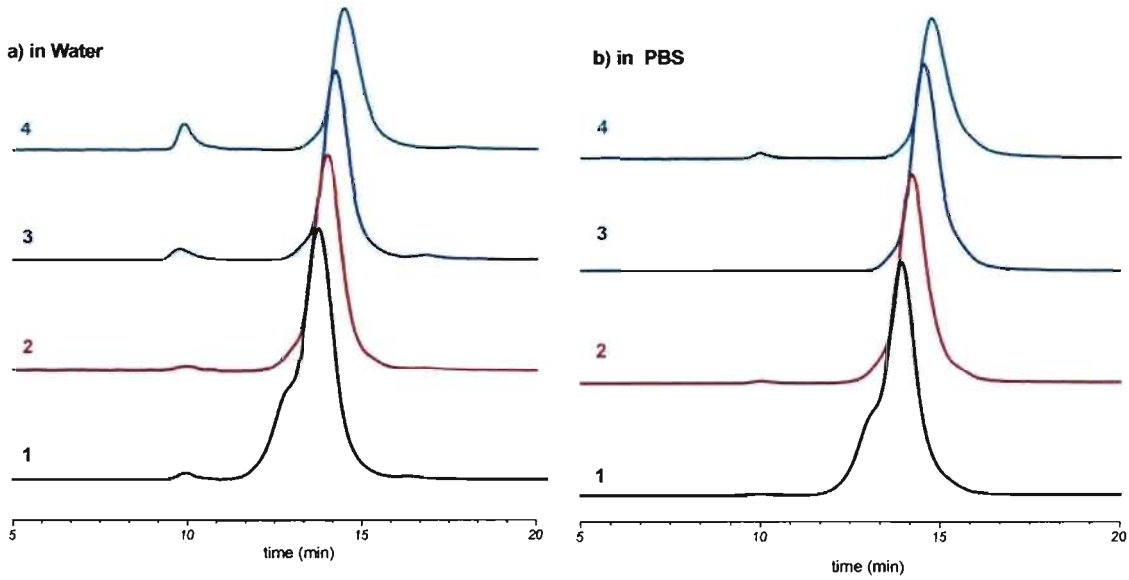

Figure 3.11. SEC-MALLS chromatogram of star shaped-polymers $CA(PEG)_4$ a) in water and b) in phosphate buffer saline solution (PBS). **Sample 1** = 19.1 kDa; **sample 2** = 15.3 kDa; **sample 3** = 12.6 kDa; and **sample 4** = 10.1 kDa.

In general, the molar masses obtained from SEC-MALLS are higher and have a greater PDI than in SEC with THF as the eluent. The SEC-MALLS is not without its limitation for the determination of molar mass of the polymers. First, the SEC-MALLS method cannot quantify low molar mass polymers below a few thousands kDa. This arises due to the uncertainty of measured radius of gyration (R_g) values increasing rapidly as the size of the polymers approaches the cut-off molar mass at which the angular

dependence of the scattered light disappears. Theoretically, light scattering can detect sizes down to about a 20th of the incident wavelength.[115] In addition, for a given concentration (c), the scattered light signal (I) is proportional to the molar mass, (M) and dn/dc:

$$I_{scattered} \propto Mc\left(\frac{dn}{dc}\right)^2 \tag{3.6}$$

This implies that for low M, relatively high concentrations are required to produce detectable light scattering signal. However, in practice the concentrations of low M polymers cannot meet the S/N requirement. If the concentration were high, the viscosities of the polymer solution would be too high to obtain good quality chromatograms, which would result in column overloading and flow problems causing poor detection limit, or high errors for the R_g at the low M.

Since SEC alone requires a calibration curve to determine the molar mass, it is considered as a relative method. However, SEC alone can provide a rapid and good estimation of molar mass when the other characterization instruments are not available. Absolute molar mass determination is possible when MALLS is combined to SEC or with MALDI-TOF. However, as mentioned above, MALDI-TOF is more sensitive for lower molar mass polymers whereas SEC-MALLS is not. Therefore for the determination of the distribution of the lower molar mass, MALDI-TOF is preferable and for higher molar mass, SEC-MALLS is better.

Determination of the Number of Arms

The Zimm-Stockmayer approach[112] was employed to determine the number of arms or branching ratio in the CA(PEG)$_4$ star-shaped polymers. As discussed above, in SEC-MALLS both the M and R_g are measured simultaneously at each elution slice of a chromatogram. For example, **sample 8** was used to determine the number of arms in the polymer. The SEC chromatograms as a function of the elution volume of the linear PEG and **sample 8** of the star-shaped CA(PEG)$_4$ polymers in water are shown in **Figure 3.12**.

Information about the branching ratio can be obtained by two methods. The first method consists of plotting the R_g against the molar mass (conformation plot) and in the second method, the molar mass is plotted against the elution volume. Since the R_g values were outside the limit of the instrument as mentioned above, the mass method was used to determine the number of arms. The mass method compares molar masses at equal elution volumes and requires overlapping of the linear and the branch plot (**Figure 3.13**).

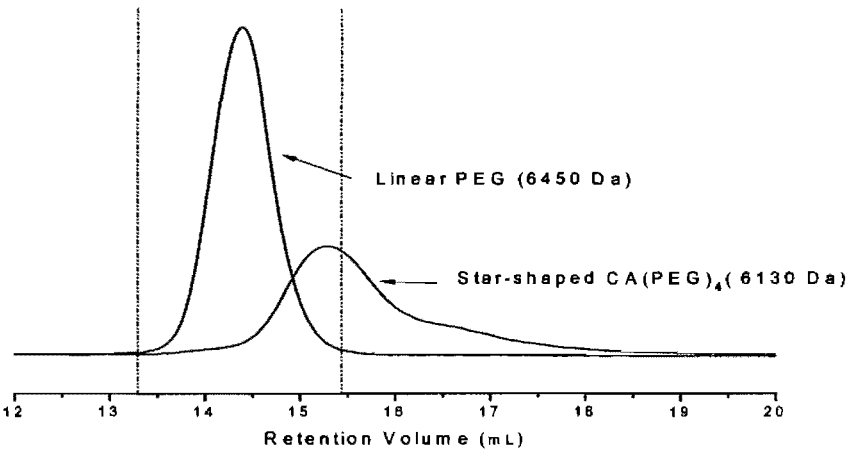

Figure 3.12. An overlay of molar mass distribution as a function of the elution volume at 90° light scattering for the linear PEG and **sample 8** of the star-shaped $CA(PEG)_4$. The two vertical lines delimit the overlapping region of the elution volume of the two polymers.

Figure 3.13 shows that both the linear and the star-shaped sample had abnormal SEC elution behaviour: the star-shaped curves up at low elution volumes and for the linear PEG, the plot curves back up at high elution volumes rather than the normal linear decrease with increasing elution volume. The curvature is usually typical of highly branched polymers.[115] However, in our case the curvature was much more pronounced for the linear sample. This may be due to the nonsize exclusion mechanisms (e.g. adsorption) that can delay some molecules. Due to this effect, the slices of higher elution volume can

contain a mixture of molecules of lower molar mass and molecules of higher molar mass that were retained by the nonsize exclusion mechanisms, which is frequent in aqueous SEC.[103] Also, the curves strongly deviate at low elution volumes. This deviation is due to the presence of branching. Branched molecules are more compact than linear ones and therefore they have smaller sizes when molar mass are equal. The retardation of the large molecules in the size exclusion separation reflects the molecular architecture of branched molecules, though the origin of the retardation remains unclear.[116] The delay in the size exclusion separation may be due to mechanical entanglements in the column packing and their later elution with smaller molecules.[117]

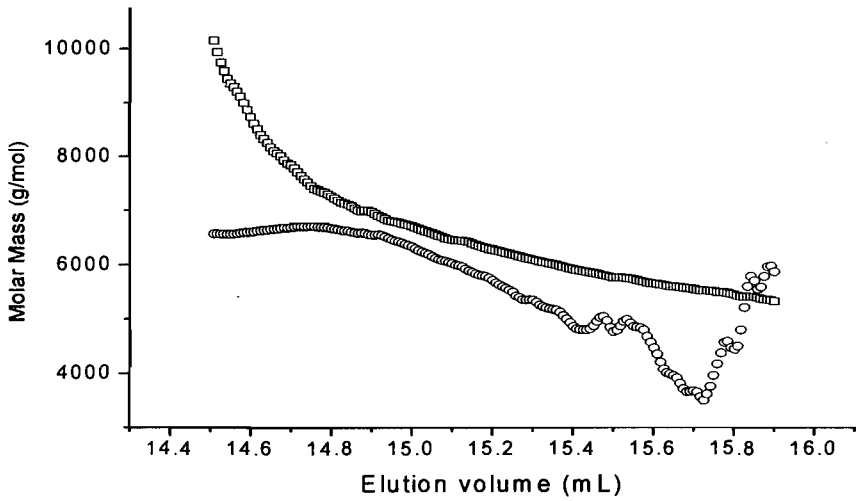

Figure 3.13. The molar mass overlap between the linear PEG (○) and star-shaped $CA(PEG)_4$ (□) at each elution volume using the data selected from the region defined by the two vertical lines in **Figure 3.12.**

In order to determine the number of arms for the star-shaped polymers, the branching ratio (g_M) must be determined first. The branching ratio (g_M) equals unity for linear polymers and decreases with increasing number of branches.

The g_M can be calculated from:

$$g_M = \left(\frac{M_{lin}}{M_{br}} \right)_V^{(1+a)/e} \tag{3.7}$$

where M_{lin} and M_{br} are the molar mass of linear and branched polymers, respectively, a is the Mark-Houwink exponent for the linear polymer, and e is the draining parameter ranging from 0.5 to 1.5. The draining parameter e is generally unknown and changes with the molar mass.[116] The ratio of the molar masses is taken at the same elution volume V and is calculated for all volume slices of the overlapping region as shown in **Figure 3.12**. The branching ratio for star-shaped CA(PEG)$_4$ polymers is shown in **Figure 3.14** where typically for PEG polymers a = 0.712 and e =1.[118]. **Figure 3.14** shows that the g_M is lower than unity meaning that there is branching in the polymer.

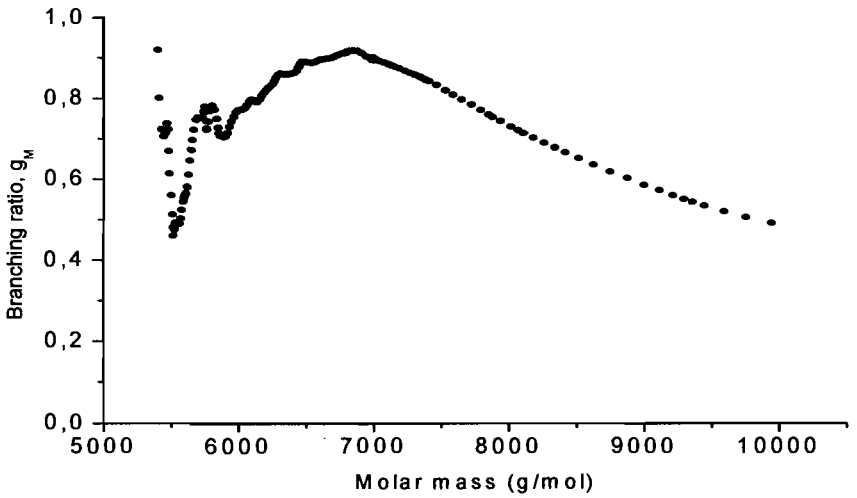

Figure 3.14. Branching ratio versus molar mass for **sample 8** of the star-shaped CA(PEG)$_4$ polymer calculated by the mass method using a = 0.712 and e = 1 in **Equation 3.7.**

A fundamental model for the determination of branching has been derived by Zimm and Stockmayer.[112] It can be used for the determination of the number of arms in a polymer from molecular weight and R_g data obtained from SEC-MALLS. The branching

ratio, g_M, is related to the average number of branching units or arms per molecule for star polymers with monodisperse arms of equal length linked together by

$$g_M = \frac{3f-2}{f^2} \tag{3.8}$$

where f is the number of arms. The model would be appropriate for star molecules produced under controlled anionic polymerization conditions where the chains emanate from a central core.[119] For **Eq. 3.8**, the left hand side g_M is known already (see **Figure 3.14**). The equation is solved for f for each slice which produced a reasonable value of g_M. Note that if g_M falls outside of 0 to 1, no value of f will be calculated for that slice. Note that when g_M equals unity it signifies no branching, whereas values lower than unity signifies that there is branching in the sample. The Astra software generated the corresponding data shown in **Figure 3.15**. By simply finding the molar mass of the branched sample that was used, in this case **sample 8** (6 130 Da), and tracing a line unto the y-axis, the number of arms can be determined, and was found to be four (**Figure 3.15**). Therefore, **sample 8** shows branching character and the star-shaped polymer most likely has four arms.

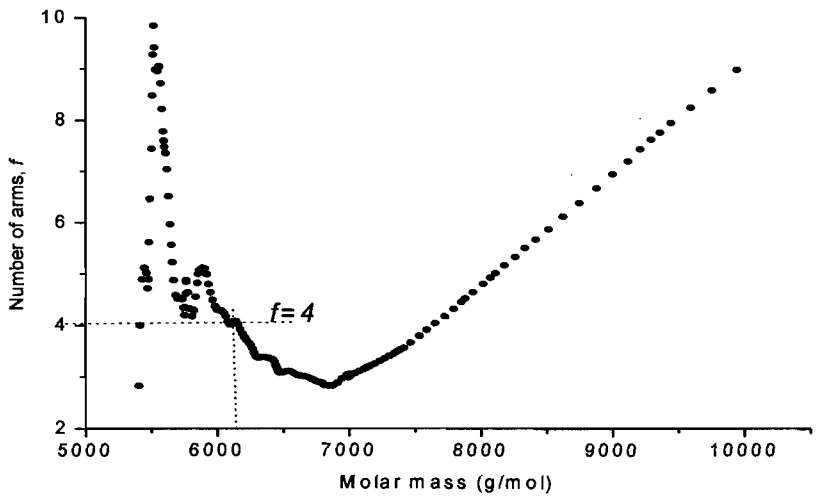

Figure 3.15. Determination of the number of arms for a star-shaped $CA(PEG)_4$ polymer of **sample 8** (6 130 Da). The number of arms (f = 4) is determined by tracing a line from 6 130 Da to the y-axis.

The determination of the number of arms by using the mass technique is not without its own limitations. The equation assumed that the polymers have the same hydrodynamic volume, when we know that star-shaped polymers are more compacted than linear polymers of the same type. What **Figure 3.15** does show is the presence of branching in the polymer and provides a good estimation of the number of arms that is present in the polymer.

3.4 Determination of the Hydrodynamic Radius, R_h

Star shaped polymers recently attract increasing interest due to their compact structures, which may lead to peculiar rheological properties. This is of particular interest for the modification of the RBC rheology. The influence of the size in aqueous environment of a macromolecule on RBC aggregation is an important factor to consider and may be even more important than the specific type of macromolecule.[6] As it was mentioned in the introduction, Armstrong et al. showed that macromolecules including non-ionic polymers and plasma proteins with a hydrodynamic radius (R_h) smaller than 4 nm were able to inhibit RBC aggregation, whereas those with R_h greater than 4 nm promoted RBC aggregation.[6] The R_h of the individual samples of the $CA(PEG)_4$ star-shaped polymers were calculated from their intrinsic viscosities using the Einstein viscosity relation.

Polymer concentrations of 1, 3, 5, 7, 13, 17, and 23 mmol were prepared by adding an appropriate amount of polymer in doubled distilled water. All solutions were clear and without evidence of precipitation. The viscosities (η) of the solutions were measured at 25 °C using a viscometer. The specific viscosity (η_{sp}) is the fractional change in viscosity upon addition of polymer and is defined as

$$\eta_{sp} = (\eta / \eta_o) - 1 \tag{3.9}$$

where η and η_o are the viscosities of the solution and of the solvent, respectively. To eliminate the effects of intermolecular interference on viscosity, it is necessary to extrapolate to infinite dilution. The intrinsic viscosity [η] (mL/g) of the polymers

solutions were determined by extrapolation of η_{sp} divided by the concentration (c) versus the concentration to infinite dilution:

$$[\eta] = \lim_{c \to 0}(\eta_{sp}/c) = \lim_{c \to 0}\{(1/c)\ln(\eta/\eta_0)\} \quad (3.10)$$

Both (η_{sp}/c) and $(1/c)\ln(\eta/\eta_0)$ showed reasonably good linear dependence on the concentration expressed in ml/g . An example for **sample 4** is shown in **Figure 3.16.**

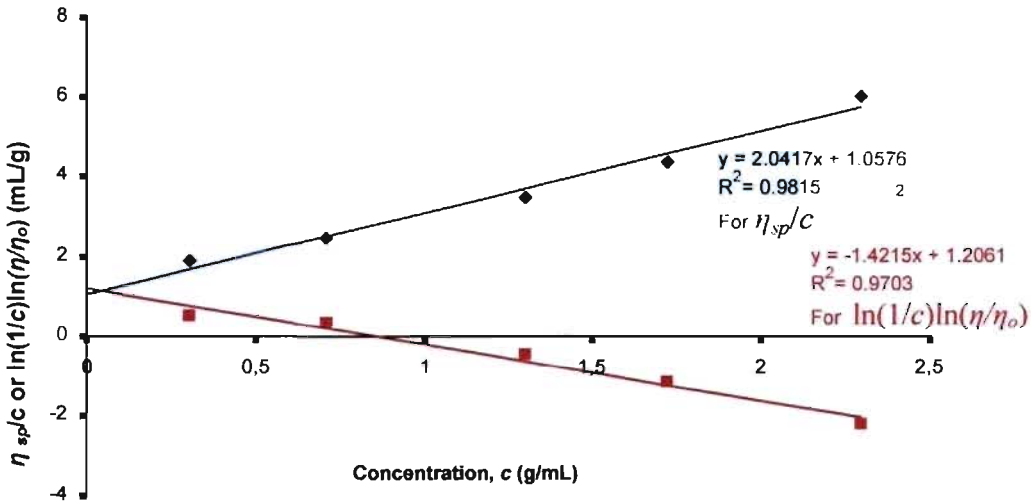

Figure 3.16. Determination of the intrinsic viscosity of the star-shaped CA(PEG)$_4$ polymer in water at 25 °C for **sample 4** with a molar mass of 10.1 kDa .

The hydrodynamic radius (R_h) of the polymers were determined by using a previously published method.[6] R_h was assessed according to Einstein viscosity relation, modeling the hydrated polymer molecules in terms of equivalent hydrodynamic spheres that would increase the viscosity to the same extent as solid spherical particles of volume V_e:

$$[\eta] = \frac{2.5NV_e}{M} \quad (3.11)$$

where M is the molecular weight of the polymer in g/mol, N is the Avogadro's number, and V_e is the volume of an equivalent spherical particle. Since $V_e=\frac{4}{3}\pi R_h^3$, rearrangement of **Equation 3.11** gives:

$$R_h = \left(\frac{3[\eta]M}{10\pi N}\right)^{1/3} (cm) \qquad (3.12)$$

The values of the R_h and the $[\eta]$ of the samples are listed in **Table 3.3** and are illustrated in **Figure 3.17.** The CA(PEG)$_4$ polymers in water have a compact structure with a R_h value less than 2 nm and a low intrinsic viscosity. The viscosity effect depends on the temperature, the nature of the solvent and polymer, the polymer concentration, and the size and shape of the macromolecules. Typically, the viscosity of a solution increases as the molar mass of the macromolecules increases. **Figure 3.17** shows a linear increase of the $[\eta]$ and R_h with increasing molar mass, however, at high molar mass (~15 kDa), the $[\eta]$ starts to increase much more rapidly than the R_h. The plot of $[\eta]$ shown in **Figure 3.17**, consists of two distinct linear regions. The second region has a relative slope value of approximately 1.8 to that of the first region. The differences between these two regions can be explained in terms of two competitive effects in polymer solutions: free volume and entanglements.[120] A polymer with shorter chains has more space to move freely, thus it has less chain entanglements. Therefore its viscosity is defined primarily by its free volume, while a polymer with longer chains has more chain entanglements and less movement. This means that its viscosity is defined mostly by chain entanglements than free volume effects. This is a common behavior for a wide range of polymers.[120]

In a polymer solution, because the solvent is inside the polymer coils, it cannot attain the velocities it would have in the absence of the polymer. These random coils can be perceived in the Einstein's equations (**Eq. 3.12**). Thus, the intrinsic viscosity method assumes that the radius of the spheres is constant, while in reality the shape of the polymer coil continuously changes as the polymer segments are in constant motion. From **Equation 3.12**, the intrinsic viscosity depends on the molar mass and this relationship is usually expressed with the Mark-Houwink equation:

$$[\eta] = KM^{a} \qquad (3.13)$$

where M represents the viscosity average-molar mass, and K and a are Mark-Houwink constants. These constants depend upon the polymer and solvent. The molar mass of the polymers were not determined by this method because it has been determined by more reliable methods such as SEC-MALLS, consequently, it was only used to determine the hydrodynamic radius.

Table 3.3. Experimental results and equivalent sphere hydrodynamic radius for the star-shaped CA(PEG)$_4$ polymers in doubled distilled water.

Sample	M_w (g/mol)	M_n (g/mol)	Intrinsic viscosity $[\eta] \pm \Delta_b$ (g/mL)	Hydrodynamic radius $R_h \pm \Delta_h$ (nm)
1	22 540	20 130	2.26 ± 0.89	1.90 ± 0.76
2	21 500	17 580	1.81 ± 0.70	1.64 ± 0.63
3	15 350	13 890	1.21 ± 0.16	1.34 ± 0.14
4	13 800	12 300	1.06 ± 0.23	1.18 ± 0.66
11	4 840	4 620	0.35 ± 0.09	0.62 ± 0.17
15	2 540	2 380	0.13 ± 0.12	0.38 ± 0.13
18	1 360	1 330	0.04 ± 0.11	0.20 ± 0.12

M_w is average molar mass determined by size exclusion chromatography coupled to multi-angle laser light scattering (SEC-MALLS) in water
M_n is the number-average molar mass determined by SEC-MALLS in water
Δ_b is the confidence limits for the intercept b for the linear regression $y = mx+b$ for N = 5 at 95% confidence interval
Δ_h is the standard deviation of R_h.

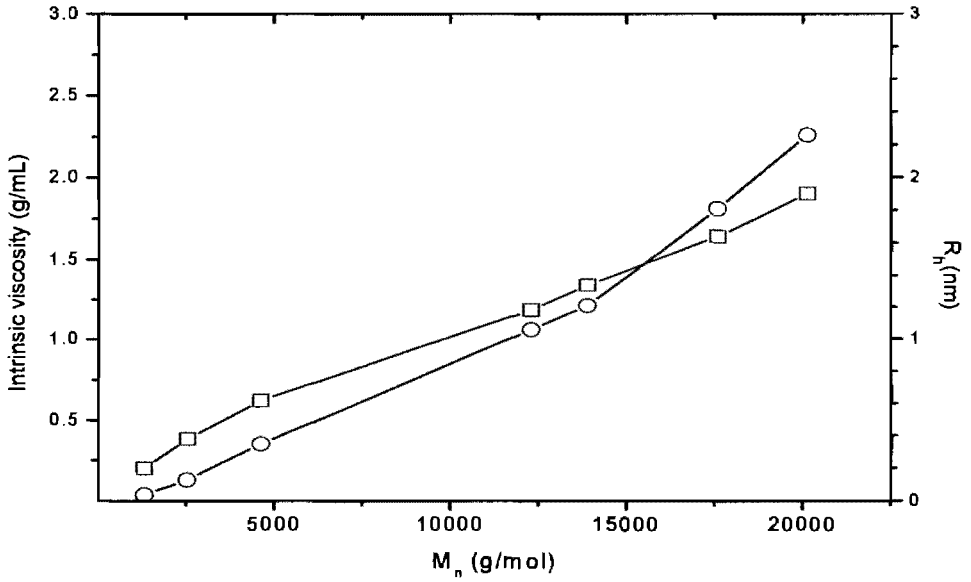

Figure 3.17. Intrinsic viscosity [η] (○) and hydrodynamic radius (R_h) (□) against the average-number molar mass (M_n) for a series of solutions of $CA(PEG)_4$ polymers in water at 25 °C.

3.5 Rheology Study of the Star-Shaped Polymers

The small size of the star-shaped $CA(PEG)_4$ polymers and branching character can lead to unique properties. These polymers are compact and have high segment density, which is unobtainable by most other types of polymers. Some of their unique properties are lower crystallinity, and lower solution viscosity than those of corresponding linear polymers. Most importantly of interest for this study are their solution viscosity properties as they pertain to the modification of red blood cell (RBC) aggregation.

The concentration dependence on the flow curves is shown in **Figure 3.18** for **sample 1** (19.1 kDa) in water. Below the concentration of 0.3% (w/v) there was no significant difference between water and the polymer solutions. Beyond 0.3%, there was a significance among flow curves with $P < 0.05$ and the viscosity increased as the

concentration increased. The increase of polymer concentration in water results in more frequent contacts between the macromolecules and the formation of chain entanglements.[19]

.

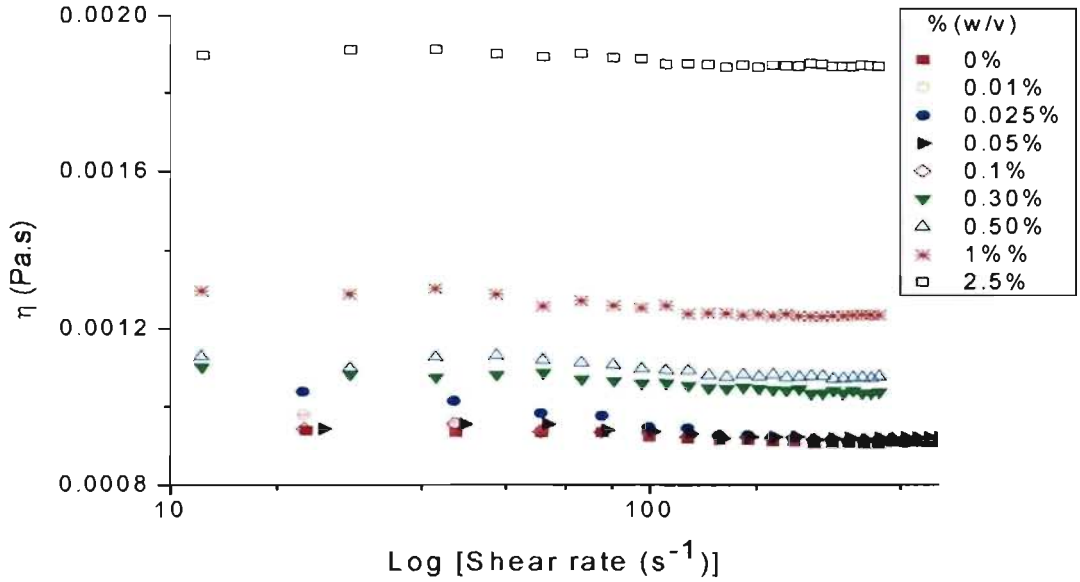

Figure 3.18. Semi log scale plot of the concentration dependence on the flow curves of star-shaped $CA(PEG)_4$ polymer of **sample 1** in water with a molar mass of 19.1 kDa at 25 °C. A significant difference was found for concentrations above 0.1% for multiple pair-wise comparisons with $P < 0.05$ using Anova test.

The molar mass dependence on the flow curves of the $CA(PEG)_4$ polymers at 0.3% (w/v) in water is depicted in **Figure 3.19**. Shear thinning occurred at low shear rates for the star-shaped polymers. Under the action of shear stress, the polymers align, orient, and disentangle themselves in order to flow more easily. The highest molar mass 19.1 k Da exhibits the highest apparent viscosity around 0.001 Pa.s and the lowest molar mass exhibits the lowest apparent viscosity around 0.00095 Pa.s. However, under shear rate, the normal increase in the apparent viscosity with the molar mass is not observed for the

molar mass 10 kDa, which shows lower apparent viscosities than the 4 kDa and the 15 kDa, which shows lower apparent viscosities than the 12 kDa. These inconsistent behaviors may be due to the fact that star polymers consisting of shorter arms, have chain stiffness and greater interaction with the core, which can cause competiting effects.[121] Though, it was shown that the star polymer had branched architectures, it is also possible that the length of each arm or the degree of polymerization is not equal for each arm. These possibilities could account for the unpredictable behavior of the molar mass effect.

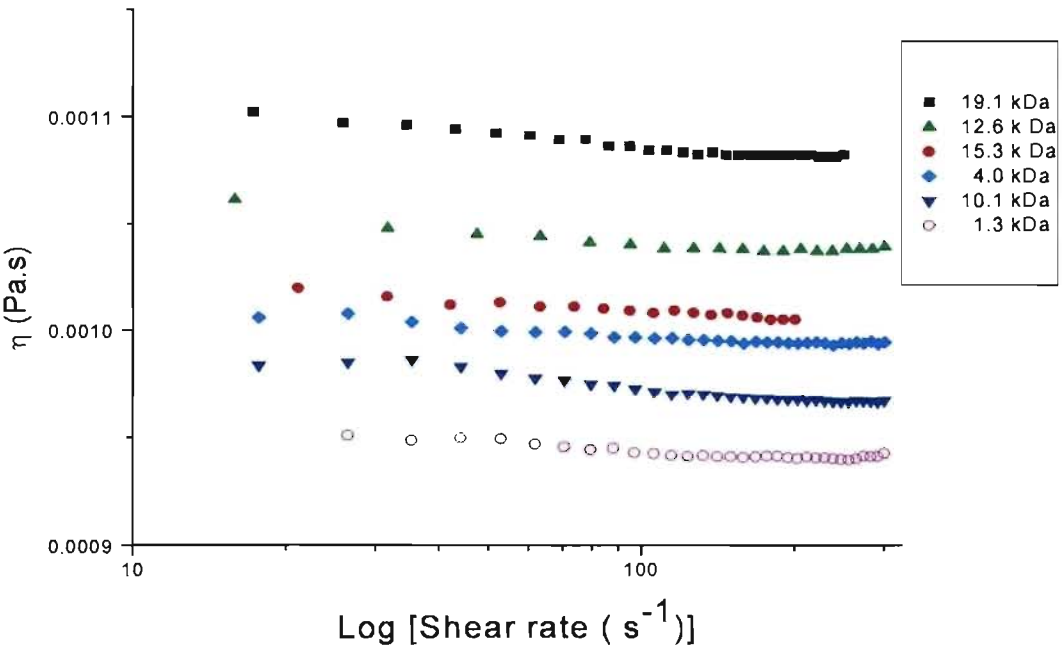

Figure 3.19. Semi log scale plot of the molar mass dependence on the flow curves for star-shaped $CA(PEG)_4$ polymer in water at 25 °C. A significant difference was found for multiple pair-wise comparisons with $P < 0.05$ for Anova test.

The viscosity profiles of different molar mass of the star-shaped polymers were also studied in phosphate buffer solution (PBS) at a concentration of 0.3 % (w/v). PBS is a buffer saline solution that is commonly used in biological applications because the

osmolarity and ion concentrations of the solution usually match that of human blood.[122] **Figure 3.20** shows pronounced shear thinning behavior for all polymers at 25 and 37 °C. This shear-thinning viscosity behavior results from the coil-like behavior of most polymer fluids.[120] Under shear, the coils rotate causing disentanglement/entanglement with their neighbors. This means high apparent viscosity at low shear rate. As the shear rate increases, the coils rotate too fast to re-entangle, so the apparent viscosity decreases. **Figure 3.20** also shows that there is no molar mass effect at the 0.3% (w/v) concentration for the star polymers in PBS and that there is no significant difference between the viscosity profiles at 25 and 37 °C with $P > 0.05$.

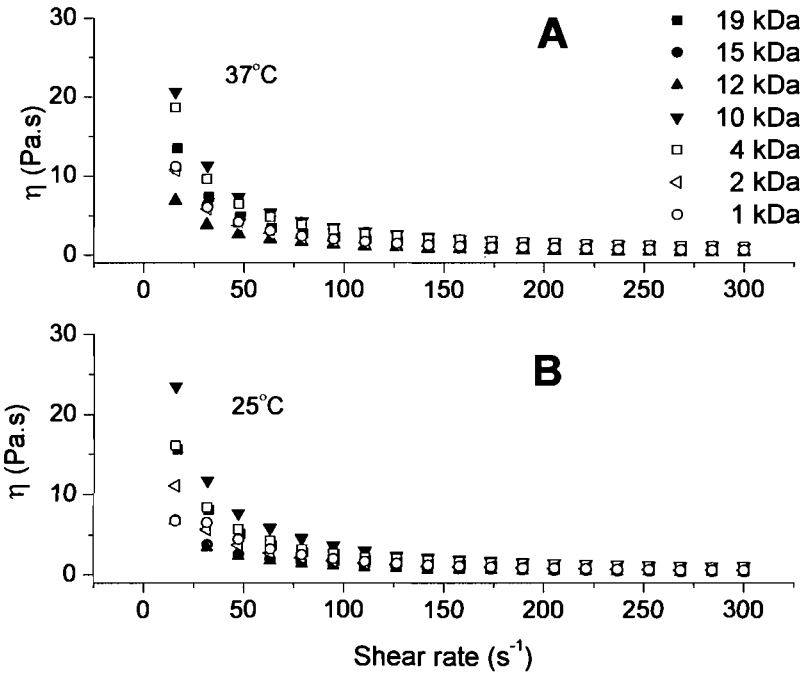

Figure 3.20. Shear thinning behavior of the viscosity profiles of $CA(PEG)_4$ polymers in phosphate buffer saline solution (PBS) at 0.3% (w/v) (**A**) at 25 °C and (**B**) at 37 °C. No significance difference was found at 25 and 37 °C for multiple pair wise comparisons ($P > 0.05$, Anova).

The presence of salts or ions in solution usually disrupts the hydrogen bonding or the ordered arrangement of the water structures along the PEO chains which should in practice decrease the viscosity.[123] However, the viscosities of the polymers in PBS are remarkably greater compared to the $CA(PEG)_4$ solutions in pure water. This suggests a more complex arrangement of the polymers in saline solutions. Clearly, this reveals that $CA(PEG)_4$ in solution possesses interesting rheological properties that merit more in depth studies.

In summary, the rheological results showed that the $CA(PEG)_4$ in solution exhibit pronounced shear thinning behaviour especially for high molar mass fraction and that the viscosity was considerably higher in PBS solution than in water.

CHAPTER 4: BLOOD EXPERIMENTS

The effect of the star-shaped $CA(PEG)_4$ polymers on RBC aggregation and viscosity were compared to linear PEGs by the following techniques: a rheometer was utilized to measure the effect of the polymer samples on blood viscosity at varying shear rates; a laser aggregometer was used to quantify the extent of RBC aggregation by measuring the rate of change of light transmission through a sheared blood sample; and light microscopy was used to evaluate the normal morphology (e.g. biconcave discs) of the treated RBCs. The results of the star-shaped polymers will be presented first and then compared to linear PEGs and to the activated PEG.

4.1 Effect of star-shaped $CA(PEGs)_4$ on human RBCs

4.1.1 Viscosity profiles of RBC samples with $CA(PEG)_4$

The molar mass effect on blood viscosity was evaluated at various shearing rates and is shown in **Figure 4.1**. The control sample (*i.e.* no polymer added) and all the polymer samples show increased blood viscosity with decreasing shear rate. This is indicative of normal RBC aggregation formation, which occurs at low shear rates. The viscosity profile data were not significantly different at a concentration of 6.6 mg/mL (polymers in PBS, $P > 0.05$). Therefore, no obvious molar mass effect was detected.

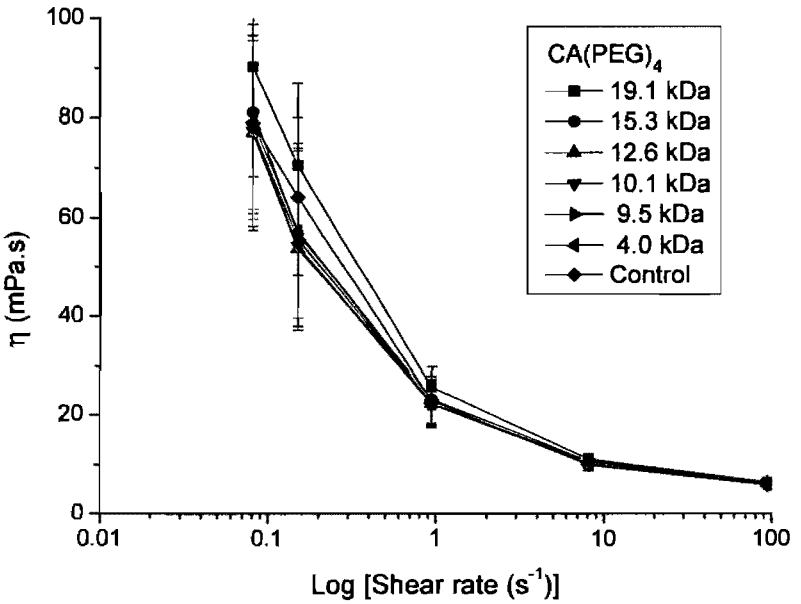

Figure 4.1 Viscosity-shear rate data of RBCs suspended in autologous plasma at 25°C with $CA(PEG)_4$ solution (6.6 mg/mL). All flow curves show typical non-Newtonian behavior for an aggregating system, the increase in viscosity with decreasing shear rate is indicative of RBC aggregation. Data are presented as mean ± standard deviation (S.D.). Data showed no significant difference with $P > 0.05$.

Another way to extrapolate more information from the viscosity profiles plotted in **Figure 4.1** is to plot a bar graph of the apparent viscosity as a function of the ratio of the low shear rate to the high shear rate (0.15 s^{-1}/ 94 s^{-1}). Such graph is depicted in **Figure 4.2**. Although a reduction of blood viscosity for the $CA(PEG)_4$ samples is observed when compared to the control (no polymer added), especially for the 10 kDa and 12 kDa, it was found not to be significant ($P > 0.05$). The rheometer is probably not sensitive enough to detect the inhibition of RBC aggregation.

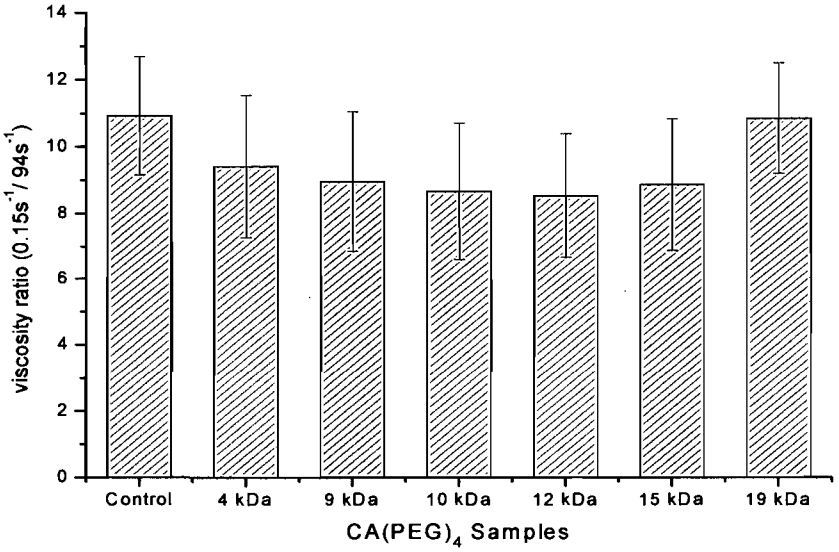

Figure 4.2. Apparent viscosity ratio (0.15 s^{-1} / 94 s^{-1}) of RBCs suspended in autologous plasma at 25°C with a $CA(PEG)_4$ at a polymer concentration of 6.67 mg/mL for n = 3 . Data are obtained from **Figure 4.1**.

There are several reasons which can account for significant variability when comparing the aggregability of RBCs from healthy donors. As aforementioned, RBC aggregability varies from individuals with different age and gender groups. When suspended in the same aggregating medium, different human donors can show up to two-fold variation in their aggregability.[6] In this study, the subjects were two males and one female from different age groups. Even within the same individuals, there can be some differences in the aggregability of RBCs because older RBCs tend to show greater aggregability compared to younger ones.[124]

4.1.2 Myrenne aggregation data of RBC samples with $CA(PEG)_4$

The effects of the molar mass of CA(PEG) on the Myrenne aggregation indices (M (stasis) and M1 (at 3 s^{-1})) of RBCs suspended in plasma were evaluated by adding a predetermined amount of polymer concentrations of 1.33, 4.0, and 6.7 mg/mL. The

resulting data are shown in **Figure 4.3** and are presented as relative values to that of the control (*i.e.* buffer added without polymer). In that manner, the influence due to simple dilution effects is eliminated. Relative aggregation values less than unity indicate reduced aggregation. The results clearly demonstrate that at a concentration of 4.0 and 6.7 mg/mL, the star-shaped $CA(PEG)_4$ is able to inhibit RBC aggregation. This is in agreement with prior studies[125], which described an optimum value for the concentration. The extent of the inhibition of RBC aggregation shows a dependence on the polymer concentration and seems to be influenced by the molar mass as well. Molar mass between 10 -16 kDa are more efficient in reducing RBC aggregation.

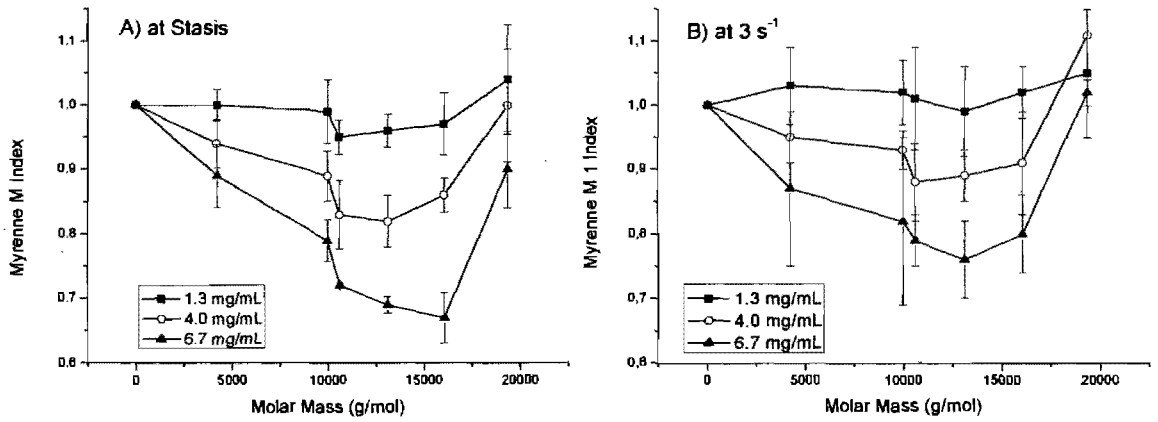

Figure 4.3. Aggregation of RBCs suspended in autologous plasma measured using a Myrenne Aggregometer. Myrenne M at stasis (**A**) and M1 at 3 s^{-1} (**B**) aggregation values normalized to control (e.g. buffer added without polymer) and presented as indices (± SD) for $CA(PEG)_4$ for each polymer concentration (1.3, 4.0 and 6.7 mg/mL). Values for M and M1 < 1 indicate inhibition of RBC aggregation. Measurements were in duplicate for each donor (n = 3).

Interpretation of these findings in terms of physicochemical mechanisms is thus of importance, but is limited by the current lack of understanding of the mechanism involved in RBC aggregation. As discussed in the introduction, the two models describing RBC aggregation are opposing. The "bridging model" predicts increased aggregation resulting from an increased polymer concentration at the RBC surface, whereas the "depletion model" predicts the opposite.[15] It is important to note that the depletion model does not require polymer adsorption onto the RBC but only requires that the concentration of the polymer in the depletion layer be less than the bulk solution to cause aggregation. Given the two models for RBC aggregation, it is possible that the star shaped $CA(PEG)_4$ decreases RBC aggregation via either decreasing (bridging model) or increasing (depletion model) the concentration of the aggregating polymer near the RBC surface. However, there has been increasing evidence to support the depletion model for polymer-induced RBC aggregation.[8,54,60] Therefore, if the depletion model was to be applied, it would seem most likely that $CA(PEG)_4$ reduces RBC aggregation via reducing the depletion effect near and the RBC soft surface layer (i.e., its glycocalyx). Considering the small size of the $CA(PEG)_4$, it is possible that it is able to penetrate the depletion layer formed by the larger pro-aggregating macromolecules (e.g. fibrinogen) such that it is able to effectively reduce the osmotic gradient between the intercellular gap and the bulk phase.[8]

Possible measurement artifacts may have affected the Myrenne data such as incomplete disruption of strongly interacting RBCs at high shear rates, and a uniform cell concentration gradient due to non-Newtonian behaviour of the medium.[6]

4.1.3 Light microscopy of blood samples with $CA(PEG)_4$

Microscopic examinations of RBCs incubated in autologous plasma and in 6.67 mg/mL of $CA(PEG)_4$ are shown in **Figure 4.4** . The microscopic examination of the morphology indicated that normal, discocytic RBC morphology was preserved for all samples. No difference in *rouleaux* structure compared to the control sample (i.e. no polymer added) was observed. This implies that polymer does not cause morphological

changes to the red cell membranes, which is a desired feature for biocompatibility. The images of the sample with the $CA(PEG)_4$ polymer did not reveal inhibition of RBC aggregation because the sample was further diluted with plasma to obtain a good image. It is possible that the dilution with plasma hindered the polymer effect.

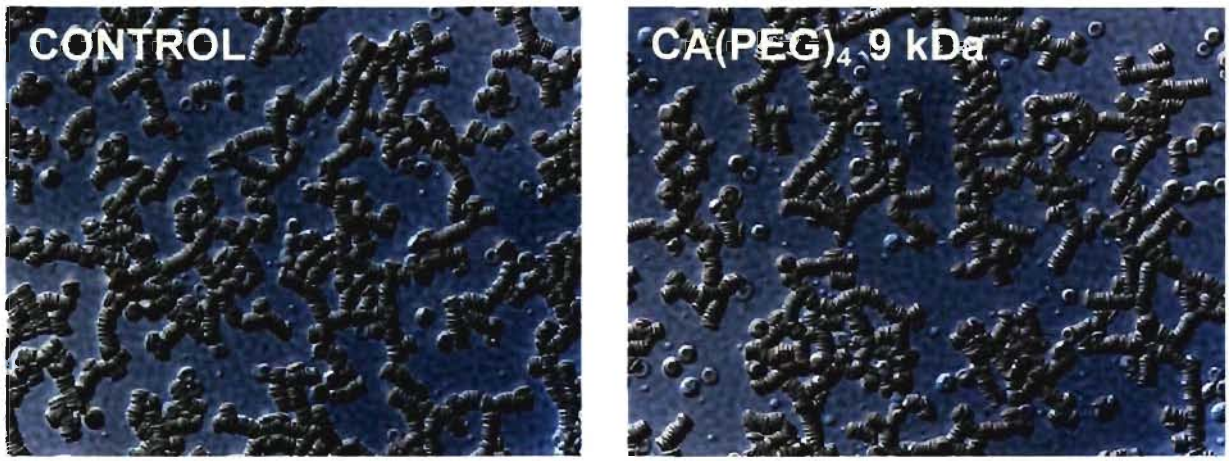

Figure 4.4. Photomicrographs of red blood cells (RBCs) in plasma with $CA(PEG)_4$ polymer at a concentration of 6.67 mg/mL taken at 400 magnification. These are enlarged microscopic images and are used for the basis of qualitative observations.

4.2 The Effect of Linear PEGs on Human RBCs

The effect of linear PEGs on blood viscosity at 25°C over a range of shear rates is shown in **Figure 4.5**. The flow curves show non-Newtonian behavior similar to the star-shaped polymers. Although the sample of the linear PEG 5 kDa appeared to be the most effective in reducing blood viscosity, it was not significant ($P > 0.05$). A similar chart to **Figure 4.2** was plotted for the linear PEGs and is displayed in **Figure 4.6**. This plot clearly shows that the reduction in blood viscosity is not significant for all linear PEG polymers. The same explanation for the variability of the measurements as for the star-shaped $CA(PEG)_4$ can be applied for the linear PEGs.

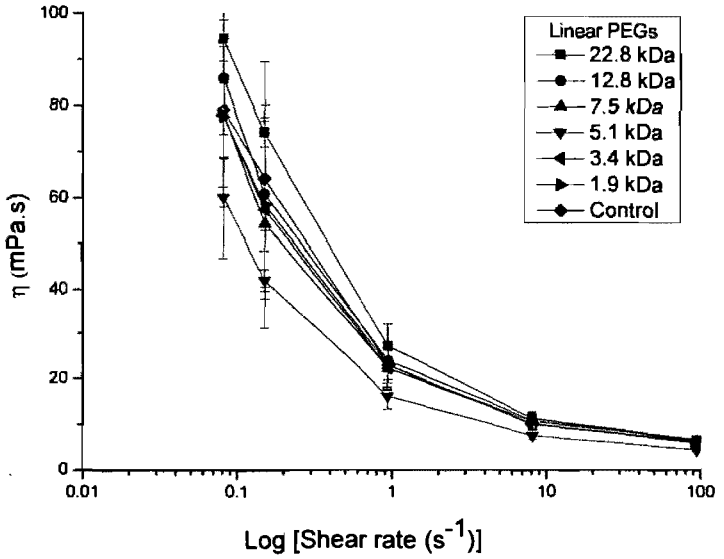

Figure 4.5. Viscosity profiles of RBCs suspended in autologous plasma at 25°C with linear PEGs (6.67 mg/mL). All flow curves show typical non-Newtonian behavior for an aggregating system. Data showed no significance difference with $P > 0.05$.

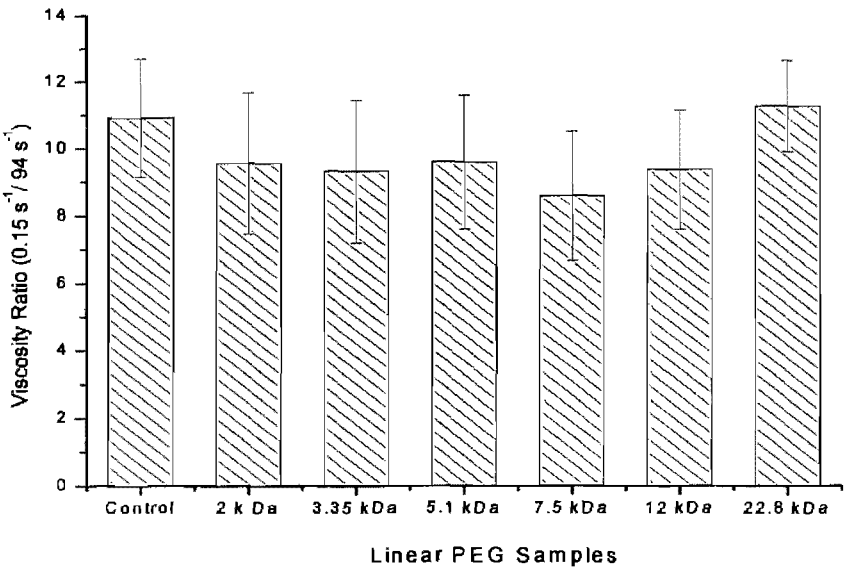

Figure 4.6. Apparent viscosity ratio (0.15 s^{-1} / 94 s^{-1}) of RBCs suspended in autologous plasma at 25 °C with linear PEGs (6.67 mg/mL). Data are obtained from **Figure 4.5.**

4.2.1 Myrenne aggregation data of RBC samples with linear PEGs

The Myrenne aggregation data were obtained in the same manner as the star-shaped $CA(PEG)_4$. As indicated in **Figure 4.7,** the linear PEGs inhibited RBC aggregation with increasing concentrations and the effect of inhibition of RBC aggregation was greater for the concentrations of 4 and 6.7 mg/mL. The 7.5 kDa linear PEG appears to be the most effective in reducing RBC aggregation. The Myrenne aggregation data for the linear PEGs are in agreement with studies that have shown that between 4 kDa to 6 kDa, linear PEG strongly inhibits RBC aggregation in whole blood.[6,126]

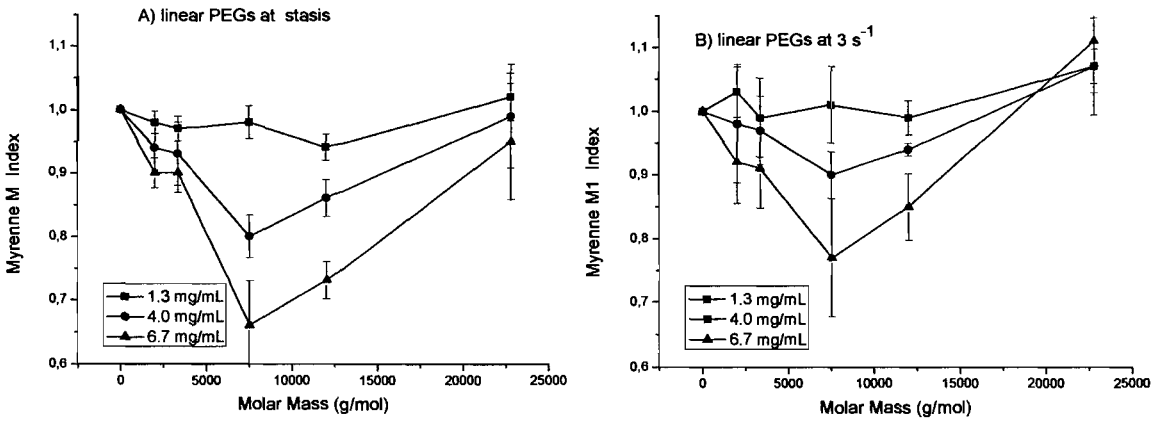

Figure 4.7. Aggregation of RBCs measured using a Myrenne Aggregometer. Myrenne M at stasis (**A**) and M1 at 3 s^{-1}(**B**) aggregation values normalized to control (*i.e.* no polymer added) and presented as Indices (mean ± standard deviation) for linear PEGs at each polymer concentration (1.3, 4.0 and 6.7 mg/mL). Values for M and M1 < 1 indicate inhibition of RBC aggregation and values > 1 indicate promotion of RBC aggregation. Measurements were in duplicate for each donor (n = 3).

4.3 Comparison of CA(PEG)s and Linear PEGs

Before comparing the results of the star-shaped $CA(PEG)_4$ with the linear PEGs, it is important to revisit some basic differences between these polymers. As it was shown in the characterization of the polymer, star-shaped $CA(PEG)_4$ have a small compact structure in solution. However, at some higher molar masses, the star-shaped $CA(PEG)_4$ and linear PEG will have the same size in solution as the effect of the core is diminished with increasing chain length. Ideally, comparing the effect of the star-shaped $CA(PEG)_4$ to linear PEGs on RBC aggregation and blood viscosity should be done on the basis of their hydrated size. Approximately, this equates to comparing polymers at an equivalent suspending phase viscosity. Examples are given in **Figure 4.8** at a high shear rate (94 s^{-1}) and a low shear rate (0.15 s^{-1}) for the star-shaped $CA(PEG)_4$ and the linear PEGs at different molar masses. It can be seen that, at a constant polymer concentration, star-shaped $CA(PEG)_4$ yield a lower bulk phase viscosity than the linear PEGs for a given molar mass, which is an indication that star-shaped PEGs have a more compacted structure in solution than linear PEGs. Though the estimated values for the star-shaped $CA(PEG)_4$ appeared lower, they are not statistically significant.

Figure 4.8 confirms the observation that no interaction between the cholane acid core and RBC surface occurred as the relationship between molar mass and inhibition of RBC aggregation is similar between star-shaped $CA(PEG)_4$ and linear PEGs.

The possible mechanisms by which the more compacted $CA(PEG)_4$ polymers affect RBC aggregation are complex. It is possible that the $CA(PEG)_4$ with the smaller radii infiltrates the interspace between RBCs membrane putative binding sites more efficiently than linear PEGs. This hypothesis has been suggested previously with low molar mass of polysaccharides, which occupy such sites and thereby reduced RBC aggregation.[7]

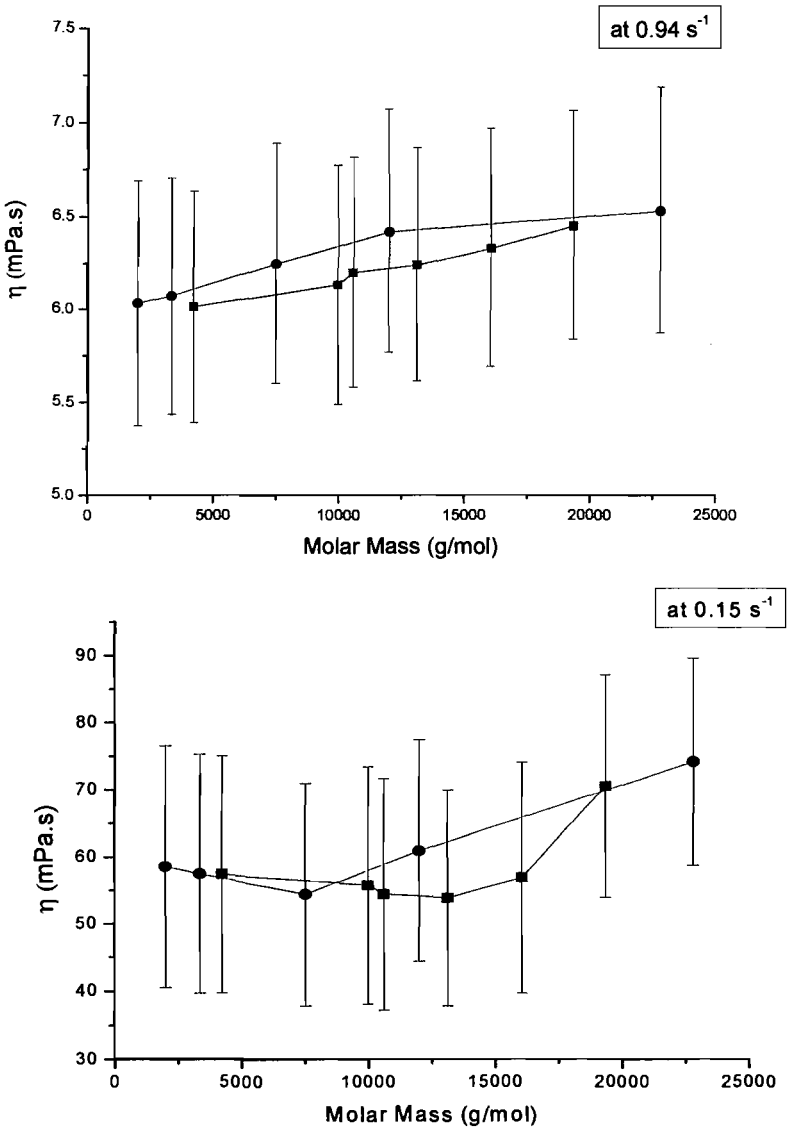

Figure 4.8. Mean viscosity at a high shear (94 s^{-1}) and a low shear (0.15 s^{-1}) of RBC samples suspended at 40% hematocrit in plasma at 25°C at a polymer concentration of 6.67 mg/mL for linear PEGs (●) and $CA(PEG)_4$ (■). Data are presented as mean ± standard deviation for n = 3.

To assess the hypothesis that the cholane core of $CA(PEG)_4$ shows greater inhibition of RBC aggregation due to the absorption of the cholane-core to the RBC membrane, a positive control, monofunctional succinimidyl propionate derivative of monomethoxy PEG (mPEG20k-SPA) of a molar mass of 20 kDa was used.[127] The mPEG20k-SPA reacts with lysine residues and terminal amines of proteins. The reaction between the activated ester of mPEG20k-SPA and amino groups forms a stable amide linkage. The covalent modification of RBCs with PEG produced immunologically attenuated cells that may reduce the risk of allosensitization in chronically transfused patients.[128]

The effects of $CA(PEG)_4$ and mPEG20k-SPA on blood viscosity at 37°C over a range of shear rates are shown in **Figure 4.9**. The RBCs that were incubated with $CA(PEG)_4$ in autologous plasma show no difference from the control sample. The RBC samples with the reactive linear PEG, mPEG20k-SPA, shows negligible RBC aggregation and a marked reduction (>60%) in low shear blood viscosity when compared to the control. This data is an agreement with a previous study that has shown that coated RBCs with monomethoxy PEG, molar mass 5 kDa and activated with cyanuric chloride, inhibited RBC aggregation and could reduced low shear blood viscosity.[127] They also showed that the reactive PEG reduced the viscosity by 30% more than the Poloxamer 188 (Pluronic F-68, 8.4 kDa) which has shown to be beneficial in clinical studies for the treatment of pain in sickle cell crisis.[10] This implies that covently "coating" RBCs with PEGs prevents the cells from adhering to each other hence reducing the RBC aggregation extent.

Also, these observations suggest that no interaction/adsorption occurs between the cholic acid core and the RBC surface. If adsorption did occur, the flow curves of the $CA(PEG)_4$ would be between that of the control and linear reactive PEG but that was not observed (**Figure 4.9**). Therefore the inhibition of RBC aggregation hence the reduction of low shear blood viscosity observed for the $CA(PEG)_4$ samples is most likely due to the polymer-polymer steric repulsion of the hydrated PEG chains between adjacent RBCs.

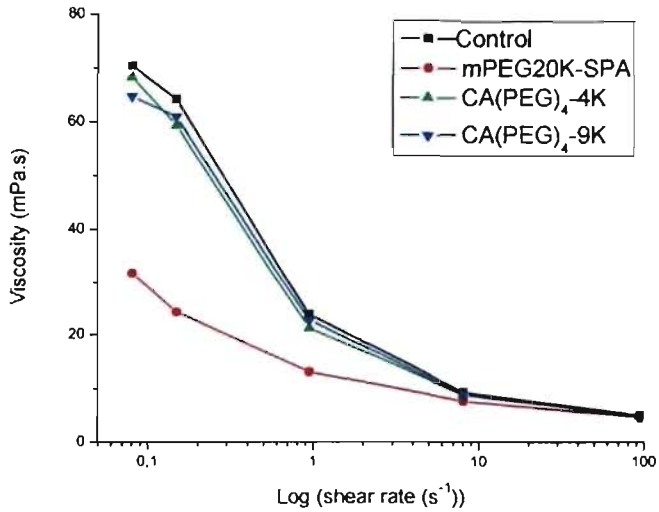

Figure 4.9. Viscosity profile of RBCs suspended in plasma at 37 °C over a range of shear rates (0.01 - 94.5s $^{-1}$). Measurements were in duplicate for each donor (n = 2).

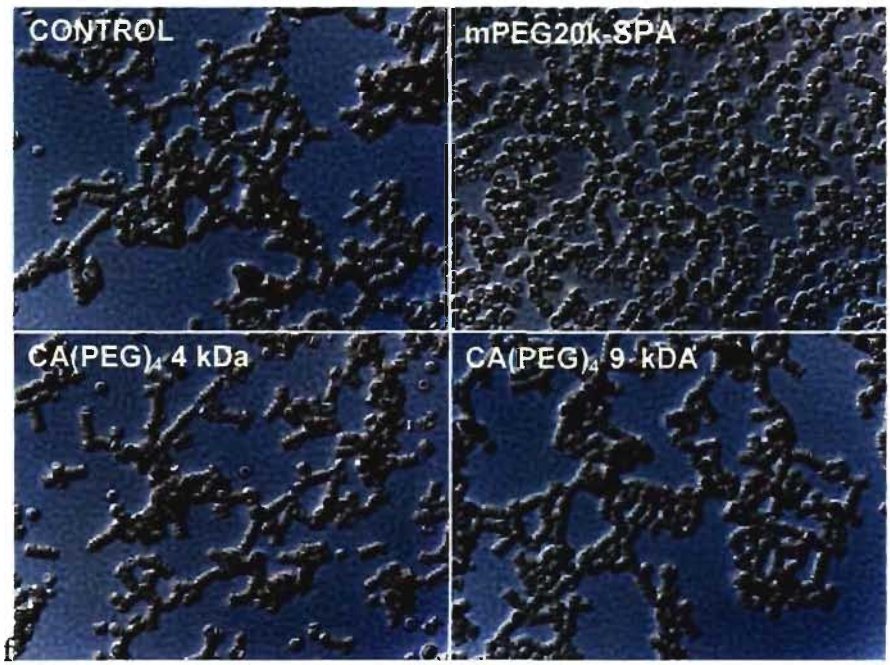

Figure 4.10. Photomicrograph images of RBCs in plasma at 40X magnification. Normal rouleaux formation was observed in control and $CA(PEG)_4$ samples. Minimal rouleaux formation was observed for mPEG20k-coated RBCs.

Microscopic examinations of RBCs suspended in plasma are shown for mPEG20k-SPA-coated RBCs and control (**Figure 4.10**). The mPEG20k-SPA-coated RBCs show minimal *rouleaux* formation compared to the control. Normal, discocytic RBC morphology was observed in all samples.

In overview, our results indicate that star-shaped $CA(PEG)_4$ can reduce RBC aggregation in a similar manner to the linear unreactive PEGs. The inhibition of RBC aggregation is dependent on concentration, molar mass, and molecular size. Though, the effect on the blood viscosity was not different for both linear and star-shaped PEGs. Also, the $CA(PEG)_4$ polymers do not adsorb or bind to the RBC's surface as it was demonstrated with the activated PEG, mPEG20k-SPA, which showed marked decreased in whole blood viscosity.

CHAPTER 5: CONCLUSION

5.1 Preparation of $CA(PEG)_4$

The objective of this work was to use a star-amphiphilic PEG polymer with cholic acid derivative as core ($CA(PEG)_4$) and as a therapeutic polymer for inhibiting RBC aggregation. The hypothesis was that the star-shaped $CA(PEG)_4$ polymer would be better than linear PEGs due to its small hydrodynamic size and solution viscosity. Also, it was suggested that these polymers would be more biocompatible than the block copolymer Pluronics, which has been clinically used to reduce RBC aggregation but had some adverse reactions.

A series of molar masses of star-shaped $CA(PEG)_4$ polymers were synthesized by anionic polymerization. The high molar mass polymers presented some bimodal characteristics in the SEC traces, which are evident of early chain terminations that were present during polymerization. Despite the difficulty in obtaining controlled high molar mass, anionic polymerization of the star-shaped $CA(PEG)_4$ provided narrowed molar mass distributions. The characterization of their molar mass distributions by MALDI-TOF proved to be accurate for small molar masses (< 5 kDa) but not for the higher molar fractions. Therefore, for higher molar masses, SEC alone and SEC-MALLS proved to be accurate. The SEC-MALLS provided additional information about the star-like architecture. The hydrodynamic radius of the polymers obtained from the intrinsic viscosity measurements confirmed the small and compact structure of the star shaped polymers (< 2 nm). The polymers also demonstrated shear-thinning behaviour in water and in PBS.

The extent of the inhibition of RBC aggregation by the star-shaped $CA(PEG)_4$, with the Myrenne aggregation data showed significant reduction when compared to the control sample, which was dependent on the concentration. However, these observations were not consistent with the blood viscosity measurements which showed no differences with the control samples. In comparison to linear PEGs, the effects on RBC aggregation and blood viscosity were not different. Under the conditions studied, neither does the

$CA(PEG)_4$ appear to absorb on the membrane of RBCs, meaning that it behave in same manner as a linear PEG regardless of its compact structure and low solution viscosity. Additional tests with a large controlled groups and patients with abnormal RBC aggregation could assess the real effect of the star-shaped $CA(PEG)_4$ polymers on RBC aggregation and blood viscosity.

Since limited success has been achieved by simply incubating blood with the $CA(PEG)_4$, covently binding the $CA(PEG)_4$ to the RBC's membrane by means of reactive groups such as succinimidyl propionate could prove to be a more promising avenue in reducing RBC aggregation. Covalently linking star-shaped $CA(PEG)_4$ could allow high surface coverage of RBC's membrane and thus preventing non-specific interactions with biological systems, which could lead to even better immune responses.

REFERENCES

1. MacRury, S. et al. Increased red cell aggregation in diabetes mellitus: association with cardiovascular risk factors. *Diabeict Medicine.* **10**, 21-26 (1993).

2. Ziegler, O. et al. Increased erythrocyte aggregation in insulin-dependent diabetes mellitus and its relationship to plasma factors: a multivariate analysis. *Metabolism* **43**, 1182-1186 (1994).

3. Shiga, T., Maeda, N. & Kon, K. Erythrocyte rheology. *Critical reviews in oncology/hematology* **10**, 9-48 (1990).

4. Somer, T. & Meiselman, H. Disorders of blood viscosity. *Annals of Medicine* **25**, 31-39 (1993).

5. Chien, S., Dormandy, J. & Ernst , E. *Clinical Hemorheology*, (Martinus Nijhoff Pub., Dordrech, 1987).

6. Armstrong, J.K., Wenby, R.B., Meiselman, H.J. & Fisher, T.C. The hydrodynamic radii of macromolecules and their effect on red blood cell aggregation. *Biophysical Journal* **87**, 4259-4270(2004).

7. Neu, B., Armstrong, J.K., Fisher, T.C. & Meiselman, H.J. Aggregation of human RBC in binary dextran-PEG polymer mixtures. *Biorheology* **38**, 53-68 (2001).

8. Toth, K., Wenby, R.B. & Meiselman, H. Inhibition of polymer-induced red blood cell aggregation by poloxamer 188. *Biorheology* **37**, 301-312 (2000).

9. Vercellotti, G., Hammerschmidt, D., Craddock, P. & Jacob, H. Activation of plasma complement by perfluorocarbon artificial blood: probable mechanism of adverse pulmonary reactions in treated patients and rationale for corticosteroids prophylaxis,. *Blood* **59**, 1299-1304 (1982).

10. Koshy, M., Wojtowicz-Praga, S. & Grindel, J. A phase III multicenter, randomized, doubled-blind, placebo-controlled study of Flocor (purified poloxamer 188) in patients with sickle cell disease in acute vaso-occlusive crisis. *Blood* **94**, 25B (1999).

11. Moghimi, S. et al. Causative factors behind poloxamer 188 (pluronic F68, Flocor (TM))-induced complement activation in human sera. A protective role against poloxamer-mediated complement activation by elevated serum lipoprotein levels. *Biochimica et biophysica acta. Molecular Basis of Disease* **689**, 103-113 (2004).

12. Peter Gasteier, A.R., Petra Schulte, Jochen Salber, Andreas Offenhäusser, Martin Moeller, Jürgen Groll,. Surface grafting of PEO-based star-shaped molecules for bioanalytical and biomedical Applications. *Macromolecular Bioscience* **7**, 1010-1023 (2007).

13. Ingraham, J. & Ingraham, C. *Introduction to Microbiology: A Case Study Approach*, 737 (Brooks/Cole-Thomson Learning, Pacific Grove, 2004).

14. García, M.F., de la Fuente, J.L., Fernández-Sanz, M. & Madruga, E.L. The importance of solvent polar character on the synthesis of PMMA-b-PBA block copolymers by atom transfer radical polymerization. *Polymer* **42**, 9405-9412 (2001).

15. Baskurt, O. & Meiselman, H. Blood rheology and hemodynamics. *Seminars in Thrombosis and Hemostatis* **29**, 435-450 (2003).

16. Nordmeyer, D., Forestner, J.E. & Wall, M.H. Advances in transfusion medicine. *Advances in Anesthesia* **25**, 41-58 (2007).

17. Hemoglobin [Online Image] Available at http://fig.cox.miami.edu/~cmallery/150ss97/hemoglobin.jpg., January 19, 2008.

18. Barnes, A. *A Handbook of Elementary Rheology*, 210 (The University of Wales Institute of Non-Newtonian Fluid Mechanics, Aberystwyth 2000).

19. Malkin, A. & Isayev, A. Rheology: Concepts, Methods, and Applications. 128 (ChemTec Publishing, Toronto, 2006).

20. Lichtman, M.A. & Rowe, J.M. Hyperleukocytic leukemias: rheological, clinical, and therapeutic considerations. *Blood* **60**, 279-283 (1982).

21. Whitmore, R.L. *Rheology of the Circurlation*, 187 (London, 1968).

22. Snyder, D. Influence of temperature and hematocrit on blood viscosity. *American Journal of Phisiology*
220(1971).

23. Wiewora, M., Sosada, K., Wylezol, M., Slowinska, L. & Zurawinski, W. Red blood cell aggregation and deformability among patients qualified for bariatric surgery. *Obesity Surgery* **17**, 365-371 (2007).

24. Hebert, H. Microvascular rheology and hemodynamics. *Microcirculation* **12**, 5-15 (2005).

25. Anatomy, G.s. Human red blood cells. in *Grey's Anatomy of the Human Body* Vol. 469 × 305 pixels (1918).

26. Stoltz, J. Hemorheologie et Aggregation Erythrocytaire. in *Compte rendu 1er Symposium international Genever 1986* (ed. Internationalees, E.M.) 175 (Geneve, 1986).

27. Merill, E., Cheny, C. & Pelletier, G. Yield stress of normal human blood as a function of endogenous fibrinogen. *Journal of Applied Physiology* **26**, 1 (1968).

28. Chien, S., Simchon, S., Abbot, R. & Jan, K. Surface adsorption on human red cell membrane. *Journal of Colloid and Interface science* **62**, 461-470 (1977).

29. Yalcin, O., Uyuklu, M., Armstrong, J., Meiselman, H. & Baskurt, O. Graded alterations of RBC aggregation influence in vivo blood flow resistance. *American Journal of Physiology. Heart and Circulatory Physiology* **287**, 2644-2650 (2004).

30. Dintenfass, L. *Blood Microrheology- Viscosity Factors in Blood Flow, Ischaemia and Thrombosis*, (London, 1971).

31. Weng, X.D., Cloutier, G., Beaulieu, R. & Roederer, G.O. Influence of acute-phase proteins on erythrocyte aggregation. *American Journal of Physiology-Heart and Circulatory Physiology* **271**, H2346-H2352 (1996).

32. Bishop, J., Popel, A., Intaglietta, M. & Johnson, P. Rheological effects of red blood cell agregation in the venous network: A review of recent studies. *Biorheology* **38**, 263-274 (2001).

33. Chien, S. Shear Dependence of Effective cell volume as a determinant of blood viscosity. *Science* **168**, 977-978 (1970).

34. Merill, E., Gilliland, E., Lee, T. & Salzman, E. Blood rheology effect of fibrinogen deduced by addition. *Circulation. Research* **18**, 437-446 (1966).

35. Brooks, D.E. The effect of neutral polymers on the electrokinetic potential of cells and other charged particles. III Experimental studies on the dextran/erythrocyte system. *Journal of Colloid and Interface Sciencee* **43**, 701-713 (1973).

36. Chien, S. & Jan, K. Red cell aggregation by macromolecules: Roles of surface adsorption and electrostatic repulsion. *Journal of Supramolecular* **1**, 385-409 (1973).

37. Chien, S. & Jan, K. Ultrastructural basis of the mechanism of rouleaux formation. *Microvascular Research* **5**, 155-166 (1973).

38. Kobuchi, Y., Tadanao, I. & Ogiwara, A. A model for rouleaux pattern formation of red blood cells. *Journal of Theoretical Biol*ogy **130**, 129-145 (1988).

39. Armstrong, J., Meiselman, H. & Fisher, T. Evidence againts macromolecular "bridging as the mechanism of red blood cell aggregation induced by nionic polymers. *Biorheology* **36**, 433-437 (1999).

40. Asakura, S. & Oosawa, F. On interaction between two bodies immersed in a solution of macromolecules. *The Journal of Chemical Physics* **22**, 1255-1256 (1954).

41. Neu, B. & Meiselman, H.J. The Role of Macromolecules in Stabilization and De-Stabilization of Biofluids. in *Bioengineering in Cell and Tissue Research* (eds. Artmann, G. & Chien, S.) 393-413 (Springer, NY, 2008).

42. Alexander, S. & Johnson, P. Microcirculation and hemorheology. *Annual Review of Fluid Mechenics.* **37**, 43-69. (2005).

43. Moncrief, J., Darin, J., Canizaro, P. & Sawyer, R. Use of Dextran to prevent arterial and venopus thrombosis. *Annals of Surgery* **158.** 553-559 (1963).

44. Stoltz, J.F. Drugs affecting blood rheology- a review. *Scandinavian Journal of Clinical & Laboratory Investigation* **41**, 287-290 (1981).

45. Brooks, D. Mechanism of red cell aggregation. in *Blood Cells, Rheology and Aging* 158-162 (Springer-Verlag, Berling, 1988).

46. Haljamäe, H., Dahlqvist, M. & Walentin, F. Artificial colloids in clinical practice: pros and cons. *Baillière's Clinical Anaesthesiology* **11**, 49-79 (1997).

47. Bruckner, U. & Messmer, K. Blood rheology and systematic oxygen transport. *Biorheology* **27**, 903-912 (1990).

48. Veronese, F.M. & Mero, A. The impact of Pegylation on biological therapies. *Biodrugs* **22**, 315-329 (2008).

49. Bailon, P. & Won, C.Y. PEG-modified biopharmaceuticals. *Expert Opinion on Drug Delivery* **6**, 1-16 (2009).

50. Wattendorf, U. & Merkle, H.P. PEGylation as a Tool for the Biomedical Engineering of Surface Modified Microparticles. *Journal of Pharmaceutical Sciences* **97**, 4655-4669 (2008).

51. Keys, K.B., Andreopoulos, F.M. & Peppas, N.A. Poly(ethylene glycol) star polymer hydrogels. *Macromolecules* **31**, 8149-8156 (1998).

52. Peppas, N.A., Keys, K.B., Torres-Lugo, M. & Lowman, A.M. Poly(ethylene glycol)-containing hydrogels in drug delivery. *Journal of Controlled Release* **62**, 81-87 (1999).

53. Murad, K.L. et al. Structureal and functional consequences of antigenic modulation of red blood cells with methoxypoly(ethylene glycol). *Blood* **93**, 2121-2127 (1999).

54. Neu, B., Armstrong, J., Fisher, T., Bäumler, H. & Meiselman, H. Electrophoretic mobility of human red blood cells coated with poly(ethylene glycol). *Biorheology* **38**, 389-403 (2001).

55. Miyauchi, Y., Inoue, T. & Paton, B. Adjunctive use of a surface-active agent in extracorporeal circulation. *Circulation* **33** (1966).

56. Grover, F., Heron, M. & Newman, M. Effects of non-ionic surface active agent on blood viscosity and platelets adhesiveness. *Circulation* **37/38**, 89 (1968).

57. Armstrong, J., Meiselman, H. & Fisher, T. Covalent binding of poly(ethylene glycol) (PEG) to the surface of red blood cells inhibits aggregation and reduces low shear blood viscosity. American Journal of Hematology **56**, 26-28 (1997).

58. Armstrong, J., Meislman, H. & Fisher, T. Inihibition or red blodd cell induced-platelet aggregationin whole-blood by a nonionic surfactan, Poloxamer 188 (Rheoth Rx injection, Thrombosis Research **79**, 437-450 (1995).

59. Baskurt, O., Yalcin, O., Ozdem, S., Armstrong, J. & Meiselman, H. Modulation of endothelial nitric oxide synthase expression by red cell aggregation. *American Journal of Physiology Heart and Circulatory Physiology* **286**, 222-229 (2004).

60. Armstrong, J.K., Meiselman, H.J., Wenby, R.B. & Fisher, T.C. Modulation of red blood cell aggregation and blood viscosity by the covalent attachment of Pluronic copolymers. *Biorheology* **38**, 239-247 (2001).

61. Grindel, J., Jaworski, T., Piraner, O., Emanuele, R. & Balasubramanian, M. Distribution, metabolism, and excretion of a novel surface-active agent, purified poloxamer 188, in rats, dogs, and humans. *Journal of Pharmaceutical Sciences* **91**, 1936-1947 (2002).

62. Papo, A., Piani, L. & Ricceri, R. Sodium phosphates as dispersing agents for calcium carbonate industrial slurries: Rheological characterization. *Silicates Industriels* **68**, 119-124 (2003).

63. Hunter, R., Papadea, C., Gallagher, C., Finlayson, D. & Check, I. Increased whole blood viscosity during coronary atery bypass surgery. Studies to evaluate the effects of soluble fibrin and Poloxamer 188. *Thrombosis and Haemostatis* **63**, 6-12 (1990).

64. Ingram, D., Forman, M. & Murray, J. Activation of complement by Fluosol attributes to the Pluronic detergent micelle structure. *Journal of Cardiovascular. Pharmacology* **22**, 456-461 (1993).

65. Hofmann, A.F. Bile acids as drugs principles, mechanisms of action and formations. *Italian Journal of Gastroenterology* **27**, 106-113 (1995).

66. Tamminen, J. & Kolehmainen, E. Bile Acids as Building Blocks of Supramolecular Hosts. *Molecules* **6**, 21-46 (2001).

67. Virtanen, E. & Kolehmaien, E. Use of Bile Acids in Pharmacological and Supramolecular Application. *European journal of organic chemistry*, 3385-3399 (2004).

68. Enhsen, A., Kramer, W. & Wess, G. Bile acids in drug discovery. *Drug Discovery Today* **3**, 409-418 (1998).

69. Albert, D. & Feigel, M. *Tetrahedron Lett* **35**, 565 (1994).

70. Zhu, X.X. & Nichifor, M. Polymeric Materials Containing Bile Acids. *Accounts of Chemical Research* **35**, 539-546 (2002).

71. Noll, O. & Ritter, H. *Macromolecular rapid communications* **17**, 553 (1996).

72. Gautrot, J. & Zhu, X. Main-Chain Bile Acid Based Degradable Elastomers Synthesized by Entropy-Driven Ring-Opening Metathesis Polymerization. Angewandte Chemie (International ed.). **45**, 6872-6874 (2006).

73. Ghedini, N., Ferruti, P., Andrisano, V., Cesaroni, M. & Scapini, G. *Synthetic communications* **13**, 701 (1983).

74. Gauthier, M.A., Simard, P., Zhang, Z. & Zhu, X.X. Bile acids as constituents for dental composites: in vitro cytotoxicity of (meth)acrylate and other ester derivatives of bile acids. *Journal of the Royal Society Interface* **4**, 1145-1150 (2007).

75. Gautrot, J.E. & Zhu, X.X. Biodegradable polymers based on bile acids and potential biomedical applications. *Journal of Biomaterials Science-Polymer Edition* **17**, 1123-1139 (2006).

76. Beher, W.T. *Chemistry and Physiology of Bile Acids and their Influence on Atherosclorosis*, 218 (Gasser & Cie AG, Basel (Switzerland), 1976).

77. Small, D. *The Bile Acids, Chemistry, Physiology and* ***Metabolism***, (Plenum Press, New York, 1971).

78. Hao, J.Q., Li, H. & Zhu, X.X. Preparation of a comb-shaped cholic acid-containing polymer by atom transfer radical polymerization. *Biomacromolecules* **7**, 995-998 (2006).

79. Benrebouh, A., Zhang, Y.H. & Zhu, X.X. Hydrophilic polymethacrylates containing cholic acid-ethylene glycol derivatives as pendant groups. *Macromolecular Rapid Communications* **21**, 685-690 (2000).

80. Denike, J.K. & Zhu, X.X. Preparation of New Polymers from Bile-Acid Derivatives. *Macromolecular Rapid Communications* **15**, 459-465 (1994).

81. Zhu, X.X. & Nichifor, M. Polymeric materials containing bile acids. *Acc. Chem. Res.* **35**, 539 (2002).

82. Belle, H.V. *Cholesterol, Bile Acids and Atherosclerosis*, (North-Holland Publishing Company, Amsterdam, 1965).

83. Messager, R., Ott, A., Chatenay, D., Urbach, W. & Langevin, D. Are giant micelles living polymers? *Physical Review Letters* **60**, 1410 (1988).

84. Aswal, V.K. & Goyal, P.S. Role of counterion distribution on the structure of micelles in aqueous salt solutions: small-angle neutron scattering study. *Chemical Physics Letters* **357**, 491-497 (2002).

85. Hofmann, B. The Function of Bile Salts in Fat aborption. *Biochemical Journal.* **89**, 57-68 (1963).

86. Zhang, Y.H. & Zhu, X.X. Polymers made from cholic acid derivatives: Selected properties. *Macromolecular Chemistry and Physics* **197**, 3473-3482 (1996).

87. Zhang, Y.H., Akram, M., Liu, H.Y. & Zhu, X.X. Characterization of new copolymers made from methacrylate and methacrylamide derivatives of cholic acid. *Macromolecular Chemistry and Physics* **199**, 1399-1404 (1998).

88. Denike, J.K. & Zhu, X.X. Preparation of new polymer from bile acid derivatites. *Macromolecular Rapid Communications* **15**, 459-465 (1994).

89. Zhu, X.X., Moskova, M. & Denike, J.K. Preparation and characterization of copolymers of new monomers from bile acid derivatives with methacrylic monomers and selective hydrolysis of the homopolymers. *Polymer* **37**, 493-498 (1996).

90. Wang, Q. Syntheses and characterizations of new polymers with bile acid derivatives as pendant groups, Universite de Montreal (2002).

91. Lele, B.S. & Leroux, J.C. Synthesis of novel amphiphilic star-shaped poly([var epsilon]-caprolactone)-block-poly(N-(2-hydroxypropyl)methacrylamide) by combination of ring-opening and chain transfer polymerization. *Polymer* **43**, 5595-5606 (2002).

92. Nichifor, M., Stanciu, M.C. & Zhu, X.X. Bile acids covalently bound to polysaccharides 2. Dextran with pendant cholic acid groups. *Reactive & Functional Polymers* **59**, 141-148 (2004).

93. Choi, Y., Bae, Y. & Kim, S. Star-shaped Poly(ether-ester) block copolymers: synthesis, characterization, and their properties. *Macromolecules* **31**, 8766-8774 (1998).

94. Jeong, B., Choi, Y.K., Bae, Y.H., Zentner, G. & Kim, S.W. New biodegradable polymers for injectable drug delivery systems. *Journal of Controlled Release* **62**, 109-114 (1999).

95. Choi, Y.R., Bae, Y.H. & Kim, S.W. Star-shaped poly(ether-ester) block copolymers: Synthesis, characterization, and their physical properties. *Macromolecules* **31**, 8766-8774 (1998).

96. Nichifor, M. & Carpov, A. Bile acids covalently bound to polysaccharides 1. Esters of bile acids with dextran. *European Polymer Journal* **35**, 2125-2129 (1999).

97. Torchilin, V.P. Structure and design of polymeric surfactant-based drug delivery systems. *Journal of Controlled Release* **73**, 137-172 (2001).

98. Alheim, M. & Hallensleben, M. Radically polymerizable cholic acid derivatives in monolayers, micelles, and vesicles. *Makromolekulare Chemie* **193**, 779-797 (1992).

99. Durand, A. Bile acids as building blocks of amphiphilic polymers. Applications and comparison with other systems. *Collection of Czechoslovak Chemical Communications* **72**, 1553-1578 (2007).

100. Knischka, R., Lutz, P.J., Sunder, A., Mulhaupt, R. & Frey, H. Functional poly(ethylene oxide) multiarm star polymers: Core-first synthesis using hyperbranched polyglycerol initiators. *Macromolecules* **33**, 315-320 (2000).

101. Guingère, G. & Zhu, X.X. Synthesis and aggregation properties of anionic star-shaped polymers with cholic acid cores and polyacrylate arms. *Journal of Polymer Science: Part A: Polymer Chemistry* **45**, 4173-4178 (2007).

102. Gouin, S. & Zhu, X. Synthesis of 3-alpha and 3-beta dimers from selected bile acids. *Steroids* **61**, 664-669 (1996).

103. Podzimek, S The use of GPC coupled with a multiangle laser light scattering photometer for the characterization of polymers. On the determination of molecular weight, size and branching. *Journal of Applied Polymer Science* **54**, 91-103 (1994).

104. Klose, H., Volger, E., Brechtelsbauer, H. & Schmid-Schonbein, L.a.H. Microrheology and light transmission of blood. *Pfluegers Arch* **333**, 126-139 (1972).

105. Taton, D. et al. Controlled polymerizations as tools for the design of star-like and dendrimer-like polymers. *Polymer International* **55**, 1138-1145 (2006).

106. Feng, X.S., Taton, D., Chaikof, E.L. & Gnanou, Y. Toward an easy access to dendrimer-like poly(ethylene oxide)s. *Journal of the American Chemical Society* **127**, 10956-10966 (2005).

107. Boileau, S. Anionic Ring-Opening Polymerisation: Epoxides and Episulfides,. in *Comprehensive Polymer Science"*, Vol. 3 467-487 (Pergamon Press, London, 1989.).

108. Chen, E.-Q. et al. Isothermal Thickening and Thinning Processes in Low-Molecular-Weight Poly(ethylene oxide) Fractions Crystallized from the Melt. *Macromolecules* **32**, 4784-4793 (1999).

109. Skoog, D., Holler, F. & Nieman, T. *Principles of Instrumental Analysis*, 849 (Nelson Thomson Learning, Toronto, 1971).

110. Montaudo, G., Garozzo, D., Montaudo, M.S., Puglisi, C. & Samperi, F. Molecular and Structural Characterization of Polydisperse Polymers and Copolymers by Combining MALDI-TOF Mass Spectrometry with GPC Fractionation. *Macromolecules* **28**, 7983-7989 (1995).

111. Luo, J., Giguere, G. & Zhu, X.X. Asymmetric Poly(ethylene glycol) Star Polymers with a Cholic Acid Core and Their Aggregation Properties. *Biomacromolecules* **in press**.

112. Zimm, B. & Stockmayer, W. The dimensions of chain molecules containing branches and rings. *Journal of Chemical Physics* **17**, 1301 (1949).

113. Wyatt, P.J. Light-Scattering and the Absolute Characterization of Macromolecules. *Analytica Chimica Acta* **272**, 1-40 (1993).

114. Kratochvi, P. *Classical Light Scattering from Polymer Solutions*, (Elsevier, Amsterdam-Oxford-New York-Tokyo, 1987).

115. Grcev, S., Schoenmakers, P. & Iedema, P. Determination of molecular weight and size distribution and branching characteristics of PVAc by means of size exclusion chromatography/multi- angle laser light scattering (SEC/MALLS). *Polymer* **45**, 39-48 (2004).

116. Podzimek, S. A review of the analysis of branched polymers by SEC-MALS. *American Laboratory* **34,** 38-45(2002).

117. Podzimek, S., Vlcek, T. & Johann, C. Characterization of branched polymers by size exclusion chromatography coupled with multiangle light scattering detector. I. Size exclusion chromatography elution behavior of branched polymers. *Journal of Applied Polymer Science* **81**, 1588-1594 (2001).

118. Huang, C.Y., Huang, S.J., Yu, Y.C., Lee, T.Y. & Shau, M.D. Viscosity and density measurements of macromolecules. *Angewandte Makromolekulare Chemie* **265**, 25-30 (1999).

119. Bywater, S. Preparation and properties of star-branched polymers in *Physical Chemistry* 89-106 (Springer Berlin / Heidelberg, 2007).

120. Allison, C. & Peacock, A. Polymer Chemisty : Properties and Applications. 106 (Hanser Verlag, Munich, 2006).

121. Huber, K., Bantle, S., Burchard, W. & Fetters, L.J. Semidilute solutions of star branched polystyrene: a light and neutron scattering study. *Macromolecules* **19**, 1404-1411 (1986).

122. Albertsson, P. *Partition of Cell Particles and Macromolecules*, (Wiley, New York, 1971).

123. B. Briscoe, P.L., S. Zhu,. Rheological properties of poly(ethylene oxide) aqueous solutions. *Journal of Applied Polymer Science* **70**, 419-429 (1998).

124. Tudral, E., Yalcin, O. & Baskurt, O. Effect of donor age on the deformability and aggregability of density-separated red blood cells *Turkish Jurnal Haematology* **19**, 303-308 (202).

125. Bauersachs, R., Wenby, R. & Meiselman, H. Determination of specific red blood cell aggregation indices via an automated system. *Clinical hemorheology and microcirculation* **9**, 1-25 (1989).

126. Geller, N., Kropachev, V., Leftov, V. & Potapova, I. The influence of polyethylene oxice on the aggregation of erythrocytes. *Polim. Med.* **11**, 83-93 (1981).

127. Armstrong, J. Covalent binding of poly(ethylene glycol) (PEG) to the surface of red blood cells inhibits aggregation and reduces low shear blood viscosity. *American Journal of Hematology* **56**, 26-28 (1997).

128. Bradley, A.J., Murad, K.L., Regan, K.L. & Scott, M.D. Biophysical consequences of linker chemistry and polymer size on stealth erythrocytes: size does matter. *Biochimica et Biophysica Acta (BBA) - Biomembranes* **1561**, 147-158 (2002).

129. Goldsmith, H. Poisseuile medal award lecture: From papermaking fibers to human blood cells. *Biorheology* **30**, 165-190 (1993).

130. Schiffman, F.J. *Hematologic Pathophysiology*, 369 (Lippincott-Raven Publishers, Philidelphia, 1998).

131. Stuart, J. & Johnson, C. Rheology of the sickle cell disorders. *Baillier's Clin Haematol* **1**, 745-775 (1987).

132. Hunter, R., Papadea, C., Gallagher, C., Finlayson, D. & Check, I. Increased whole blood viscosity during coronary atery bypass surgery. Studies to evaluate the effects of soluble fibrin and Poloxamer 188. *Thrombosis and Haemostatis* **63**, 6-12 (1990)

133. Kesmarky, G., Toth, K. & Habon, L. Hemorheological parameters in coronary artery disease. *Clinical hemorheology and microcirculation* **18**, 245-251 (1998).

134. Hinshaw, L. Sepsis/septic shock: participation of the microcirculation. An abbreviated review. *Critical Care Medicine* **24**, 1072-1078 (1996).

135. Baskurt, O.K., Temiz, A. & Meiselman, H.J. Red blood cell aggregation in experimental sepsis. *The Journal of laboratory and clinical medicine* **130**, 183-190 (1997).

136. Chen, S. et al. Enhanced aggregability of red blood cells of beta-thalessemia major patients. *American Journal of Physiology* **270**, H1951-H1956 (1996).

137. Miller, J. *Chromatography: concepts and contrasts*, 490 (John Wiley and Sons, San Francisco, 2005).

138. Creel, H. *Trends in Polymer Science* **1**, 336-342 (1993).

APPENDIX 1

Steady Laminar Flow

The relationship between vessel diameter and/or blood viscosity and their influence on blood flow can be best described by the Hagen-Poiseuille equation:[129]

$$Q = P\frac{\cdot r^4 \cdot \pi}{8 \cdot \eta \cdot L} \qquad \text{(a1.1)}$$

where Q is the rate of flow, P is the pressure, r the radius, η the viscosity, and L, the vessel length. According to Equation (a.1.1), blood flow in a capillary is directly proportional to the pressure and the diameter with power of 4, and indirectly proportional to the viscosity and the length of the blood vessel. This implies that the vessel diameter may be more important than viscosity for normal blood flow. Poiseuille law is only valid under a constant pressure gradient and when the blood flow is defined as laminar flow of a homogenous fluid in a rigid cylindrical tube. Thus, in the vascular systems the Poiseuille law only serves as a mathematical approximation of the in vivo model of blood flow.

Disorders Related to Abnormal RBC Aggregation

Sickle cell disease (SCD) is one of the most important clinical hemapathologies. It is an inherited blood disorder that affects red blood cells and is common among African-American, Africans, natives of central India, Mediterranean, and natives of the Middle East.[130] People with sickle cell disease have red blood cells that contain mostly hemoglobin *S, an abnormal type of hemoglobin that arises from a point mutation in the beta-globin chain gene. Sometimes these red blood cells become sickle-shaped (crescent shaped) and have difficulty passing through capillaries (**Figure a1.1**). When sickle-shaped cells block small blood vessels, less blood can reach that part of the body. A tissue

that does not receive a normal blood flow eventually becomes damaged. Periods of painful crisis in sickle cell disease are associated with alteration of the circulating red cell population with elevated levels of fibrinogen and plasma viscosity.[131] Sickled RBCs get entrapped in the microcirculation, thereby causing ischemia or organ damage throughout the body. Standard treatments are aimed at relieving some symptoms and include oxygen, analgesics, fluid therapy, and blood transfusion. However, there is currently no universal cure for sickle cell disease and blood transfusion accompanied by polymer coating of RBCs to inhibit aggregation would certainly be clinically beneficial if such coating strategy is succeeding.

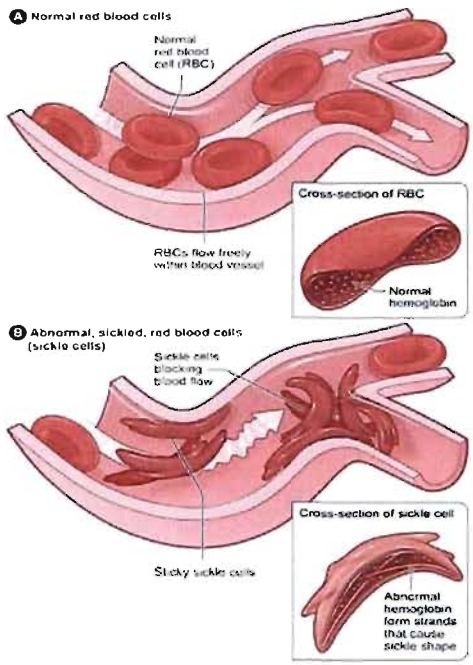

Figure a1.1. **(A)** Normal red blood cells flow freely in a blood vessel. The inset image shows a cross-section of a normal red blood cell with normal hemoglobin. **(B)** Abnormal, sickled red blood cells clump and block the blood flow in a blood vessel. The inset image shows a cross-section of a sickled red blood cell with abnormal strands of hemoglobin. Taken from ref. [132]

Cardio vascular diseases

Cardio vascular disease is one of the clinical disorders for which the effect of hemorheological consequences has been well established. The observable outcomes of cardio vascular diseases such as increased blood viscosity, increased RBC aggregation, and impaired RBC deformability have been reported.[5] For instance, ischemic diseases of various organs are known to be associated with blood flow impairment.[133]

Diabetes mellitus

Diabetes mellitus is a disease of metabolic malfunction, most notably abnormal glucose metabolism, accompanied by characteristic long-term complications. The complications of diabetes mellitus represent microcirculatory disorders and damage many types of tissues including nerves, skin, retina, heart, kidney, and brain. In all these tissues, the major cause of damage is vascular disease affecting both microvasculature and macrovasculatrure. Diabetes mellitus is affected by a microcirculatory disturbance which gives rise to higher blood and plasma viscosity, enhanced RBC aggregation, and impaired RBC deformability. Both the velocity of *rouleaux* formation and the cohesion of the rouleaux network are significantly elevated in diabetic patients. Plasma viscosity and whole-blood viscosity measured at a low shear rate (0.95 s^{-1}) are also significantly elevated in the diabetic group.[2] Another study showed that an increased in RBC aggregation may be a mechanism by which some cardiovascular risk factors could promote cardiovascular disease in diabetes.[1]

Sepsis syndrome

Sepsis syndrome represents one of the most dramatic disturbances in hemorheological and is a leading cause of death in non-coronary intensive care units worldwide. The sepsis syndrome is a complex systematic inflammatory condition associated with infection. Both clinical and experimental studies showed that sepsis is

significantly marked by increased in RBC aggregation and impaired RBC deformability.[134,135] These deformabilities may lead to severe vascular problems encountered in sepsis syndrome such as impaired oxygen delivery to tissues and organ failure.

Thalassemia

Thalassemias are inherited disorders characterized by a defective production of the globin chain subunits of hemoglobin.[130] In alpha or beta thalessemia, the alpha or globin chain is reduced or absent. Major thalessemic syndromes are associated with morphological and functional RBC anomalies, leading to shortening of the red cells life span and chronic anemia. It has been reported that major thalessemia patients exhibit enhanced aggregability forming large clusters, and higher-than-normal shear force is required to disperse these aggregates.[136] Thalessemias are most commonly in people form Southeast Asia and China, Mediterranean origin, and Blacks.[130] These areas were historically affected by malaria. This thought to be because the RBCs of people diseased with Thalessemia are relatively resistant to infection with the malaria parasite.

Obesity

The prevalence of obesity is a concern today especially in North America. Morbidly obese patients or those that qualify for bariatric surgery possess a severe risk for deep vein thrombosis and pulmonary embolism. RBC rheological properties play an instrumental role in determining the blood-flow resistance in microcirculation and RBC hyperaggregation has a significant influence on the microcirculation blood flow, both are determinant factors in whole blood viscosity and are known to be altered in obese patients. Obesity is associated with an increase in the degree of aggregation and a decrease in RBC deformability as well as an alteration in the RBC aggregation kinetics. [23] The deformability factor is important in RBC aggregation because it leads to a shear-dependent-behaviour of blood viscosity and minimizes the blood-flow resistance in

capillaries. Thus the necessity to introduce a therapy to correct or improve RBC rheological properties, which in turn may improve blood flow in microcirculation and prevent post-operative complications after bariactric surgery, is a need.

APPENDIX 2

Differential Scanning Calorimetry (DSC)

Differential scanning calorimetry (DSC) is a technique that measures heat flow into or out of a material as a function of time or temperature. Polymer crystallinity can be determined with DSC by quantifying the heat associated with melting (fusion) of the polymer. In DSC the sample and the reference pan (usually an empty pan) are heated at the same rate to keep the temperature identical (**Figure a2.1**). The heater output at the sample is different from the reference. The heat output difference, which depends on differences in heat capacity (amount of heat it takes to get temperature increase), is plotted as a function of temperature. A preheated purge gas is present to provide additional baseline stability as well as the desired sample/atmosphere interaction.

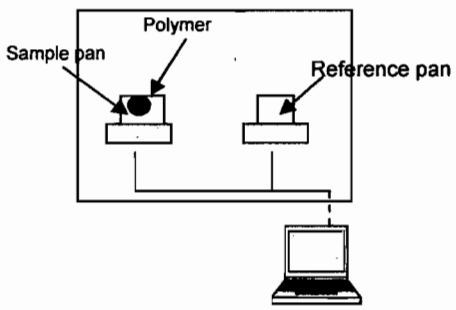

Figure a2.1. Representation of Differential Scanning Calorimetry (DSC).

The heat capacity changes at the glass transition (T_g.). Glass transitions may occur as the temperature of an amorphous solid is increased. These transitions appear as a step in the baseline of the recorded DSC signal. This is due to the sample undergoing a change in heat capacity; no formal phase change occurs. As the temperature increases, an amorphous solid will become less viscous. At some point the molecules may obtain enough freedom of motion to spontaneously arrange themselves into a crystalline form.

This is known as the crystallization temperature (T_c) (**Figure a2.1**). This transition from amorphous solid to crystalline solid is an exothermic process, and results in a peak in the DSC signal. As the temperature increases the sample eventually reaches its melting temperature (T_m). The melting process results in an endothermic peak in the DSC curve. The ability to determine transition temperatures and enthalpies makes DSC an invaluable tool in producing phase diagrams for various chemical systems.

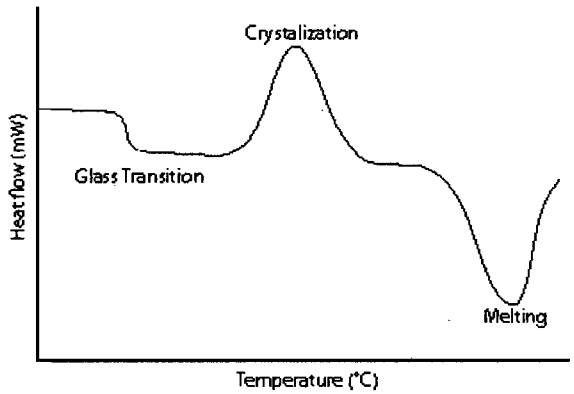

Figure a2.2. Schematic differential Scanning Calorimetry (DSC) demonstrating the appearance of several common features

Determination of the molar mass

Polymers are a chain consisting of large molecules made up of a linked series of repeated simple monomers. The individual polymer chains rarely have the exact same degree of polymerization and molar mass, and there is always a distribution around an average value. The molar mass distribution (or molecular weight distribution) in a polymer describes the relationship between the number of moles of each polymer species (N_i) and the molar mass (M_i) of that species.

As a consequence of the molar mass distribution (**Figure a2.3**), different techniques can yield different molar mass values. Colligative properties such as size

exclusion chromatography depend on the number of molecules in solution, and such properties correspondly yield a number-average molar mass $\overline{M}_n$ as given by

$$\overline{M}_n = N_A \sum N_i M_i / \sum N_i \qquad \text{(a2.1)}$$

where N_A is the Avogadro number, 6.023 x 10^{23} molecules/mole. In a distribution of molecular weights, the number average is bias for the lower values.

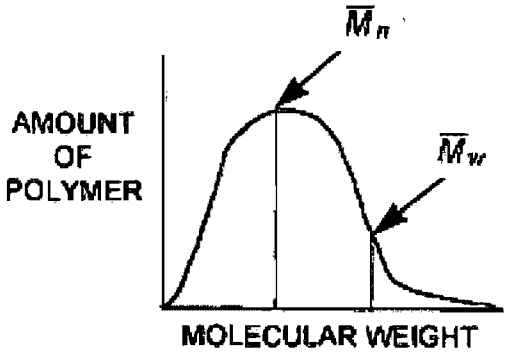

Figure a2.3. Distribution of molar mass in a typical polymer.

Figure a2.3 shows a graph of molecular weight distribution for a typical polymer. Polymers with a narrow spread in molecular weights can be obtained by anionic polymerization or other living polymerization techniques.

Some experimental methods for the determination of molecular weight depend on the masses or size of the solute molecules, rather then their number. An example of such method is in light scattering (LS) and the weight-average molar mass, $\overline{M}_w$ is given by

$$\overline{M}_w = N_A \sum N_i M_i^2 / \sum N_i , M_i \qquad \text{(a2.2)}$$

The ratio, $\overline{M}_w / \overline{M}_n$ is known as the polydispersity index (PDI). Polymers produced by free radical polymerization give a ratio of 2. However, polymers produced by anionic polymerization may be almost unity or monodisperse as it is technically referred.

Size Exclusion Chromatography

This technique depends on the size of the polymer in solution. The stationary phase is composed of crosslinked polymers which contain surface pores of various sizes (**Figure a2.4**). The large molecules do not fit into the pores so they travel fast whereas the small molecules travel slower because they are retained longer.

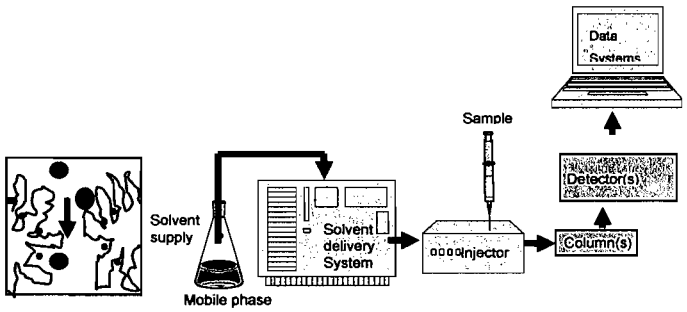

Figure a2.4. Diagram of size exclusion chromatography (SEC).

The molar mass-log retention volume plot can be used to determine the molar mass and molar mass distribution of a polymer sample if monodisperse calibration standards are available for that polymer.[137] The SEC chromatogram of a polymer will show a broad peak. The broadening effect is a result of the large number of unresolved oligomers in the samples. Commercially available SEC software is able to divide the peak into a number of slices. Each slice has a retention volume, V_R; and if the slice is sufficiently narrow, it can be assumed to be effectively monodisperse and to have a molar mass M_i which can be read off the calibration plot, to give molar mass of the polymer as a function of V_R. The software also determines the area A_i of each slice. Since the area of each slice is proportional to the weight of the polymer as a function of V_R, the software integrates it to produce the cumulative weight percent. Finally, the software makes the cross-plot of cumulative weight percent vs. log M, which is the molar mass distribution.

Size exclusion chromatography with multiangle laser light scattering (SEC-MALLS)

Coupling the SEC instrument with molecular weight sensitive laser light-scattering overcomes the need of a calibration and yields absolute molecular weights provided that the value *dn/dc* (differential refractive index increment) or the total mass of the eluting solute is known. In the SEC-MALLS system as shown in **Figure a2.5** DAWN EOS photometer is attached to a pump system. Polymer solutions injected to the system are brought downstream to the columns by the mobile phase for fractionation. When the eluent leaving the column flows through the MALLS, light scattering measurements are made almost simultaneously at each different angle photometer and are recorded before passing through the differential refractive index detector (DRI) where their concentrations are quantified. Data collection and processing are generated by the Wyatt Technology Corporation ASTRA. SEC-MALLS provides the molecular weight distribution, branching information, and molecular information (R_h, R_g).

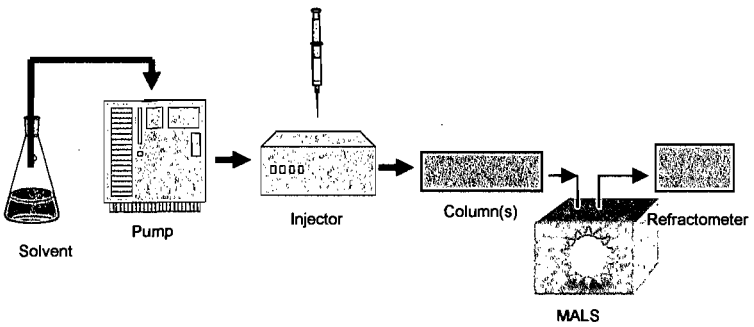

Figure a2.5. Simplified diagram of SEC-MALLS set-up

Matrix-assisted laser desorption/ionization time-of-flight (MALDI-TOF) mass spectrometry

MALDI-TOF mass spectrometer (**Figure a2.6)** is a relatively novel in which a co-precipitate of an UV-light absorbing matrix and a macromolecule is irradiated by a nanosecond laser pulse. Most of the laser energy is absorbed by the matrix, which

prevents unwanted fragmentation of the macromolecule. The ionized macromolecules are accelerated in an electric field and enter the flight tube. During the flight in this tube, different molecules are separated according to their mass to charge ratio and reach the detector at different times. In this way each molecule yields a distinct signal. The method is used for detection and characterization of macromolecules, such as proteins, peptides, and polymers. The m/z scale of the mass spectrometer is calibrated with a known sample that can either be analyzed independently (external calibration) or pre-mixed with the sample and matrix (internal calibration). The analyzer and detector of the mass spectrometer, and often the ionisation source too, are maintained under high vacuum to give the ions a reasonable chance of traveling from one end of the instrument to the other without any hindrance from air molecules.

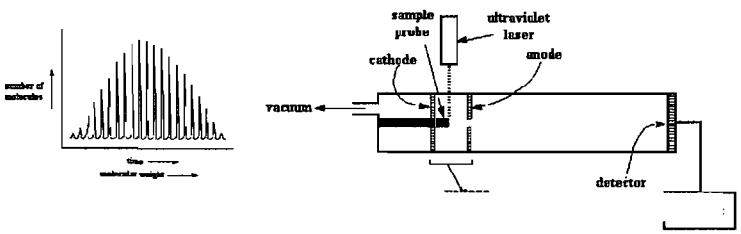

Figure a2.6. Simplified diagram of MALDI apparatus and output (Taken from [138])

APPENDIX 3

NMR Spectra

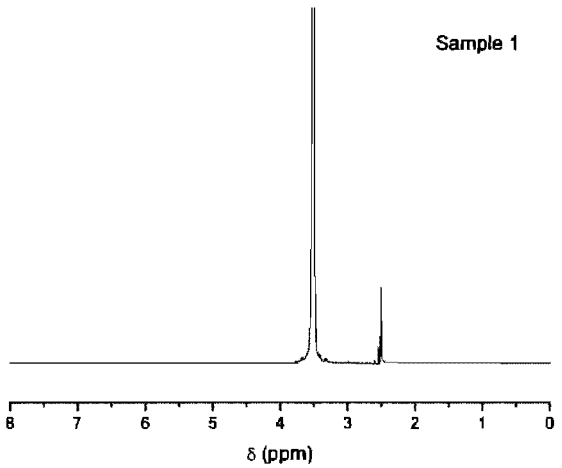

Figure. a3.1. NMR spectra of $CA(PEG)_4$ of sample 1 see**Table 2.1** for details.

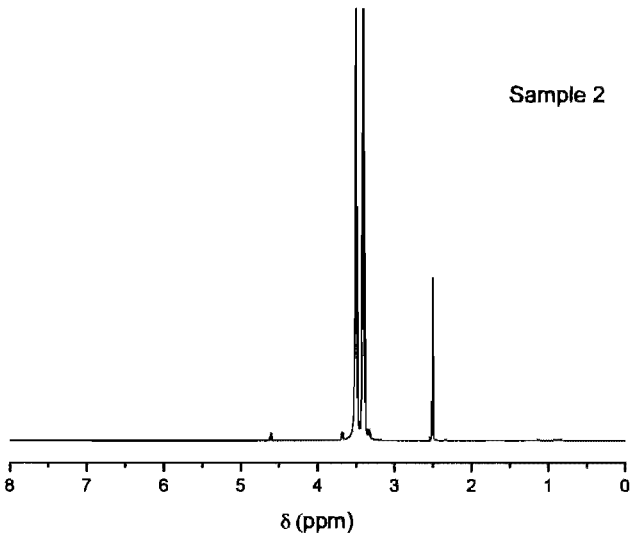

Figure. a3.2. NMR spectra of $CA(PEG)_4$ of sample 2 see**Table 2.1** for details.

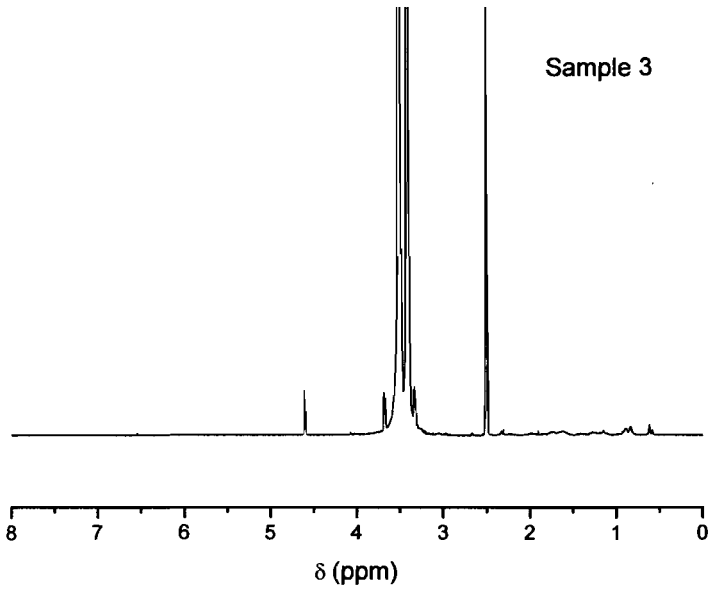

Figure. a3.3. NMR spectra of $CA(PEG)_4$ of sample 3 seeTable 2.1 for details

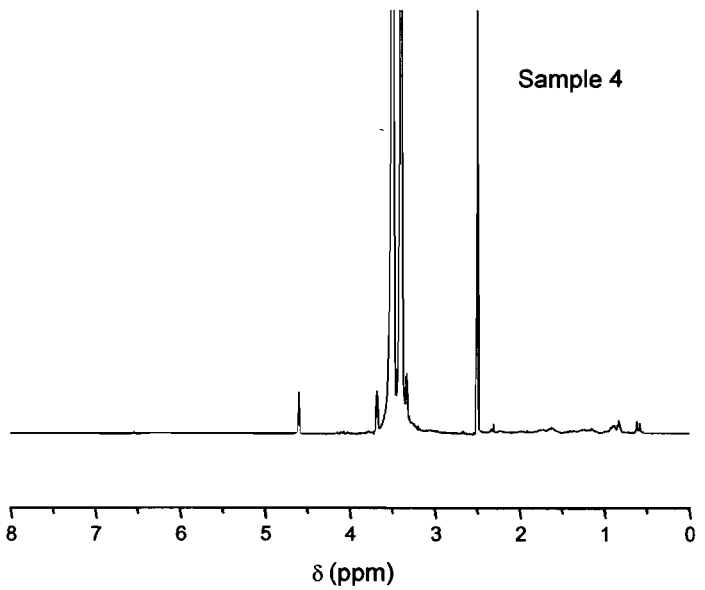

Figure. a3.4. NMR spectra of $CA(PEG)_4$ of sample 4 seeTable 2.1 for details

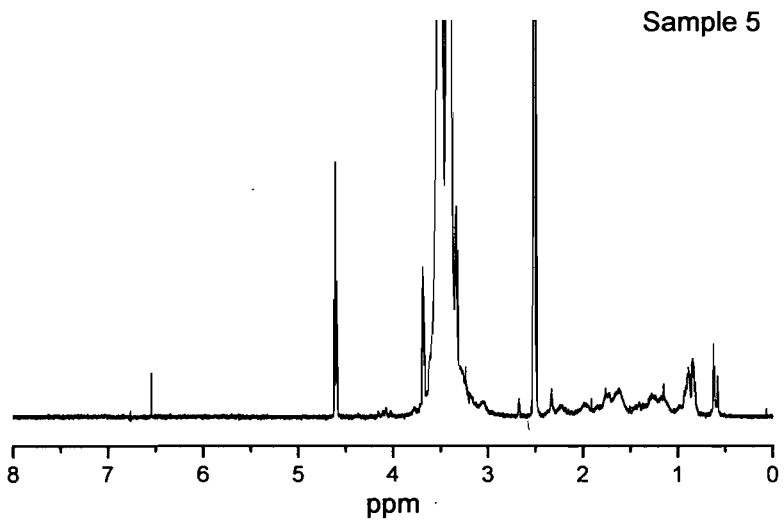

Figure. a3.5. NMR spectra of $CA(PEG)_4$ of sample 5 seeTable 2.1 for details

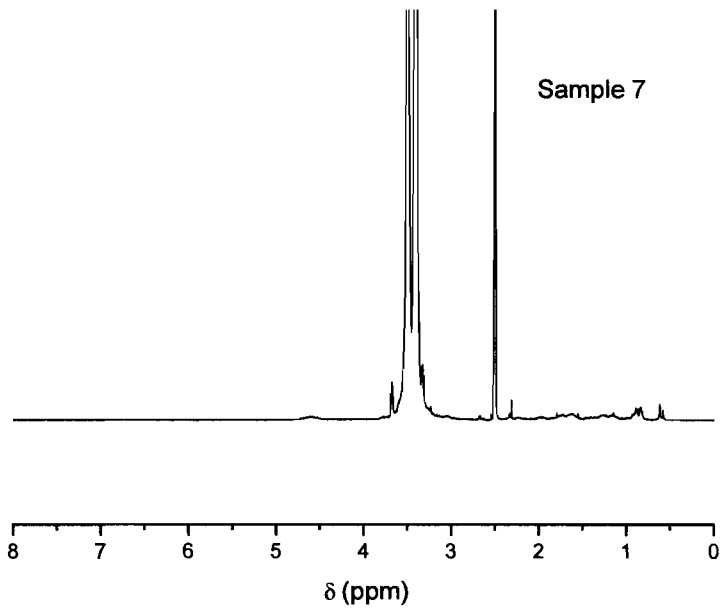

Figure. a3.6. NMR spectra of $CA(PEG)_4$ of sample 7 seeTable 2.1 for details

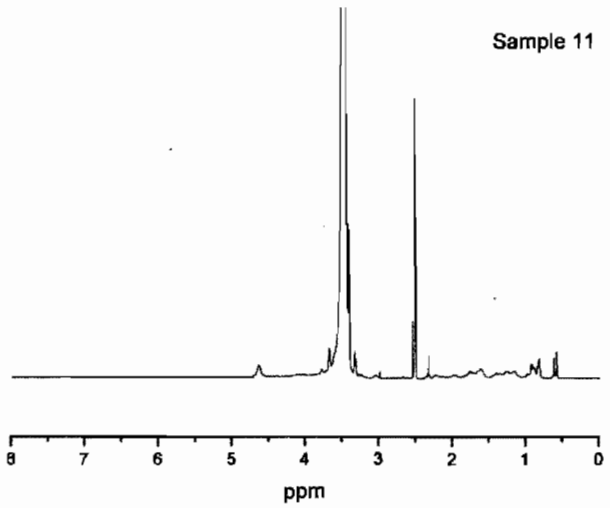

Figure. a3.7. NMR spectra of $CA(PEG)_4$ of sample 11 seeTable 2.1 for details

---

i